Sphingosine-1-phosphate receptor 3 signaling is a critical modulator of stroke outcome

Doctoral thesis

to obtain a doctorate (PhD)

from the Faculty of Medicine

of the University of Bonn

Hana Matuskova

from Teplice, Czech Republic

2022

Written with authorization of

the Faculty of Medicine of the University of Bonn

First reviewer: Prof. Dr. Anja Meissner

Second reviewer: Prof. Dr. Gabor Petzold

Day of oral examination: 09.06.2022

From the University Hospital Bonn, Neurology Department

Director: Prof. Dr. Thomas Klockgether

Table of Contents

List of abbreviations

List of abbreviations

αSMA	Alpha smooth muscle actin
ABC	ATP-binding cassette
ACSA2	Astrocyte cell surface marker 2
AIF	Apoptosis-inducing factor
ASL	Arterial spin labeling
ATP	Adenosine triphosphate
BBB	Blood-brain barrier
BSA	Bovine serum albumin
Ca^{2+}	Calcium
CBF	Cerebral blood flow
CCA	Common carotid artery
Cdh5	Cadherin 5
Cer	Ceramide
CNS	Central nervous system
Cnx43	Connexin 43
COX-2	Cyclooxygenase-2
Cyt C	Cytochrome C
DAG	Diacylglycerol
DAMP	Damage-associated molecular pattern

EC	Endothelial cell
ECA	External carotid artery
EDTA	Ethylenediaminetetraacetic acid
EHSB	Extra high salt buffer
eNOS	Endothelial nitric oxide synthase
ER	Endoplasmic reticulum
ERK	Extracellular signal-regulated kinase
FACS	Fluorescence-activated cell sorting
Gfap	Glial fibrillary acidic protein
GSL	Glycosphingolipid
HA	Hemagglutinin
HSB	High salt buffer
HT	Hemorrhagic transformation
ICA	Internal carotid artery
IL	Interleukin
IP_3	Inositol trisphosphate
I/R	Ischemia/reperfusion
K^+	Potassium
MACS	Magnetic-activated cell sorting
MCA	Middle cerebral artery

MCAo	Middle cerebral artery occlusion
MEK	Mitogen activated kinase
Mfsd2	Major facilitator superfamily domain-containing protein 2
MMP	Matrix metalloproteinase
MRI	Magnetic resonance imaging
N_2O	Nitrous oxide
Na^+	Sodium
NK-κB	Nuclear factor kappa-light-chain-enhancer of activated B cells
NO	Nitric oxide
NVU	Neurovascular unit
O_2	Oxygen
ORF	Open reading frame
PBS	Phosphate buffer saline
PGDB	Protein G Dynabeads
PIP_2	Phosphatidylinositol 4,5-bisphosphate
PIP3K	Phosphoinositide 3-kinase
PKC	Protein kinase C
PLC	Phospholipase C
pMCAo	Permanent middle cerebral artery occlusion
PPA	Pterygopalatine artery

PSB	Polysome buffer
PTEN	Phosphatase and tensin homolog
ROCK	Rho-associated protein kinase
ROS	Reactive oxygen species
RT	Room temperature
RT-qPCR	Real-time quantitative polymerase chain reaction
S1	Supernatant 1
S1P	Sphingosine-1-phosphate
S1Pr	Sphingosine-1-phosphate receptor
$S1Pr3^{-/-}$	Sphingosine-1-phosphate receptor 3 knockout
SEM	Standard error of the mean
SM	Sphingomyelin
Sox9	SRY-box transcription factor 9
Sph	Sphingosine
SphK1/2	Sphingosine kinase 1/2
Spns2	Spinster homolog 2
SPP1/2	Sphingosine-1-phosphate phosphatase 1/2
tMCAo	Transient middle cerebral artery occlusion
tPA	Tissue plasminogen activator
TTC	2, 3, 5-Triphenyltetrazolium chloride

VEGF	Vascular endothelial growth factor
VSMC	Vascular smooth muscle cell
WT	Wild type

1. Introduction

1.1. Etiology and pathogenesis of stroke

Stroke is the second leading cause of death worldwide (https://www.who.int/news-room/fact-sheets/detail/the-top-10-causes-of-death). Various risk factors are known to be associated with the development of stroke, these includes hypertension, diabetes, hyperlipidemia and age, the most prominent non-modifiable factor (Boehme et al., 2017). Stroke is classified based on its origin into ischemic and hemorrhagic type. Hemorrhagic stroke is caused by blood vessel rupture and subsequent bleeding to the brain tissue and accounts 13 % of all cases (Chauhan & Debette, 2016; Koh & Park, 2017); (**Fig. 1**). As a result, a hematoma compresses the surrounding brain tissue, which causes brain edema followed by secondary brain injury (Shao et al., 2019). Ischemic stroke is the most prevalent type of stroke and leads to a complete interruption of blood flow. While this event results in irreversible changes and cell death in the ischemic core within minutes, the surrounding area, the so-called penumbra, has potential to be rescued and is therefore a target for developing neuroprotective therapy (Lo, 2008; Xing et al., 2012); (**Fig. 1**). Currently, tissue plasminogen activator (tPA) is the only approved treatment. It is, however, only suitable for 15 % of stroke patients mainly due to the narrow administration time window, which is limited to 3–4.5 hours after the onset of the ischemic event (Zaheer et al., 2011), as later administration is associated with a high risk of hemorrhagic transformation (HT); (Peña et al., 2017).

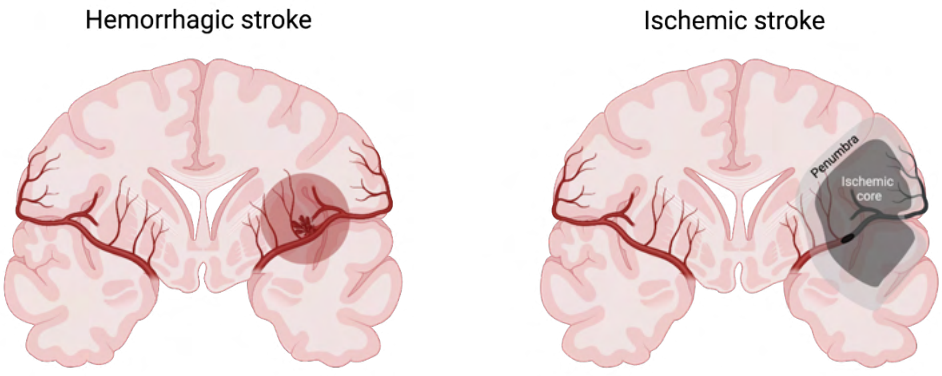

Fig. 1: Schematic illustration of ischemic vs hemorrhagic stroke. Ischemic stroke occurs due to the obstruction of blood vessel, which results in a drop of blood flow under 10 ml/100 g/min in the ischemic core inducing irreversible changes. The surrounding penumbra has perfusion below 17 ml/100 g/min, which leads to neuronal dysfunction, however, the ionic gradients are not yet disrupted (Zhou & van Zijl, 2012). Hemorrhagic stroke is a result of a ruptured blood vessel followed by bleeding to the brain parenchyma. *Created with BioRender.com.*

1.2. Pathophysiology of ischemic stroke

The brain has high energetic demands and consumes 20 % of the body's total oxygen supply, which is used for generation of adenosine triphosphate (ATP). During cerebral ischemia, ATP production is impaired which prevents ATPases from keeping the ionic hemostasis (Doyle et al., 2008). Increased influx of sodium (Na^+) and efflux of potassium (K^+) leads to depolarization of the neuronal plasma membrane, resulting in release of the excitatory neurotransmitter glutamate. Glutamate binds to its receptors, which allows excessive calcium (Ca^{2+}) influx, leading to activation of degrading enzymes (i.e., caspases and calpains) and cell death in the ischemic core (Doyle et al., 2008; Rodrigo et al., 2013; Xing et al., 2012). Increased intracellular concentrations of Ca^{2+} induce the formation of reactive oxygen species (ROS) and release of pro-inflammatory mediators (Dirnagl et al., 1999). Due to the uncontrolled movement of ions through the membrane, spreading depolarization occurs and contributes to secondary ischemic brain injury. Frequency of spreading depolarization positively correlates with the extent of the ischemic lesion (Hartings et al., 2003); (**Fig. 2**).

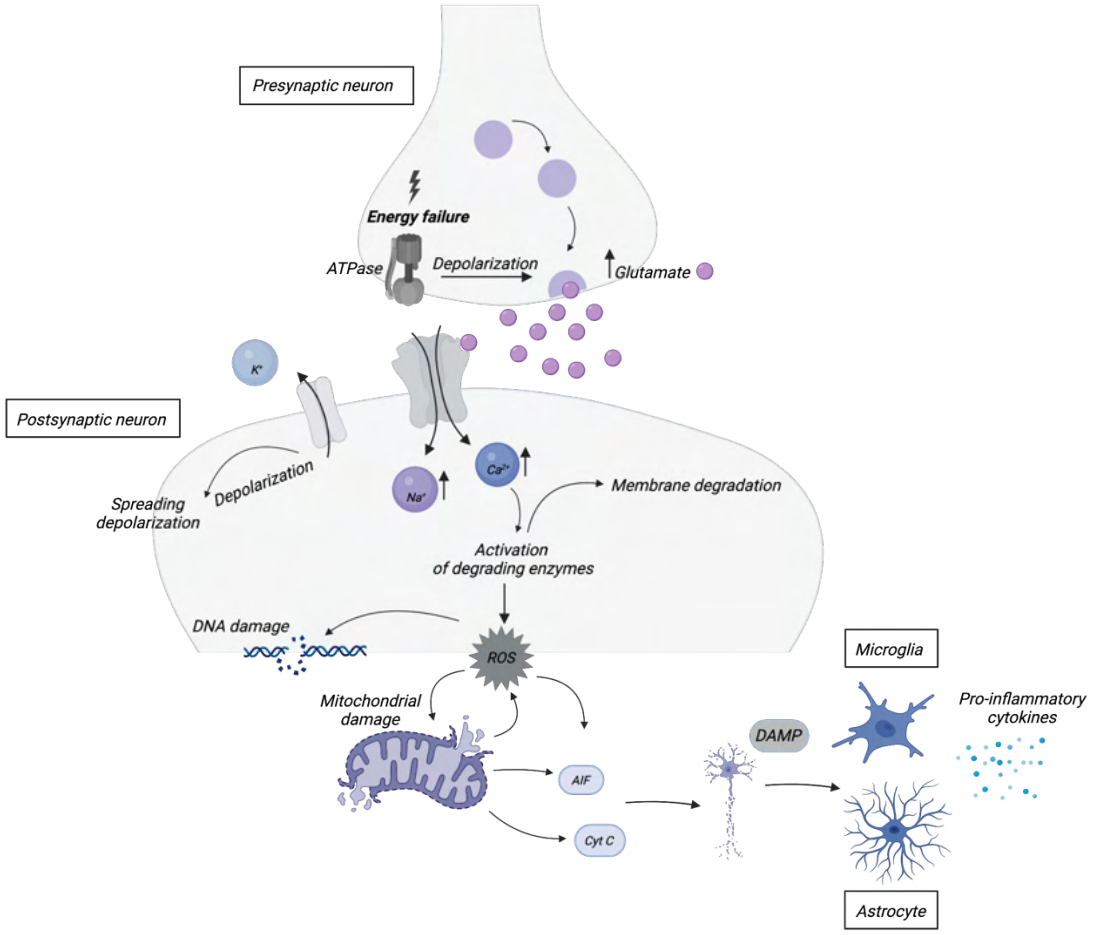

Fig. 2: Schematic illustration of molecular mechanisms of stroke. Insufficient blood supply to the brain leads to failure of ATP production, which results in ionic imbalance and depolarization. Increased release of glutamate activates glutamate receptors resulting in increase of intracellular Ca^{2+} and Na^{+}. Excess of intracellular Ca^{2+} overactivates degrading enzymes. Increased ROS production induces DNA and mitochondrial damage. As a result, disrupted mitochondria release Cyt C or AIF triggering apoptosis. DAMP molecules, which are released by necrotic neurons activate astrocytes and microglia and they in turn release pro-inflammatory cytokines. The same cell can depolarize again due to the release of K^{+} leading to spreading depolarizations (Dirnagl et al., 1999; Jayaraj et al., 2019). *Created with BioRender.com.*

AIF – apoptosis-inducing factor; ATP – adenosine triphosphate; Ca^{2+} – calcium; Cyt C – cytochrome C; DAMP – damage-associated molecular pattern; K^{+} – potassium; Na^{+} – sodium; ROS – reactive oxygen species.

1.2.1.1. Inflammatory mechanisms in ischemic stroke

Inflammation as a defense mechanism is initiated by damage-associated molecular pattern (DAMP) molecules and purines released from necrotic cells which together activate the immune system within minutes after ischemic brain damage (Iadecola & Anrather, 2011). It is a complex of highly regulated cascades which can, depending on time of occurrence, be either beneficial or destructive (Lambertsen et al., 2019). The first cell type reacting to the ischemic insult are microglia, the resident macrophages of the central nervous system (CNS); (Xing et al., 2012). Under ischemic conditions, microglia undergo morphological changes and start to proliferate and accumulate at the site of injury. Many studies have shown that upon activation, microglia polarize into different phenotypes. As such heterogeneous cell population, they release a wide range of pro- and anti-inflammatory substances and thereby may have both beneficial and detrimental effects (Hu et al., 2012; S. Xu et al., 2020; S. C. Zhao et al., 2017). Hours to a few days after stroke onset, blood-derived leukocytes are recruited into the site of ischemia. Neutrophils are the first immune cells migrating from the peripheral blood into the brain, which was shown to be associated with release of ROS and proteolytic enzymes. This further worsens neurological outcome by disrupting the blood-brain barrier (BBB), inducing blood flow obstruction or contributing to HT (Doyle et al., 2008; Lambertsen et al., 2019; Yin & Yang, 2016). In addition to neutrophils, ischemia induces brain infiltration of monocytes and macrophages, which were initially associated with aggravation of tissue injury. However, studies showed that, similarly to microglia, they acquire different phenotypes and are important contributors to tissue regeneration by for instance, phagocytizing dead cells (Chu et al., 2015; Perego et al., 2016). Later after the ischemic brain damage, lymphocytes (T and B cells) infiltrate the infarcted brain tissue. Their presence in the acute stages was reported to be mainly associated with detrimental effects due to the secretion of pro-inflammatory mediators such as interleukin (IL) 17, IL-23 or IL-1 (Beuker et al., 2021; Brait et al., 2012; Iadecola & Anrather, 2011; Selvaraj & Stowe, 2017). However, also lymphocytes are a highly heterogeneous cell population and thus, their role during brain ischemia remains to be fully elucidated (Chen et al., 2012; Doyle et al., 2015; Kleinschnitz et al., 2013; Liesz et al., 2009).

Although activation of the immune system after stroke is initiated in order to salvage the affected brain tissue, immune cell infiltration partially contributes to tissue damage in the ischemic brain. Thus, it is therefore of utmost importance to better understand the precise mechanisms of the action of the different immune system components and how exactly they affect the post-stroke brain. This knowledge is critical to develop new therapeutic targets that could help to reduce the extent of brain damage following stroke.

1.3. The role of astrocytes in health and stroke-induced ischemic damage

1.3.1. Classification of astrocytes

Astrocytes are the most abundant glial cell type and crucial regulators of ischemic brain damage (S. Zhang et al., 2021). Glial cells were originally assigned only minor functions of passive supporters of brain cells (Temburni & Jacob, 2001). This view has changed over the past years due to intensive research, which underlined the complexity and necessity of glial cells in essential brain functions (Jäkel & Dimou, 2017).

Astrocytes are a highly heterogeneous cell population, which can be classified into distinct classes based on their morphology, localization and expression pattern (Ben Haim & Rowitch, 2016). The traditional classification dates back to the 19th century and includes protoplasmic and fibrous astrocytes (Andriezen, 1893). Gray matter protoplasmic astrocytes have a branched morphology and ensheath synapses (Allen & Eroglu, 2017; Ben Haim & Rowitch, 2016). The elongated processes of fibrous astrocytes, on the other hand, are in contact with oligodendrocytes and myelinated axon tracts in the white matter (Sofroniew & Vinters, 2009). Development of new molecular and imaging techniques further confirmed the extent of astrocytic heterogeneity within and between brain regions based on their electrophysiological properties (Matthias et al., 2003), Ca^{2+} activity (Takata & Hirase, 2008) or gene expression pattern (Batiuk et al., 2020; John Lin et al., 2017).

1.3.2. The role of astrocytes in the tripartite synapse

Astrocytes are in close contact with neuronal synapses in a functional unit called tripartite synapse. Additionally, they form networks with each other via gap junctions (Araque et al., 1999; Benarroch, 2016). Such an organization enables astrocytes to spread detected signals across brain regions and regulate synaptic transmission including maintaining physiological pH, neurotransmitter and water homeostasis and regulating ion concentration (Benarroch, 2016; Blutstein & Haydon, 2013; Deitmer et al., 2019; Perea et al., 2009).

As neuronal activity is coupled to the acidic environment, maintaining the physiological pH between 7.2–7.3 is essential for the continuous information processing in the brain (Deitmer et al., 2019; Theparambil et al., 2020). Astrocytes possess the main H^+ buffering system in form of electrogenic sodium-bicarbonate cotransporter and carbonic anhydrases II and IV (Deitmer et al., 2019). Various ionotropic and metabotropic receptors expressed by astrocytes detect neuronal activity via transient increases of astrocytic intracellular Ca^{2+} levels. Activation of Ca^{2+}-dependent signaling pathways is followed by the release of gliotransmitters, which ultimately leads to regulation of synaptic activity (Liu et al., 2018). Another way how astrocytes modulate synaptic activity is via a mechanism known as glutamate/glutamine cycle, which protects from accumulation of neurotransmitters in the synaptic cleft (Bak et al., 2006; Watts et al., 2018). Astrocytes take up neurotransmitters such as glutamate via glutamate/GABA transporters and convert them to glutamine, which can then be taken up into neurons that convert it back to glutamate/GABA (Benarroch, 2016; C. Y. Liu et al., 2018). In addition, astrocytic end-feet are in contact with blood vessels, which enables glucose uptake from blood and thus, serves as a main storage of glycogen to support high neuronal energetic demand (P.Magistretti, L.Pellerin, D.Rothman, 1999; Sofroniew & Vinters, 2009).

1.3.3. Astrocytes as part of the neurovascular unit

The brain vasculature possesses an important role in regulating the transport of molecules and ions from the periphery into the brain. This physical and chemical barrier is called the BBB. It consists of tightly interconnected endothelial cells (EC), astrocytes, and pericytes, which together with neurons and microglia form the neurovascular unit (NVU); (Obermeier

et al., 2013). The NVU couples high energy demands of brain cells with local blood flow (Muoio et al., 2014).

The highly selective transport across the BBB is ensured by ECs located on the luminal part of blood cells interconnected via tight and adherens junctions (Betz et al., 1980; McConnell et al., 2017). Additionally, polarized expression of receptors, ion channels and transporters additionally allow ECs to deliver nutrients to the brain and eliminate metabolic waste products out of the brain (Bell et al., 2020). The basal side of ECs is surrounded by a basement membrane, which is composed of extracellular matrix proteins of the glycoprotein families and has mainly supporting functions (Sweeney et al., 2016; Thomsen et al., 2017). The outer part of the basement membrane consists of embedded pericytes. Their localization between ECs and astrocytes enables them to modulate BBB integrity mainly via regulation of ECs tight junction protein expression and polarizing of astrocytic end-feet (Armulik et al., 2010). In addition to that, pericyte processes express contractile proteins which regulate blood vessel diameter (Daneman, R., Prat, 2008). Astrocytes act as a connecting unit between neurons and ECs and possess essential functions in cerebral blood flow regulation in response to neuronal activity. Astrocytes also release growth factors in order to maintain the BBB (Cabezas et al., 2014; Guérit et al., 2021; Muoio et al., 2014).

1.3.3.1. The neurovascular unit during ischemia

One of the early hallmarks of stroke is NVU dysfunction, which subsequently leads to BBB disruption (Nian et al., 2020). Early after stroke onset, the lack of oxygen and glucose leads to an ionic imbalance. As a result, Na^+ accumulates within the cells and causes their swelling, a phenomenon called cytotoxic edema. The activation of the inflammatory cascade induces an overexpression of matrix metalloproteinases (MMP), a family of proteolytic enzymes which degrade tight junction proteins and extracellular matrix (Wang et al., 2021). This increase of BBB permeability enables the infiltration of peripheral immune cells into the brain, which contribute to ischemic injury progression (Qiu et al., 2021). Moreover, BBB disruption further allows macromolecules to enter the brain tissue, creating an osmotic gradient which leads to excessive water accumulation in the extracellular space, called vasogenic edema (Bernardo-Castro et al., 2020). Aquaporin-4

water channels that are highly expressed on astrocytic end-feet play an important role in the generation of cytotoxic edema at initial stages of BBB breakdown (Yao et al., 2015). However, it has been reported that Aquaporin-4 is necessary for water clearance and thus, resolution of vasogenic edema at later stages post-stroke (Papadopoulos et al., 2004). Furthermore, BBB disruption positively correlates with the severity of HT, which is a common complication occurring after ischemic stroke (Latour et al., 2004). As mentioned above, the risk of HT increases with tPA treatment especially when administered outside the 4.5 hour time window due to its effect on MMPs that in turn, promote ROS production and microglia activation (Jickling et al., 2014; Kim, 2019).

1.3.4. Astrocytes during ischemia

Intensive research since the 19th century uncovered the prominent role of astrocytes under physiological and pathological conditions such as stroke. Ischemic insult induces a series of morphological and functional changes in a subpopulation of astrocytes referred to as reactive astrocytes. These typically increase the expression of glial fibrillary acidic protein (Gfap) together with other intermediate filament proteins such as vimentin and nestin, and SRY-box transcription factor 9 (Sox9); (Liddelow et al., 2017; W. Sun et al., 2017; Zamanian et al., 2012). As cessation of blood supply to the brain causes massive cell death in the infarct core, a subgroup of reactive astrocytes proliferate and form a physical barrier around the necrotic area to separate and protect the healthy tissue (Sofroniew, 2020). At first, the astroglial border was associated with detrimental effects on axonal regeneration after stroke (Busch & Silver, 2007). However, experiments examining outcome after experimental stroke without the presence of reactive astrocytes revealed larger ischemic lesions, augmented immune cells infiltration, impaired vascular remodeling and worsened sensorimotor function (Bush et al., 1999; Nawashiro et al., 2000; Williamson et al., 2021). Thus, reactive astrogliosis was verified as a necessary part of the recovery process. Nevertheless, not all reactive astrocytes proliferate, subpopulation of non-proliferative astrocytes maintain their physiological functions in the less damaged tissue and depending on the severity of the injury, they display gene expression alterations and changes in their morphology (Sofroniew, 2020). Additionally, astrocytes are involved in regulation of adaptive and innate immune response after ischemic brain damage. During the acute stages of stroke, DAMPs and ROS released by

necrotic cells activate astrocytes, which in response secrete a wide range of cytokines and chemokines that regulate immune responses (S. Xu et al., 2020). Considering this, it is not surprising that astrocytes are thought to play a dual role in the context of stroke. Specifically, they contribute to neurodegeneration after stroke as they guide peripheral immune cells towards the injured area and release various pro-inflammatory cytokines. On the other hand, they promote angiogenesis and BBB repair via the release of growth factors (e.g. angiopoetin-1, glia-derived neurotrophic factor, transforming growth factor-β); (Becerra-Calixto & Cardona-Gómez, 2017; S. Zhang et al., 2021) and confine inflammation by forming glial scar (Sofroniew, 2015).

As astrocytes are critically involved in a defense response to ischemic brain damage, unraveling the precise mechanism of their action could significantly contribute to developing mechanism-based therapeutics that help to reduce the extent of brain tissue damage after stroke.

1.4. Sphingosine-1-phosphate metabolism

Sphingosine-1-phosphate (S1P) is a bioactive lipid molecule involved in a wide range of physiological functions and disease conditions (S. Pyne et al., 2016). S1P is generated via degradation of sphingomyelin and glycosphingolipids in the plasma membrane and lysosomes or via *de novo* synthesis in the endoplasmic reticulum. S1P production depends on the activity of its generating enzymes sphingosine kinase 1 and 2 (SphK1/2), which generate S1P via phosphorylation of sphingosine. Once S1P is produced, it is transported outside of the cell via S1P-specific transporters (e.g., spinster homolog 2, Spns2; major facilitator superfamily domain-containing protein 2a and b, Mfsd2a/b; ATP-binding cassette, ABC). Since S1P has pleiotropic functions, its levels need to be tightly controlled, which is ensured by an intimate interplay between SphKs and S1P degradation enzymes (S1P lyase and phosphatases); (Proia & Hla, 2015; Venkataraman et al., 2008); (**Fig. 3**). Under homeostatic conditions, red blood cells and ECs represent the major sources of plasma S1P, helping to maintain an S1P gradient with the highest concentration in plasma ~1 μM followed by lymph ~0,1 μM and the lowest concentration in interstitial tissue <1 nM (Yanagida & Hla, 2017). Such gradient is critical for maintaining physiological functions, including lymphocyte egress from lymphoid organs (Schwab et al., 2005), maintaining vascular integrity (Camerer et al., 2009) and cell migration (Kleinwort et al., 2018).

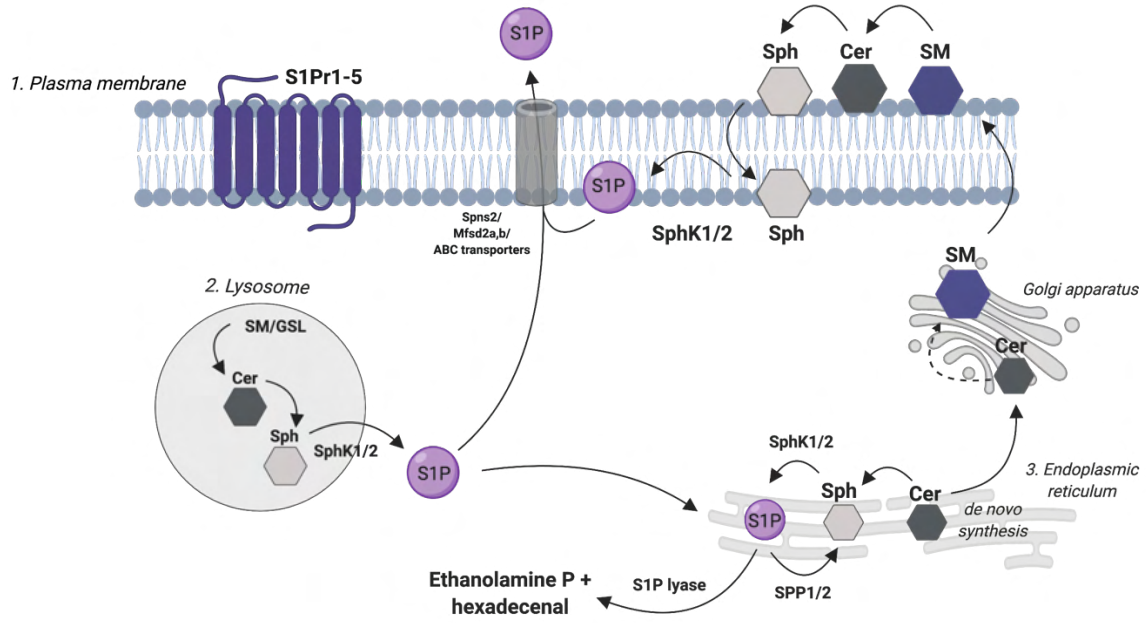

Fig. 3: Schematic illustration of S1P metabolism. S1P generation takes place in the plasma membrane, lysosome or ER. In the plasma membrane, SM is hydrolyzed into Cer followed by its deacetylation into Sph. In the last step, Sph is phosphorylated by SphK1/2 forming S1P. In lysosomes, S1P can be additionally generated via breakdown of GSL (Van Echten-Deckert & Alam, 2018). Finally, *de novo* pathway in the ER generates S1P through a chain of reactions leading to production of Cer. Alternatively, Cer is transported to the Golgi apparatus for production of SM which is then delivered to the plasma membrane via vesicular transport (Grassi et al., 2019; Kroll et al., 2020). Generated S1P is transported through cell type-specific transporters - Spns2, Msfd2a/b and ABC outside of the plasma membrane where it signals through five specific S1Pr1-5. S1P levels are further regulated via its degradation by S1P lyase or SPP1/2 exclusively in the ER; (Cantalupo & Di Lorenzo, 2016; Grassi et al., 2019; Kroll et al., 2020; Proia & Hla, 2015). *Created with BioRender.com.*

ABC – ATP-binding cassette; Cer – ceramide; ER – endoplasmic reticulum; GLS – glycosphingolipids; Msfd2a/b – major facilitator superfamily domain containing 2a/b; S1P – sphingosine-1-phosphate; S1Pr1-5 – sphingosine-1-phosphate receptor 1-5; SM – sphingomyelin; Sph – sphingosine; SphK1/2 – sphingosine-1-phosphate kinase 1/2; Spns2 – spinster homolog 2; SPP1/2 – S1P phosphatase1/2.

1.4.1. Sphingosine-1-phosphate signaling

S1P acts as an intracellular second messenger as well as an extracellular ligand that activates five specific G-protein coupled S1P receptors (S1Pr1-5) via specific signaling pathways (**Fig. 4**). While S1Pr1-3 are ubiquitously expressed, S1Pr4 and S1Pr5 are rather characteristic for hematopoietic/lymphatic tissue and immune/nervous system, respectively (Golfier et al., 2010; Jozefczuk et al., 2020).

S1Pr1, originally characterized as a highly abundant transcript in ECs, is the most studied receptor out of all S1Prs (based on Pubmed.com search); (Hla & Maciag, 1990; N. J. Pyne & Pyne, 2017). S1Pr1 is essential for vascular development as $S1Pr1^{-/-}$ mice die between E12.5 – E14.5 due to severe hemorrhage (Liu et al., 2000). Upon activation, S1Pr1 couples exclusively with $G_{i/o}$ with implications for various functions in the vascular system such as maintaining vascular integrity (Fischl et al., 2019) and inducing vasodilation (Cantalupo et al., 2017). Furthermore, S1Pr1 plays a crucial role in immune cell egress from the lymphoid organs (Allende et al., 2004, 2010; Finley et al., 2013; Weichand et al., 2013).

Compared to S1Pr1, S1Pr2 couples with several G proteins, $G_{i/o}$, $G_{12/13}$ and G_q leading to a regulation of various downstream effector pathways. Even though $S1Pr2^{-/-}$ mice were shown to be viable without any obvious developmental abnormalities (Kono et al., 2004), later on it was discovered that these mice suffer from deafness by 1 month after birth, pointing to a crucial role of S1Pr2 signaling in auditory system functionality (Kono et al., 2007). S1Pr2 activation is considered with opposing effects to S1Pr1 by promoting vascular permeability and a pro-inflammatory phenotype (Sanchez et al., 2007).

Similar to S1Pr2, S1Pr3 signals via $G_{i/o}$, $G_{12/13}$ and G_q and is involved in an array of physiological functions (Bryan & Del Poeta, 2018). S1Pr3 itself is not essential for embryonic development however, $S1Pr2^{-/-}$ $S1Pr3^{-/-}$ double and $S1Pr1^{-/-}$ $S1Pr2^{-/-}$ $S1Pr3^{-/-}$ triple knockout mice exhibit increased lethality and vascular bleeding (Kono et al., 2004). Specifically, S1Pr3 potentiates angiogenesis via activation of adherens junction assembly in ECs *in vitro* and increase expression of vascular endothelial growth factor (VEGF) and basic fibroblast growth factor 2 *in vivo* (M. J. Lee et al., 1999). Additionally, S1Pr3 involvement has been shown in the regulation of vascular tone where S1Pr3 and S1Pr1

induce vasodilation via generation of nitric oxide in ECs, while stimulation of S1Pr3 and S1Pr2 in vascular smooth muscle cells (VSMC) leads to vasoconstriction (Murakami et al., 2010; Nofer et al., 2004). Furthermore, S1Pr3 plays an important role during cell proliferation and migration (Fan et al., 2021).

S1Pr4-5 are the least studied S1P receptors (based on Pubmed.com search) and signal via $G_{i/o}$ and $G_{12/13}$ (Bryan & Del Poeta, 2018). S1Pr4 has an essential role in development of megakaryocytes (Golfier et al., 2010), neutrophil migration (Pankratz et al., 2016) and indirect regulation of dendritic cells migration (Olesch et al., 2017). S1Pr5 is highly expressed in oligodendrocytes and their precursor cells as well as in natural killer cells. S1Pr5 activation induces retraction of processes in immature oligodendrocytes, whereas S1Pr5 signaling in mature oligodendrocytes is important for their survival (Jaillard et al., 2005). In addition, it was shown that S1Pr5 plays a role in the egress of natural killer cells from the bone marrow (Walzer et al., 2007).

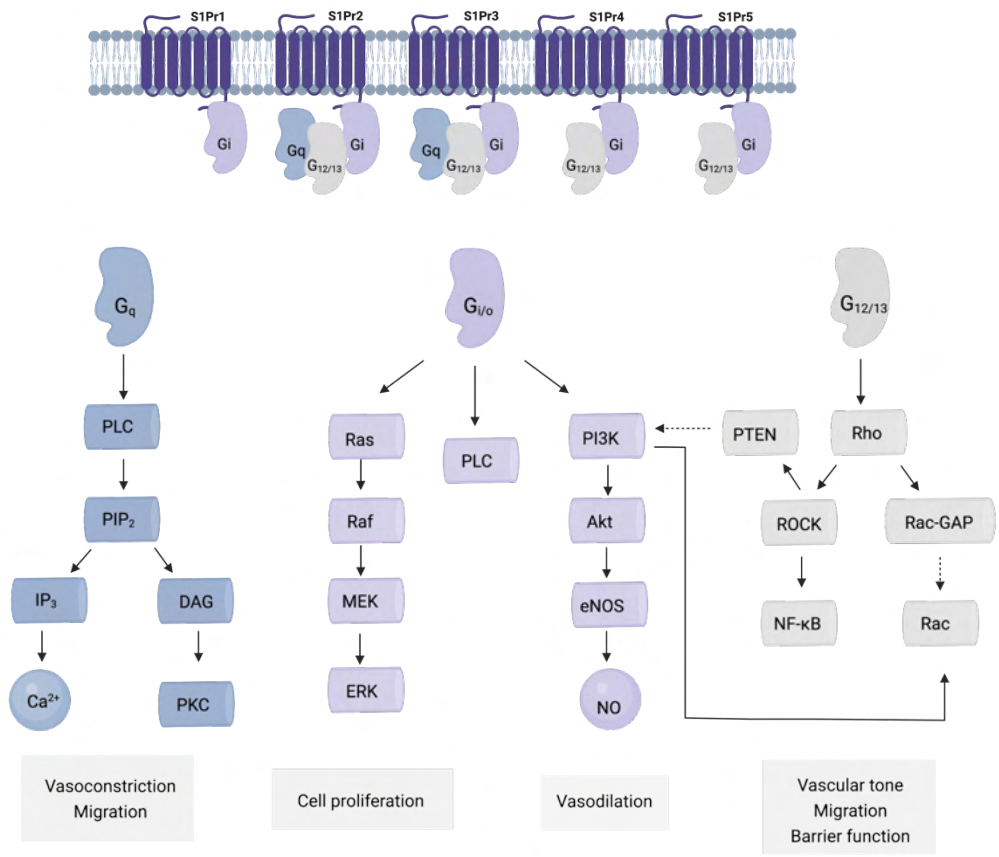

Fig. 4: Schematic illustration of S1P downstream signaling pathways. Upon activation, S1Prs couples with $G_{i/o}$, $G_{12/13}$, G_q which leads to various cell responses (examples given in the scheme). The straight and dotted lines represent activation and inhibition, respectively (Brunkhorst et al., 2014; Okamoto et al., 2011; Prager et al., 2015). *Created with BioRender.com.*

Ca^{2+} – calcium; DAG – diacylglycerol; eNOS – endothelial nitric oxide synthase; ERK-extracellular signal-regulated kinase; IP_3 – inositol 1,4,5–trisphosphate; MEK – mitogen activated kinase; NF-κB – nuclear factor kappa-light-chain-enhancer of activated B cells; NO – nitric oxide; PI3K – phosphoinositide 3-kinase; PIP_2 – phosphatidylinositol 4,5–bisphosphate; PKC – protein kinase C; PLC – phospholipase C; PTEN – phosphatase and tensin homolog; ROCK – Rho-associated protein kinase.

1.4.2. Sphingosine-1-phosphate signaling during ischemia

Research regarding the role of S1P signaling in the context of ischemic brain damage has verified its importance during CNS pathologies. S1Pr1 signaling is harnessed as a mechanistic basis for an immunomodulatory drug called Fingolimod (FTY720). Fingolimod binds nonselectively to all S1Prs, excluding S1Pr2. Its action induces internalization of S1Pr1, which results in functional antagonism (Huwiler & Zangemeister-Wittke, 2018). Fingolimod is approved for the treatment of relapsing-remitting multiple sclerosis since 2010 and is currently in several clinical trials for stroke (ClinicalTrials.gov Identifier: NCT04629872, NCT04718064, NCT02002390, NCT04088630). Experimental stroke studies have mostly shown beneficial effect of Fingolimod treatment following stroke, specifically concerning inhibition of infiltrating lymphocytes and neutrophils, reduction of neuronal apoptosis, preservation of BBB integrity, reduction of infarct lesion and improvement of neurological outcome (Czech et al., 2009; Hasegawa et al., 2010; Malone et al., 2021; Z. Wang et al., 2020; Wei et al., 2011). However, some studies could not reproduce the same positive effects (Kleinschnitz et al., 2013; Liesz et al., 2011; Salas-Perdomo et al., 2019). Moreover, potential side effects associated with Fingolimod treatment should be considered as stroke patients have a high risk of developing infection due to the phenomenon called stroke-induced immunosuppression of the peripheral immune system (Faura et al., 2021; Meisel et al., 2005). Furthermore, a recent study suggested the use of the S1Pr1 selective agonist CYM-5442 instead, which might be superior to Fingolimod due to its short half-life in plasma and thus, induction of an only transient suppression of the immune system and reduced risk of adverse effects on vascular integrity (Nitzsche et al., 2021).

S1Pr2 signaling has been repeatedly reported to contribute to disruption of vascular integrity after stroke. Genetic S1Pr2 deletion and pharmacological inhibition with the S1Pr2 antagonist JTE013 improved neurological outcome, which was further associated with smaller infarct lesions (Kim et al., 2015; Sapkota et al., 2019). On a molecular level, S1Pr2 inhibition leads to decreased MMP9 activity, which corresponds with diminished cerebrovascular permeability *in vitro* (Kim et al., 2015), augmented migration of neural progenitor cells towards infarcted area (Kimura et al., 2008), and reduced expression of microglial pro-inflammatory markers (Sapkota et al., 2019).

Compared to S1Pr1 and S1Pr2, there are less studies regarding the involvement of S1Pr3 in ischemic brain damage. Dusaban et al. (2017) revealed S1Pr3 up-regulation during *in vitro* scratch injury-induced neuroinflammation in astrocytes (Dusaban et al., 2017). Contrary to that, study of Dong et al. (2018) showed that the improved outcome after Fingolimod administration is not only associated with S1Pr1 as mentioned above but also with S1Pr3 as silencing of S1Pr3 abolished Fingolimod's anti-inflammatory effect (Dong et al., 2018). These findings point to dual effects of S1Pr3 that are dependent on the condition. Additionally, an *in vivo* study using the S1Pr3 antagonist CAY10444 in experimental murine stroke showed reduced infarct lesions and improved neurological outcome. This positive effect was associated with attenuated microglial proliferation and a reduction of activated microglia and astrocytes, which was attributed to the $G_{i/o}$ downstream signaling pathway (Gaire et al., 2018). Similar results using CAY10444 were obtained in a model of hemorrhagic stroke where researchers additionally observed a reduction of immune cell recruitment (D. Xu et al., 2021).

Currently, studies regarding the involvement of S1Pr4 and S1Pr5 signaling during ischemic brain damage are missing.

Taken together, studies have shown a critical involvement of S1P signaling during stroke pathology. Despite existing knowledge gaps regarding the S1P signaling axis and its effects post-stroke, current findings encourage the speculation that targeting the S1P signaling axis is a promising way to improve post-stroke recovery.

1.5. Aim of the study

Stroke is a highly complex pathological condition lacking effective treatment beyond the 4.5 hours administration time window without serious consequences. S1P has been repeatedly reported to be involved in cardiovascular diseases including stroke, however, research is mainly focused on S1Pr1 and S1Pr2 signaling in the context of stroke compared to the other S1Prs. Recently, several *in vitro* studies revealed an activation of S1Pr3 under inflammatory conditions. Thus, the main goal of this study was to investigate the role of S1Pr3 signaling in stroke pathology. We started with the assessment of S1Pr3 expression in the whole tissue in acute stages of two different murine stroke models in wild type (WT) mice and S1Pr3 knockout ($S1Pr3^{-/-}$) mice. Using cell-specific approaches, we next aimed at elucidating the cell type-specific contribution to the activation of S1Pr3 signaling during ischemic brain damage. Subsequently, we pharmacologically modulated the S1Pr3 signaling pathway via administration of an S1Pr3 antagonist 4 hours and 8 hours post-stroke.

2. Material & Methods

2.1. Mouse lines and husbandry

All animal experiments performed in this study were approved by LANUV of North Rhine-Westphalia (81-02.04.2019.A214/01) and by the institutional ethics committee at Lund University (5.8.18-08160/2021) and were conducted in accordance with European animal protection laws. Mice (3-5 months old) were housed on 12/12 hours light-dark cycle with access to food and water *ad libitum* and kept under specific pathogen-free conditions. Mice were housed in groups of maximum five in individually ventilated cages (Tecniplast) or in transparent polycarbonate cages (for experiments performed at Lund University).

C57BL/6N WT mice were purchased from Charles River (Sulzfeld, Germany) or Taconic (Ejby, Denmark; experiments performed at Lund University) and were given 5 days acclimatization period upon arrival.

RiboTag ($Rpl22^{tm1.1Psam}$) mice were generated by inserting loxP site 5' to the wild type exon 4 of *Rpl22* gene followed downstream by a modified exon 4 carrying 3 sequence repeats of the hemagglutinin (HA) epitope tag before endogenous stop codon at 3' site.

RiboTag mice were crossbred with Cre recombinase-expressing mice either under astrocyte-specific promotor connexin 43 (Cnx43), $Gja1^{tm5(cre/ERT)Kwi}$ ($Cnx43^{Cre\text{-}ER(T)}$) to generate $Cnx43^{Cre\text{-}ER(T)}$/RiboTag mouse line or under endothelial-specific promotor Cadherin 5 (Cdh5), VE-$Cdh5^{CreER(T)}$ to generate VE-$Cdh5^{CreER(T)}$/RiboTag. Tamoxifen injection induced Cre recombinase expression leading to deletion of the wild type exon 4 and recombination of the HA-tagged exon 4 of the *Rpl22* gene.

$S1Pr3^{-/-}$ mouse line was generated by inserting loxP site upstream to the open reading frame (ORF) of exon 2 of S1Pr3 gene and downstream to the neo cassette. The ORF together with the neo cassette were deleted between loxP sites by Cre recombinase. Generated $S1Pr3^{-/-}$ are viable and have no phenotypic abnormality other than smaller litter size compared to the WT mice.

Transgenic mouse lines and their references are listed in Table 1.

Tab. 1: Transgenic mouse lines and their references

Mouse line	Background	Generated by	References	MGI
RiboTag	C57BL/6N	Paul S. Amieux	(Sanz et al., 2009)	MGI: 4355967
$Cre^{Cre\text{-}ER(T)}$	C57BL/6N	Klaus Willecke	(Kretz et al., 2003)	MGI:2676327
$S1Pr3^{-/-}$	C57BL/6N	Jerold Chun	(Ishii et al., 2001)	MGI: 2182637

2.2. Surgical models of ischemic stroke

2.2.1. Transient middle cerebral artery occlusion (tMCAo)

Mice were anesthetized with 3 % Isoflurane (Vetflurane; Virbac) in an induction chamber and afterwards kept under anesthesia with 1–1.5 % Isoflurane in nitrous oxide (N_2O); (70 % N_2O/ 30 % O_2) delivered via a vaporizer (Tec-3, Cyprane Ltd.). The body temperature was monitored by a closed-loop controlled rectal probe and an electric blanket (CODA® Monitor; Kent Scientific) and kept at 37 ± 0.5 °C during the whole procedure. The mouse was placed in a prone position and the scalp was disinfected with Octenisept® (Schülke & Mayr) and locally anesthetized with 1 % xylocaine (Dentsply Sirona). A 1 cm long incision was made from the superior nuchal line to the nasion to expose the skull. A laser Doppler plastic fiber probe (0.5 mm diameter) was fixed perpendicular to the surface in a small hole (approx. 2 mm) drilled directly under the temporal muscle (1 mm posterior and 5 mm lateral to the bregma) in the territory of the left middle cerebral artery (MCA). A laser Doppler device (Moor Instruments) was used to monitor the blood flow during the surgery, particularly to confirm successful occlusion and reperfusion. Afterwards, mice were turned to a supine position and a median transverse neck incision was made. The large pair of salivary glands were separated from each other and placed to the side. The common carotid artery (CCA), the external carotid artery (ECA) and the internal carotid artery (ICA) were exposed and dissected after removing connective and fatty tissue. The vagus nerve was bluntly separated from the CCA which was then temporarily closed with the vascular suture (7/0; Suprama). The distal part of the ECA was permanently closed and another loose suture was prepared close to the bifurcation. The ICA was closed with a vascular clip. A small incision was made with micro-scissors in the ECA between the two sutures and the silicon coated filament (9–10 mm coating length, 0.19 ± 0.01 mm tip diameter;

Doccol) was introduced and secured by tightening the suture. The ECA was cut between the two sutures, the vascular clip on the ICA was removed and the filament further advanced through the ICA until the MCA was occluded, which was confirmed by the drop (> 75 % of the baseline) of the regional blood flow (CBF) controlled by laser Doppler flowmetry (**Fig. 5**). After 60 min, the filament was withdrawn and the suture around the ECA was permanently closed while the CCA suture was removed to induce reperfusion. The reperfusion needed to reach > 75 % of the baseline in order to include the mouse in the study. The incision on the neck and the head was sutured with a silk suture (Braun; #C0762130). After the surgery, mice were transferred to a recovery chamber at 37 °C. Sham surgery was performed identically except from inserting the filament and occluding the MCA.

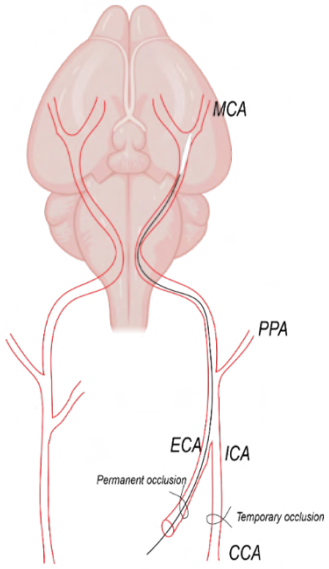

Fig. 5: Schematic illustration of the tMCAo procedure according to Longa's method. Filament was introduced to the ECA and advanced to the ICA until it occluded the MCA. After 60 min of occlusion, the filament was withdrawn and the suture around the CCA was removed in order to induce reperfusion.

CCA – common carotid artery; ECA – external carotid artery; ICA – internal carotid artery; MCA – middle cerebral artery; PPA – pterygopalatine artery; tMCAo – transient middle cerebral artery occlusion.

2.2.2. Permanent middle cerebral artery occlusion (pMCAo)

Anesthesia was initiated by 3 % Isoflurane (IsoFlo® vet 100 %) with 1 L/min oxygen and reduced to 1–1.5 % for the surgical procedure. The body temperature was kept at 37 ± 0.5 °C with a heating pad. The mouse was placed on the side and 1 cm incision was made between the left orbit and the external auditory meatus. The temporal muscle was carefully detached from the skull using electrocoagulation forceps set at 12 W (ICC50). The MCA was identified below the transparent skull. Right above the MCA bifurcation, 1–2 mm area of the skull was thinned using the dental drill until the part of the skull was possible to remove. The MCA was coagulated with electrocoagulation forceps set at 7 W proximal to the bifurcation followed by transection of the vessel to ensure successful occlusion. The temporal muscle was relocated back to its original position and the wound was sutured with a silk suture (Braun; #C0762130). Mice were placed under the infrared lamp (Beurer) to recover from anesthesia.

Sham surgery followed the same protocol except from the MCA coagulation.

2.3. Pre- and post-surgical care

Mice received Buprenorphine (0.05 mg/kg; Reckitt Benckiser Healthcare, #PZN 00345928) injected subcutaneously 30 min before the surgical intervention. Bepanthen ointment (Bayer) was applied on eyes to protect drying. After the surgery, 100 μl of saline was injected subcutaneously in addition to one dose of Buprenorphine (0.05 mg/kg) which was injected subcutaneously every 12 hours for maximally two days.

2.4. Tamoxifen treatment

In order to induce Cre recombinase activation in Cnx43$^{Cre\text{-}Er(T)}$/RiboTag or VE-Cdh5$^{CreER(T)}$/RiboTag mouse line, tamoxifen (Sigma-Aldrich, #T5648) was intraperitoneally injected for five consecutive days at dose 100 mg/kg. Tamoxifen was dissolved in 100 μl of ethanol (100 %) and 900 μl sunflower oil (Sigma-Aldrich, #47123) to the final concentration 20 mg/ml. Three weeks after the last injection, mice underwent tMCAo surgery.

2.5. S1Pr3 antagonist injection

S1Pr3 antagonist CAY10444 (Cayman, #10005033) was dissolved in 0.375 % Tween 80 and injected at dose 1 mg/kg intraperitoneally in 100 μl of saline 4 or 8 hours after the pMCAo.

2.6. Neuroscore

Neurological function was evaluated using scoring system 1 and 3 days after tMCAo. The sum of general and focal deficits gave a total score which was in the range from 0 (no deficits) to 56 (poor performance in all observed categories); (see **Tab. 2**).

Tab. 2: Neurological scoring system

General deficits	Score	Focal deficits	Score
Hair	0 – 2	Body symmetry	0 – 4
Ears	0 – 2	Gait	0 – 4
Eyes	0 – 4	Climbing	0 – 4
Posture	0 – 4	Circling behavior	0 – 4
Spontaneous activity	0 – 4	Forelimb symmetry	0 – 4
Epileptic behavior	0 – 12	Compulsory circling	0 – 4
		Whisker response	0 – 4

2.7. Tissue homogenization

Twenty-four or 72 hours after the surgery, mice were perfused with phosphate buffer saline (PBS; 137 mM NaCl, 2.7 mM KCl, 10 mM Na_2HPO_4, 1.8 mM KH_2PO_4) and brains were collected. For all experiments described below, the olfactory bulbs and cerebellum were removed and the rest of the brain tissue was separated into ipsilateral (ischemic) and contralateral hemisphere. Brain tissue was homogenized in 1 ml of PBS with ceramic beads (VWR, # 432–0356) using the tissue homogenizer Precellys® 24 (Bertin–Instruments). The homogenized tissue was stored at -80 °C until use for different molecular techniques described below.

2.8. Gene expression

2.8.1. RNA extraction from the brain tissue

For the isolation of RNA, 200 µl of the brain homogenate was mixed with 1 ml TRIzol™ (ThermoFisher, # AM9738) and incubated for 5 min at room temperature (RT). After solubilization, 200 µl Chloroform (Sigma-Aldrich, # 472476) was added, gently mixed and incubated for 2–3 min at RT followed by centrifugation at 12 000 g for 15 min at 4 °C. The clear upper phase containing RNA was transferred to the new tube and precipitated by mixing with 1.5 x sample volume of 100 % ethanol. The RNA was isolated using RNeasy® Plus Mini Kit (Qiagen, # 74134) according to the manufacturer's instructions. In the last step, RNA was eluted with 60 µl of RNase-free water.

2.8.2. Cell-specific mRNA immunoprecipitation with RiboTag

Brain tissue was collected from Cnx43$^{Cre\text{-}ER(T)}$/RiboTag or VE-Cdh5$^{CreER(T)}$/RiboTag mice and each brain hemisphere was homogenized in 1 ml of polysome buffer (PSB; **Tab. 3**) using the tissue homogenizer Precellys® 24. The homogenate was transferred to a new tube and mixed with 1 ml of PSB followed by centrifugation at 10 000 g, for 10 min at 4 °C to prepare supernatant 1 (S1). For isolation of total mRNA used as a control sample, 100 µl of S1 was mixed with 700 µl QIAzol (Qiagen, #79306) and stored at -80 °C for later mRNA extraction (as described in 2.8.1.). The rest of the sample was pre-cleared by 30 min incubation with 75 µl Protein G Dynabeads on a rotor (PGDB; Life Technologies, #10004D) at 4 °C. PGBDs were washed twice with 500 µl PBS followed by single wash with 500 µl PSB for equilibration before using. The pre-cleared homogenate was placed on magnetic rack (DynaMag-2, Thermo Fischer Scientific) to let the PGDB adhere to the wall. Supernatant was transferred to a tube containing 12 µl of anti-HA antibody (12CA5; Sigma-Aldrich, #11583816001) and incubated on a rotor for 45 min at 4 °C. The lysate with the antibody was added to equilibrated PGDB and incubated on a rotor for 80 min at 4 °C. Finally, samples were placed on a magnetic rack to allow PGDBs adhere completely to the wall and the supernatant, the unbound fraction, was discarded. PDGBs were washed three times with 500 µl high salt buffer (HSB; **Tab. 3**) for 4 min at 4 °C followed by additional three washes with 500 µl extra high salt buffer (EHSB; **Tab. 3**) to reduce the

background. In the last washing step with the EHSB, samples were split to two 250 µl aliquots. Washing buffer was discarded from all samples and one aliquot of beads from each sample was stored in -80 °C as a technical replicate and the second aliquot was mixed with 700 µl QIAzole and placed on Eppendorf mixer for 15 min, 1400 rpm at RT in order to elute polysomes followed by mRNA extraction.

Tab. 3: Buffers used for astrocyte-specific mRNA immunoprecipitation

Buffer	Reagent	Final concentration
PSB	Tris, pH 7.5	50 mM
	KCl	100 mM
	$MgCl_2$	12 mM
	Nonidet P-40	1 %
	Dithiothreitol	1 mM
	RNase inhibitor	3.75 µl/ml
	Cyclohexamide	100 µg/ml
	Protease inhibitor	2x
	Phosphatase inhibitor	1x
HSB	Tris, pH 7.5	50 mM
	KCl	300 mM
	$MgCl_2$	12 mM
	Nonidet-P40	1 %
	Dithiothreitol	1 mM
	RNase Inhibitor	1.25 µl/ml
	Cyclohexamide	10 µg/ml
	Protease inhibitor	0.5x
	Phosphatase inhibitor	1x
EHBS	Tris, pH 7.5	50 mM
	KCl	300 mM
	NaCl	300 mM
	$MgCl_2$	12 mM
	Nonidet P-40	1 %
	Dithiothreitol	1 mM

	RNase Inhibitor	1.25 µl/ml
	Cyclohexamide	10 µg/ml
	Protease inhibitor	0.5x
	Phosphatase inhibitor	1x

2.8.2.1. RNA extraction

After polysomes were eluted from the samples, 140 µl chloroform was added and vortexed for 15 s followed by incubation for 2 min at RT and centrifugation at 13 000 g, for 15 min at 4 °C. The upper aqueous phase was transferred into a new tube and mRNA was isolated using RNeasy Micro Kit (Qiagen, #74004) according to the manufacturer's instructions. The mRNA was eluted with 28 µl of RNase-free water.

RNA quality was determined with the Agilent RNA 6000 pico Kit (Agilent Technologies, #5067–1513) according to the manufacturer's instructions and measured in the Agilent 2100 Bioanalyzer.

2.8.3. Reverse transcription of RNA

RNA concentration was determined with a Nanodrop 2000 (Thermo Fisher Scientific) using 1 µl RNase-free water as a blank and 1 µl of sample for the measurement. Volume corresponding to 500 ng (whole tissue)/50 ng (RiboTag) of RNA was calculated for each sample and reversely transcribed into cDNA using High-Capacity cDNA Reverse Transcription Kit (Thermo Fisher Scientific, #4368814). First, 10 µl 2x reverse transcription master mix was prepared according to the manufacturer's instructions (see **Tab. 4**) and mixed with calculated volume of RNA adjusted to 10 µl with RNase-free water. Reverse transcription was performed with C1000 Thermal Cycler (Bio-Rad); (see **Tab. 5**). cDNA was diluted 1:30 (whole tissue)/1:5 (RiboTag) in RNase-free water and stored -20 °C.

Tab. 4: RT-qPCR master mix

2x RT-qPCR master mix	Reagent	Volume
	10 x RT Buffer	2 µl
	25 x dNTP Mix	0.8 µl
	10 x RT Radom Primers	2 µl
	MultiScribe™ Reverse Transcriptase	1 µl
	RNase Inhibitor	1 µl
	RNase-free water	3.2 µl

Tab. 5: Program for cDNA synthesis

Step	Temperature (°C)	Time (min)
Primer annealing	25	10
DNA polymerization	37	120
Enzyme deactivation	85	5
Cooling	4	∞

2.8.4. Real-time quantitative polymerase chain reaction (RT-qPCR)

SYBR-green based RT-qPCR was used to determine relative gene expression. The RT-qPCR reaction mix contained 5 µl PrimaQUANT 2x CYBR Blue (Steinbrenner - Laborsysteme, #SL-9912B), 1.5 µl reverse/forward primer of the gene of interest (see **Tab. 6**) and 3.5 µl cDNA. Primer-specific standard curves were prepared for each plate separately by serial 5-fold 1:2 dilution of the mixture containing calculated volume from all samples used for the given experiments. Measurements were performed in 384-well plate using C1000 Touch Thermal Cycler (Bio-Rad); (see **Tab. 7**). The relative gene expression was calculated from the standard curve and normalized to the housekeeping gene.

Tab. 6: RT-qPCR primers

Name	Oligoname	Sequence (5' -> 3')
L14	L14 Forward	GGCTTTAGTGGATGGACCCT
	L14 Reverse	ATTGATATCCGCCTTCTCCC
Gfap	Gfap Forward	AAGGTCCGCTTCCTGGAA
	Gfap Reverse	GGCTCGAAGCTGGTTCAGTT

S1Pr3	S1Pr3 Forward	CAAGCCTAGCGGGAGAGAAA
	S1Pr3 Reverse	ACTGCGGGAAGAGTGTTGAA
VEGF	VEGF Forward	CCTGGGACCACTTGGCAT
	VEGF Reverse	CTTTCTGCTCTCTTGGGTGC

Tab. 7: RT-qPCR program

Step	Temperature (°C)	Time (s)	
Pre-denaturation	95	180	
Denaturation	95	10	39 x
Annealing	55	30	
Extension	95	10	
Melting curve	65 (+ 0.5)	5	

2.8.5. *In situ* hybridization based on multiplex fluorescent RNAscope

Multifluorescent RNAscope (Advanced Cell Diagnostics, #320850) was used to spatially localize mRNA transcripts with probes against S1Pr3 (ACD, Bio-Techne, #435951), Sox9 (ACD, Bio-Techne, #401051-C3), and Gfap (ACD, Bio-Techne, #313211-C2). Positive control (Bio-Techne, #32088) was used to assess RNA integrity of used sections. Negative control (Bio-Techne, #320871) was used to determine background fluorescence. Each probe was labeled with fluorophores, Atto 488 – C3, Atto 550 – C1, Atto 647 – C2. The procedure was performed as per manufacturer's instructions (see **Tab. 8**). For this purpose, mice were transcardially perfused with PBS and the brains were subsequently removed and embedded in OCT medium (Fisher Scientific, #12678646) and snap-frozen in pre-cooled 2 -Methylbutane on dry-ice. Brains were sectioned to 20 μm slices using a Cryostat (CryoStar NX70; Thermo Fisher Scientific) and directly transferred on the coated glass slides (Thermo Fisher Scientific, #10149870) and stored in -80 °C.

Tab. 8: RNAscope protocol

Step	Reagent	Time (min)	Temperature (°C)
Wash	PBS	3	Ice-cold
Fixation	4 % PFA	30	Ice-cold
Wash	PBS	3	RT
Dehydration	50 % Ethanol	5	RT
	70 % Ethanol	5	RT
	2 x 100 % Ethanol	5 (each)	RT
Air dry	Hydrophobic barrier outline (Biozol Diagnostica, #VEC-H4000)		RT
Digestion	Protease IV	12	RT
Wash	2 x PBS	3 (each)	RT
Probe hybridization (Dilution 50: 1: 1)	Ms-S1Pr3-C1 Ms-Gfap-C2 Ms-Sox9-C3	120	40 °C
Wash	2 x PBS	5 (each)	RT
Amplification 1	Amp-1	30	40 °C
Wash	2 x PBS	2 (each)	RT
Amplification 2	Amp-2	15	40 °C
Wash	2 x PBS	2 (each)	RT
Amplification 3	Amp-3	30	40 °C
Wash	2 x PBS	2 (each)	RT
Amplification	Amp Alt-4C	15	40 °C
Wash	2 x PBS	2 (each)	RT
Nuclei staining	Dapi (ACD,Bio-Techne, #320858)	0.5	RT
Mounting	Prolong Gold Antifade with Dapi (Life Technologies, #P36931)		

2.8.5.1. Imaging and analysis of multiplex fluorescent RNAscope

Whole brain fluorescent images were obtained using a slide scanning microscope AxioScan.Z1 from Zeiss. Images were acquired with 20x objective and x,y-resolution of 0.22 μm/pixel.

Zeiss LSM900 microscope was used to acquire 40x oil images with z-stack. For detection of colocalization of S1Pr3/Sox9/Gfap, z-stacks of 4 μm with a z-slice interval of 0.19 μm were imaged with 40x objective and x,y-resolution of 0.156 μm/pixel. Thirty images per hemisphere were sampled from each slice. Using the Zen software, z-stacks were further processed by calculating the maximum intensity projections.

To detect cells positive for the used probes, a customized pipeline was designed in CellProfiler (version 3.1.9). Images with maximum intensity projection were first converted from czi to tif with separated channels in ImageJ (version 2.1.0; https://imagej.nih.gov/ij/download.html) which were then used for analysis in CellProfiler. Primary objects were identified based on Dapi (staining cell nuclei) with a diameter range 70–300 pixels units and lower and upper threshold set at 0.01–1. Each detected primary object was expanded by 80 pixels units to include the cell cytosol. In each channel, mRNA represented as a small dot was detected in a diameter 3–15 pixels units and related to the expanded nuclei. Finally, from the list of detected cells with related number of dots per channel were identified cells positive for S1Pr3 defined with ≥ 5 dots/cell, Sox9 and Gfap defined with ≥ 8 dots/cells.

2.9. Protein expression

2.9.1. Protein isolation

To isolate protein, 200 μl of brain homogenate (see Chapter 2.5) was mixed with 200 μl of 2x RIPA buffer containing 20 mM Tris (pH 8), 2 mM EDTA, 2 % Triton X-100, 0.2 % sodium deoxycholate, 0.2 % SDS, 280 mM NaCl supplemented with protease (Thermo Fisher Scientific, #87785) and phosphatase (Thermo Fisher Scientific, #78420) inhibitors, vortexed and incubated for 30 min on ice followed by centrifugation at 15 000 g for 30 min at 4 °C to remove the insoluble material. The supernatant was transferred into the new tube and protein concentration was measured using Pierce™ BCA Protein Assay Kit (Thermo Fisher Scientific, #23227) as per manufacturer's instructions. The absorbance was measured at 562 nm on a microplate reader FLUOstar Omega (BMG Labtech). Protein concentration was interpolated from the standard curve.

2.9.2. Vessel-parenchyma fractionation

Vessel-parenchyma fractionation was performed following an optimized protocol published by Matthes et al. (2021); (Matthes et al., 2021). Mice were transcardially perfused with PBS and brains were removed and hemispheres were separated. Each hemisphere was homogenized in 1 ml B1 buffer (HBSS; Carl Roth, #9117.1 with 10 mM HEPES) with 21 G cannula mounted on 2 ml syringe followed by centrifugation at 2000 g for 10 min at 4 °C. Parenchyma fraction present in the supernatant was transferred to a new tube and mixed with an equal volume of 2x RIPA buffer supplemented with protease and phosphatase inhibitors and stored in -80 °C until protein isolation (see Chapter 2.9.1.). Pellets containing vessels were resuspended with 2 ml B2 buffer (B1 with 18 % dextran, ~70000; Sigma-Aldrich, #31390), mixed properly and centrifuged at 4400 g for 15 min at 4 °C. Myelin together with supernatant was discarded and the pellet was resuspended with 1 ml B3 buffer (B1 with 1 % bovine serum albumin (BSA); Carl Roth, #8076.2) and applied on 20 μm cell strainer (PluriSelect, #43-10020) with subsequent centrifugation at 200 g for 1 min at 4 °C to collect vessels. Collected vessels were washed twice by resuspending with 1 ml B3 buffer followed by centrifugation. Vessels were collected from the strainer with 1 ml B3 buffer, transferred to a new tube and centrifuged at 2000 g for 5 min at 4 °C. The supernatant was discarded and the pellet was resuspended with 1 ml B1 buffer and centrifuged at 2000 g for 5 min at 4 °C in order to remove BSA presented in B3 buffer. Finally, the supernatant was discarded and sedimented vessels were stored at -80 °C.

2.9.2.1. Protein isolation from the vessel fraction

Purified vessels were thawed on ice followed by snap freezing in liquid nitrogen, which was repeated three times. After the last freezing step, vessels were mixed with 100 μl 1x RIPA buffer (see Chapter 2.9.1.) supplemented with protease and phosphatase inhibitors and homogenized in a glass micro homogenizer (Radnoti) followed by vigorous vortexing and incubation for 30 min on ice. The insoluble material was pelleted by centrifugation at 20 000 g for 10 min at 4 °C and protein concentration was measured (see Chapter 2.9.1.).

2.9.3. SDS- Polyacrylamide gel electrophoresis (PAGE) and Western blot

First, 15 μg (whole tissue/parenchyma)/ 5 μg (vessel fraction) of protein was mixed with 4x sample buffer (Thermo Fisher Scientific, #NP0007) and 2.5 % β-mercaptoethanol (Sigma-Aldrich, #63689) and heated for 8 min at 95 °C. Precast NuPAGE™ 4–12 % gel (Thermo Fisher Scientifc, #WG1402BOX) with 1x NuPAGE™ SDS Running Buffer (ThermoFisher Scientific, #NP0002) were used to separate proteins and 8 μl Precision Plus Protein™ Kaleidoscope™ ladder (Bio-Rad, #161-0375) was used to determine the size of protein of interest. Proteins were separated at 100 V for 2,5 hours. After protein separation, proteins were transferred onto PVDF membranes using a semi-dry blotter (Cytiva) set to 240 mV for 45 min subsequent to an activation of the membrane by a short incubation in 100 % methanol followed by brief washing in transfer buffer containing 25 mM Tris, 192 mM glycine, 20 % methanol. Following transfer, the PVDF membranes were blocked in 5 % non-fat dry milk in PBS with 0.05 % Tween 20 (PBST; Thermo Fisher Scientific, #233362500) for 1 hour followed by primary antibody incubation overnight (see **Tab. 9**). The next day, membranes were washed three times for 10 min with PBST and incubated with the secondary antibody for 2 hours at RT (see **Tab. 10**). Membranes were washed with PBST and incubated for 1 min in the enhanced chemiluminescence solution (see **Tab. 11**) or SuperSignal™ West Femto Maximum Sensitivity Substrate (ThermoFisher Scientific, #34095) as per manufacturer's instruction. Membranes were imaged with the Stella imaging system (Bio-Imaging) and subsequently re-probed with the housekeeping protein (β-actin; see **Tab. 9**) which was used as a reference. Primary and secondary antibodies were diluted in 5 % non-fat dry milk in PBST. Relative protein expression to the housekeeping protein was analyzed using ImageJ.

Tab. 9: Primary antibodies

Antigen	Species	Dilution	Company	Order number
S1Pr3	Rabbit	1:2000	OriGene	#TA329055
eNOS	Mouse	1:1000	Abcam	#ab76198
αSMA	Mouse	1:5000	Sigma Aldrich	#A5228
Claudin-5	Rabbit	1:1000	Abcam	#ab131259
β-actin	Mouse	1:5000	Merck	#MAB1501

Tab. 10: Secondary antibodies

Antigen	Species	Conjugate	Dilution	Company	Order number
Rabbit IgG	goat	HRP	1:10 000	Cell Signaling Technology	#7074S
Mouse IgG	goat	HRP	1:10 000	Dianova	#115-035-062

Tab. 11: ECL solution recipe

Solution	Reagent	Final concentration/volume
A (10 ml)	Luminol + Tris, pH 8	100 mg/ml 0.1 M
B	p-Coumaric acid	1 ml
	Hydrogen Peroxide	6 µl

2.9.4. Magnetic resonance imaging (MRI)

MRI was performed at Lund University Bioimaging Centre (LBIC) using a preclinical 9.4 T MRI scanner with Bruker BioSpec AVIII electronics (Bruker) operating with ParaVision 6.0.1 and a gradient strength of 670 mT/m. The coils used were a quadrature volume resonator (112/087) for transmission and a mouse brain 2x2 phased array coil for reception. Both coils were from Bruker. Mice were anesthetized with 3.5 % isoflurane (Vetflurane) with a mixture of NO_2/O_2 (1:1). Anesthetized mice were transferred onto a MR bed heated with warm water with a nose mask delivering 1.5–2.5 % isoflurane to keep respiration between 65–90 breaths. The head was fixed with a teeth bar. Additionally, mice were covered with a heating blanket to ensure constant temperature between 36–37 °C. The body temperature and respiration rate were controlled with the SA Instrument (Stony Brook) monitoring system throughout the whole imaging.

T2-weighted images of the whole brain were acquired using Rapid Imaging with Refocused Echoes (RARE) sequence with repetition time = 3.4 s, echo time = 33 ms, 30 slices with 0.5 mm thickness, resolution of 100x100 μm^2, field of view 20x12 mm^2 and 13 averages.

To assess CBF, the arterial spin labeling (ASL) method was utilized using a Look-Locker FAIR TrueFISP with repetition time = 20 s, echo time = 1.2 ms and acquisition time =

127.2 ms (Gottschalk, 2020). Three to four coronal slices were imaged per mouse and thirty inversion-recovery points were sampled over 7.63 s. The resolution was 233x234 μm^2, with field of view 17x15 μm^2, slice thickness 2 mm and 32 repetitions.

2.9.4.1. Data processing and analysis

Images from LL TrueFISP were pre-processed by Michael Gottschalk from LBIC in MATLAB (Gottschalk, 2020). Infarct lesion (presented as mm^3) and CBF (presented as ml/100 g/min) were analyzed in OsiriX Lite (version 12.0.4).

2.9.5. 2, 3, 5-Triphenyltetrazolium chloride (TTC) staining

TTC staining was used to determine infarct lesion size. Mice were perfused with PBS and brains were removed and cut on the brain matrix to 1 mm coronal slices which were directly transferred to 2 % TTC (Sigma-Aldrich, #93140) in saline. After 20 min incubation at 37 °C, sections were scanned with the scanner (Epson). The infarct lesion was analyzed with ImageJ and calculated as a percentage of the contralateral hemisphere.

2.9.6. ELISA

2.9.6.1. Plasma isolation and S1Pr3 plasma concentration measurement

Blood was collected from vena cava before transcardial perfusion using a syringe coated with Heparin-Natrium (25000I.E/5 ml, Ratiopharm) and kept in ethylenediaminetetraacetic acid (EDTA) coated tubes (Sarstedt, #41.1395.105) and kept at RT. Plasma was separated by centrifugation at 1000 g for 10 min at RT.

Concentration of S1Pr3 in plasma was measured using a Mouse S1Pr3 ELISA kit (Nordic BioSite, #EKX-UXD4XY-96) as per manufacturer's instruction. Plasma was diluted 1:2 with Sample Dilution Buffer. Absorbance was measured at 450 nm in a Microplate reader FLUOstar Omega (BMG Labtech) and concentration was interpolated from the standard curve.

2.9.7. Statistics

Statistical analysis was performed in GraphPad Prism (version 9.2.0). Data were first tested for normal (Gaussian) distribution using Shapiro-Wilk normality test. Student's t-test (parametric)/Mann-Whitney test (nonparametric)/Wilcoxon matched-pairs test (nonparametric) were used to compare two groups. Repeated measures two-way ANOVA (parametric) followed by Šidák's multiple comparison test were used to compare multiple groups defined by two factors. Data are expressed as ± standard error of the mean (SEM). Statistical difference $P < 0.05$ was considered as significant and denoted by asterisks (* $P < 0.05$; ** $P < 0.01$, *** $P < 0.001$). N represents number of mice in the group specified in the legend for each group.

3. Results

3.1. Ischemic stroke induces increased S1Pr3 expression

To investigate temporal alterations of S1Pr3 after stroke, two different timepoints post-tMCAo in WT mice were used (**Fig. 6A**). The tMCAo model mimics the clinical scenario, in which CBF is restored by either administration of tPA or via surgical removal of the clot (Llovera et al., 2021). Because only 15% of patients suffering from a large vessel occlusion receive this type of treatment (McBride & Zhang, 2017), we also used a second stroke model without reperfusion (pMCAo); (data presented as part of 3.3).

Relative gene expression was investigated in the ipsilateral (ischemic) and contralateral hemisphere after tMCAo. Sham surgeries were used to control for surgery side effects (**Supplementary Fig. 1A, B**). S1Pr3 mRNA expression was significantly elevated in the ipsilateral hemisphere 1 day post-tMCAo ($p = 0.0006$); (**Fig. 6B**). This up-regulation was also observed at 3 days post-tMCAo ($p = 0.0078$); (**Fig. 6B**). A similar S1Pr3 increase in the ipsilateral hemisphere was detected on protein level 1 day ($p = 0.0296$); (**Fig. 6C**) but not at 3 days after tMCAo ($p = 0.1487$); (**Fig. 6C**). These results suggest an involvement of S1Pr3 signaling in the acute phase after stroke. Previously published *in vitro* studies reported early on activation of the S1Pr3 signaling pathway, which was associated with pro-inflammatory responses and promotion of vasoconstriction (Dusaban et al., 2017; Murakami et al., 2010). To confirm our hypothesis that S1Pr3 inversely correlates with stroke outcome, S1Pr3-depleted mice were subjected to tMCAo and neurological function as well as infarct size were determined. Neurological function after tMCAo was assessed using a 56-point neuroscore test. The extended neuroscore test enables the detection of general and focal deficits without putting animals under additional stress as it is based mainly on visual observations. The higher the score the higher is the impairment of neurological function after experimental stroke. Neurological function tested 1 day post-tMCAo revealed significantly improved neurological function of mice lacking S1Pr3 compared to WT mice ($p = 0.0028$); (**Fig. 6D**). Additionally, TTC staining was performed to assess infarct lesions. Ischemic lesions were significantly reduced in $S1Pr3^{-/-}$ mice compared to WT mice ($p = 0.0140$); (**Fig. 6E**).

Taken together, stroke elevates S1Pr3 expression which is associated with worse neurological outcome and extended infarct lesion in WT mice.

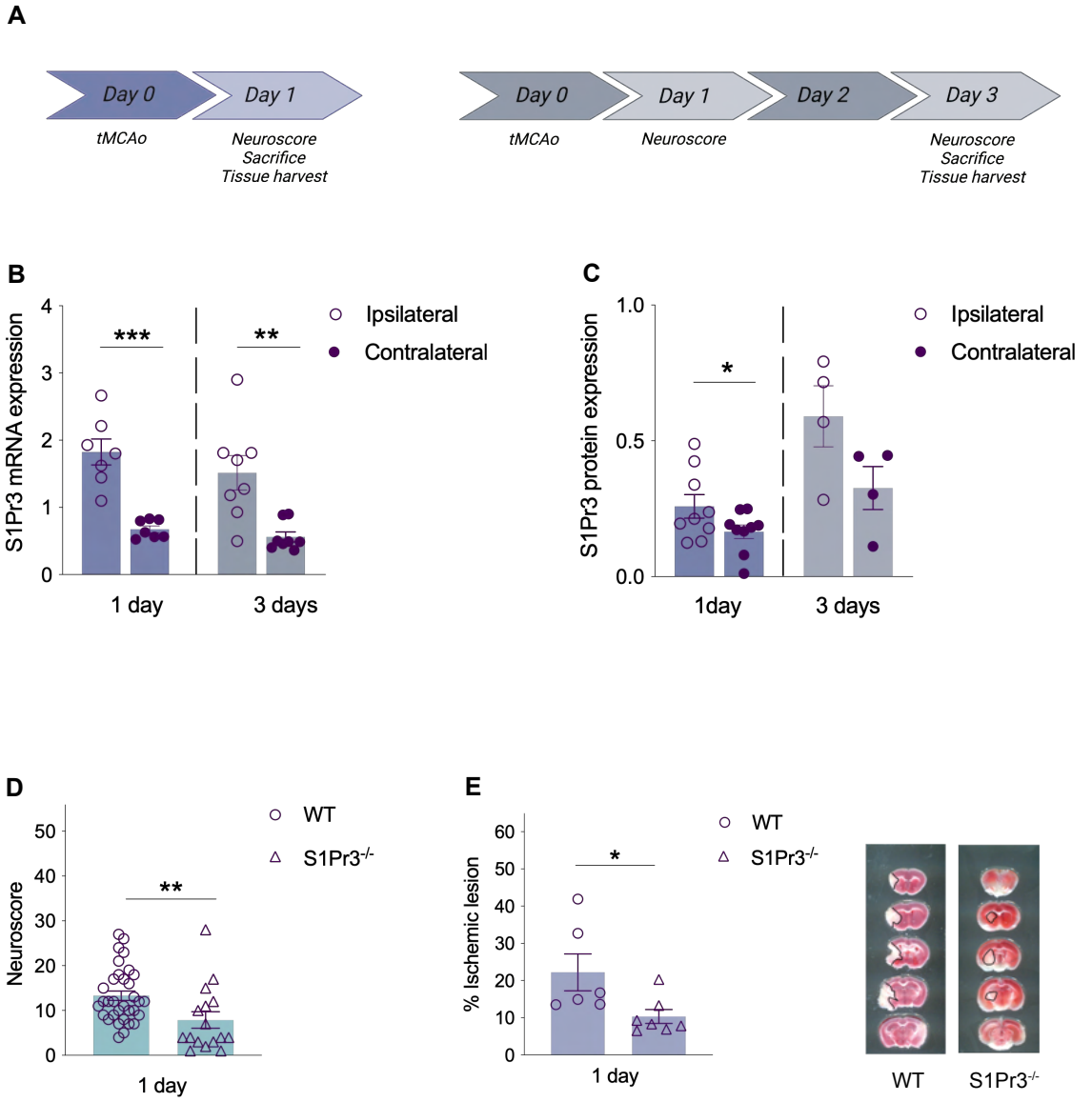

Fig. 6: S1Pr3 is up-regulated in a mouse model of stroke following tMCAo. **A)** Overview of experimental timeline. **B)** S1Pr3 gene expression (normalized to L14) in the ipsilateral and contralateral hemisphere 1 day (n = 7) and 3 days (n = 8) after tMCAo. **C)** S1Pr3 protein expression (normalized to β-actin) in the ipsilateral and contralateral hemisphere 1 day (n = 9) and 3 days (n = 4) after tMCAo. **D)** Neuroscore evaluation of WT mice (n = 33) compared to S1Pr3$^{-/-}$ mice (n = 16) 1 day after tMCAo. **E)** Quantification and representative images of infarct lesion after TTC staining of WT (n = 6) and S1Pr3$^{-/-}$ mice (n = 7) 1 day after tMCAo expressed as a percentage of the contralateral hemisphere. Data expressed as mean ± SEM.

* denotes P ≤ 0.05, ** denotes P ≤ 0.01, *** denotes P ≤ 0.001 for paired t-test when comparing the ipsilateral and contralateral hemisphere or unpaired t-test when comparing two independent groups. Dotted line represents two independent statistical tests.

S1Pr3 – sphingosine-1-phosphate; S1Pr3$^{-/-}$ – S1Pr3 knockout; SEM – standard error of the mean; tMCAo – transient middle cerebral artery occlusion; TTC – 2,3,5-Triphenyltetrazolium chloride; WT – wild type.

3.2. Astrocytes are critical contributors to S1Pr3 up-regulation after stroke

To further detect cell type-specific contribution to S1Pr3 up-regulation, vessel-parenchyma fractionation was performed (**Fig. 7A**). We optimized this technique for protein isolation of vessels and parenchyma fractions from small amounts of tissue (i.e., from one brain hemisphere); (Matthes et al., 2021). As a proof of concept, we used vessel-specific markers (endothelial nitric oxide synthase – eNOS, alpha smooth muscle actin - αSMA, Claudin 5) to confirm successful fractionation (**Fig. 7B**). Evaluation of S1Pr3 protein expression in vessel and parenchyma fractions revealed exclusive association of S1Pr3 with vessels 1 day after tMCAo (**Fig. 7C**). These data suggest several cell types forming the BBB as potential contributors to S1Pr3 elevation. We started investigating astrocytes and ECs as these cell types were shown to highly express S1Pr3 in the healthy brain (Y. Zhang et al., 2014). For this purpose, endothelial-specific Cdh5$^{Cre\text{-}ER(T)}$/RiboTag and astrocyte-specific Cnx43$^{Cre\text{-}ER(T)}$/RiboTag mouse models were utilized. RiboTag models enable the immunoprecipitation of mRNA from cell type-specific polysomes, which is subsequently used for RT-qPCR (**Fig. 7D**). Every mRNA isolation followed control RT-qPCR using primers against astrocytic (aldehyde dehydrogenase 1 family member 1, solute carrier family 1 member 2, Gfap) or endothelial genes (P-selectin, E-selectin, intracellular adhesion molecule 1) to confirm successful enrichment (data not shown).

First, endothelial-specific S1Pr3 expression was investigated. Although S1Pr3 was enriched in the endothelial fraction compared to the total fraction 3 days post-tMCAo (**Supplementary Fig. 2A**), no significant differences between the ipsilateral and contralateral hemisphere 1 day (p = 0.2493) and 3 days (p = 0.9696) post-tMCAo were detected (**Fig. 7E**). Next, astrocytic S1Pr3 gene expression was quantified in the acute and later stages after tMCAo. Similar to endothelial cells, S1Pr3 was enriched in the

astrocytic fraction compared to the total fraction (**Supplementary Fig. 2B**), however, astrocyte-specific S1Pr3 was significantly increased in the ipsilateral hemisphere compared to the contralateral hemisphere 1 day ($p = 0.0095$) and 3 days ($p = 0.0175$) after tMCAo (**Fig. 7F**). These results point to the involvement of astrocytes as important contributors to S1Pr3 up-regulation after experimental stroke. To further confirm and spatially localize astrocyte-specific S1Pr3 expression, multiplex fluorescent RNAscope was performed. Astrocyte-specific probes, Sox9 and Gfap were used to identify all astrocytes and reactive astrocytes, respectively, in addition to co-labeling with S1Pr3. Since Gfap expression rapidly increases after stroke in the ipsilateral hemisphere in the area where the glial scar is formed, Sox9-specific S1Pr3 expression was quantified first to determine co-labeling with S1Pr3 in all astrocytes independent of their activation status (W. Sun et al., 2017). The majority of detected Sox9 positive cells expressed S1Pr3 whose expression was significantly higher in the ipsilateral hemisphere compared to the contralateral hemisphere 1 day ($p = 0.0240$) but not 3 days (0.0611) post-tMCAo (**Fig. 7G**). Representative images from the ipsilateral and contralateral hemisphere demonstrate examples of dot-like stained mRNA using S1Pr3, Gfap and Sox9 probes (**Fig. 7I**). Astrocyte-independent expression of S1Pr3 was determined by assessing the proportion of Sox9-negative S1Pr3-positive cells. Quantification of the ipsilateral hemisphere revealed that expression of S1Pr3 by cell-types other than astrocytes was significantly lower 1 day ($p = 0.0202$) and 3 days ($p = 0.0113$) post-tMCAo (**Fig. 7H**). Next, we addressed the expression of S1Pr3 in Gfap positive cells that represent a group of reactive astrocytes. The whole brain images revealed strong colocalization of S1Pr3 with Gfap 1 day and 3 days after tMCAo. Figure 7J depicts the overlaying area where the expression of Gfap and S1Pr3 were detected. Moreover, the S1Pr3 expression seems to mark the shape of the glial scar. Since Gfap expression rapidly increases after stroke solely in the hemisphere with the infarct lesion, comparison between hemispheres would be misleading and for that reason the quantification is not presented.

In summary, astrocytes were identified as a major contributor to S1Pr3 increase post-tMCAo. Moreover, S1Pr3 up-regulation was mainly localized along the glial scar and colocalized with reactive astrocytes detected based on the Gfap marker. Together, these

data point towards an involvement of astrocytic S1Pr3 signaling in the acute stages after stroke.

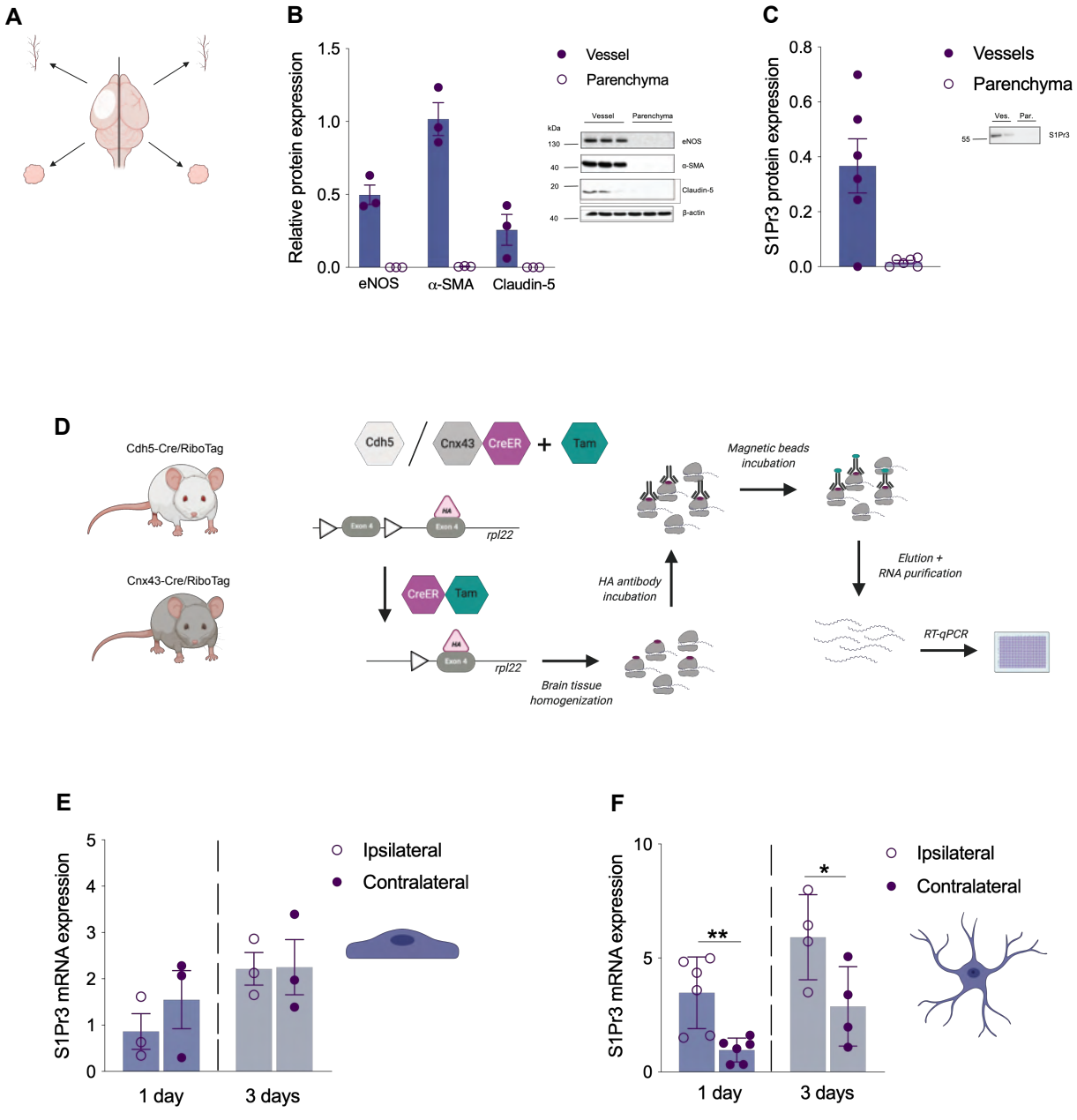

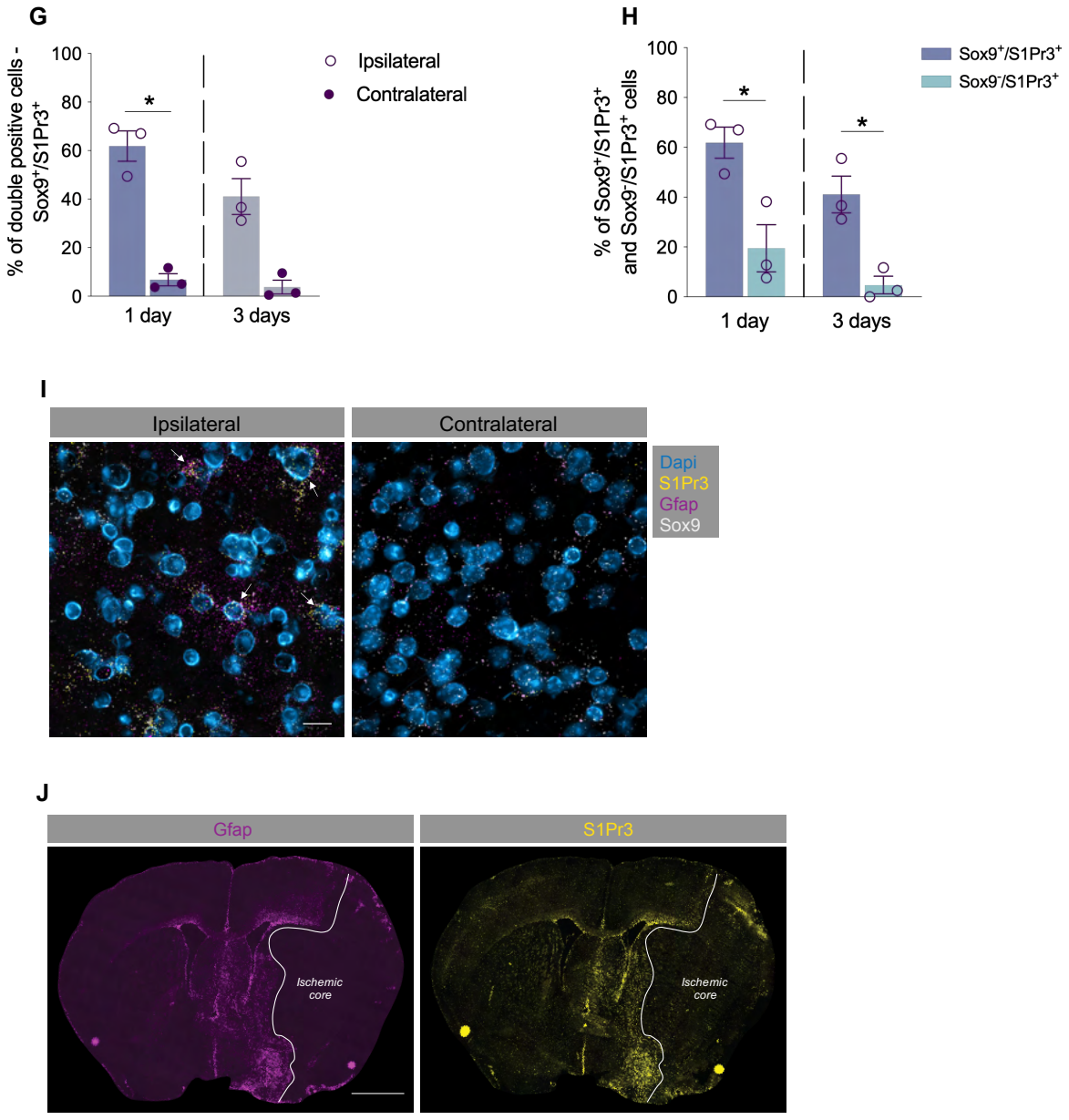

Fig. 7: Astrocytes significantly contribute to the S1Pr3 up-regulation following tMCAo. **A)** Schematic illustration of the vessel-parenchyma fractionation technique. **B)** Proof of concept of the vessel-parenchyma fractionation technique. Graph depicts relative protein expression (normalized to β-actin) of eNOS, αSMA and Claudin-5 in the vessel-parenchyma fraction (n = 3). **C)** S1Pr3 protein expression in the vessel and parenchyma fraction (normalized to β-actin) 1 day after tMCAo (n = 6). **D)** Schematic illustration of the astrocyte-specific mRNA purification from Cnx43^{CreERT}/RiboTag and Cdh5^{CreERT}/RiboTag mice. **E)** Endothelial cells-specific S1Pr3 gene expression (normalized to L14) in the ipsilateral and contralateral hemisphere 1 day (n = 3) and 3 days (n = 3) after tMCAo. **F)**

Astrocyte-specific S1Pr3 gene expression (normalized to L14) in the ipsilateral and contralateral hemisphere 1 day (n = 6) and 3 days (n = 4) after tMCAo. **G)** RNAscope quantification of $Sox9^+/S1Pr3^+$ double positive astrocytes out of all $Sox9^+$ astrocytes in the ipsilateral compared to the contralateral hemisphere 1 day and 3 days post-tMCAo (n = 3). **H)** RNAscope quantification of $Sox9^+/S1Pr3^+$ and $Sox9^-/S1Pr3^+$ in the ipsilateral hemisphere 1 day and 3 days after tMCAo (n = 3). **I)** Representative images acquired from the ipsilateral and contralateral hemisphere with visualized Dapi (blue), S1Pr3 (yellow), Gfap (violet) and Sox9 (white). Arrows point to astrocytes expressing S1Pr3. The scale bar in the image represents 50 μm. **J)** Whole brain slice image with visualized Gfap (violet) and S1Pr3 (yellow) mRNA 1 day after tMCAo. The white line indicates the glial scar. The scale bar in the image represents 1 mm.

* denotes $P \leq 0.05$, ** denotes $P \leq 0.01$, *** denotes $P \leq 0.001$ for paired t-test when comparing the vessel/parenchyma fraction or ipsilateral/contralateral hemisphere; unpaired t-test when comparing two independent groups. Dotted line represents two independent statistical tests.

αSMA – alpha smooth muscle actin; Cdh5 – cadherin 5; Cnx43 – connexin 43; eNOS – endothelial nitric oxide synthase; Gfap – glial fibrillary acidic protein; RT-qPCR –real-time quantitative polymerase chain reaction; S1Pr3 – sphingosine-1-phosphate receptor 3; SEM – standard error of the mean; Sox9 – SRY-box transcription factor 9; tMCAo – transient middle cerebral artery occlusion.

3.3. Activation of S1Pr3 signaling following pMCAo

A large proportion of ischemic stroke patients are not eligible for recanalization treatment and as a result, they remain without reperfusion (McBride & Zhang, 2017). Therefore, we tested S1Pr3 alterations in a model of pMCAo in which the distal part of the MCA is permanently occluded by electrocoagulation (**Fig. 8A**). This experimental stroke model results in a defined infarct lesion in the cortical area.

RT-qPCR revealed significant S1Pr3 up-regulation of gene expression in the ipsilateral hemisphere compared to the contralateral hemisphere at both timepoints, 1 day ($p = 0.0005$); (**Fig. 8B**) and 3 days post-pMCAo ($p = 0.0124$); (**Fig. 8C**). Furthermore, Gfap revealed similar expression patterns 1 day ($p = 0.0036$); (**Fig. 8B**) and 3 days post-pMCAo ($p = 0.0042$); (**Fig. 8C**), supporting our previous results showing an apparent association with reactive astrocytes. Next, vessel-parenchyma fractionation technique was performed on the brain tissue harvested 3 days after pMCAo. Similar to the tMCAo stroke model, S1Pr3 was exclusively associated with vessels (**Fig. 8D**) Furthermore, western blot performed only with vessel fractions of the ipsilateral and contralateral hemisphere revealed significant increases of vessel-associated S1Pr3 in the ipsilateral hemisphere 3 days post-pMCAo ($p = 0.0074$); (**Fig. 8E**). These results indicate an apparent involvement of S1Pr3 signaling in ischemic brain damage independently of reperfusion.

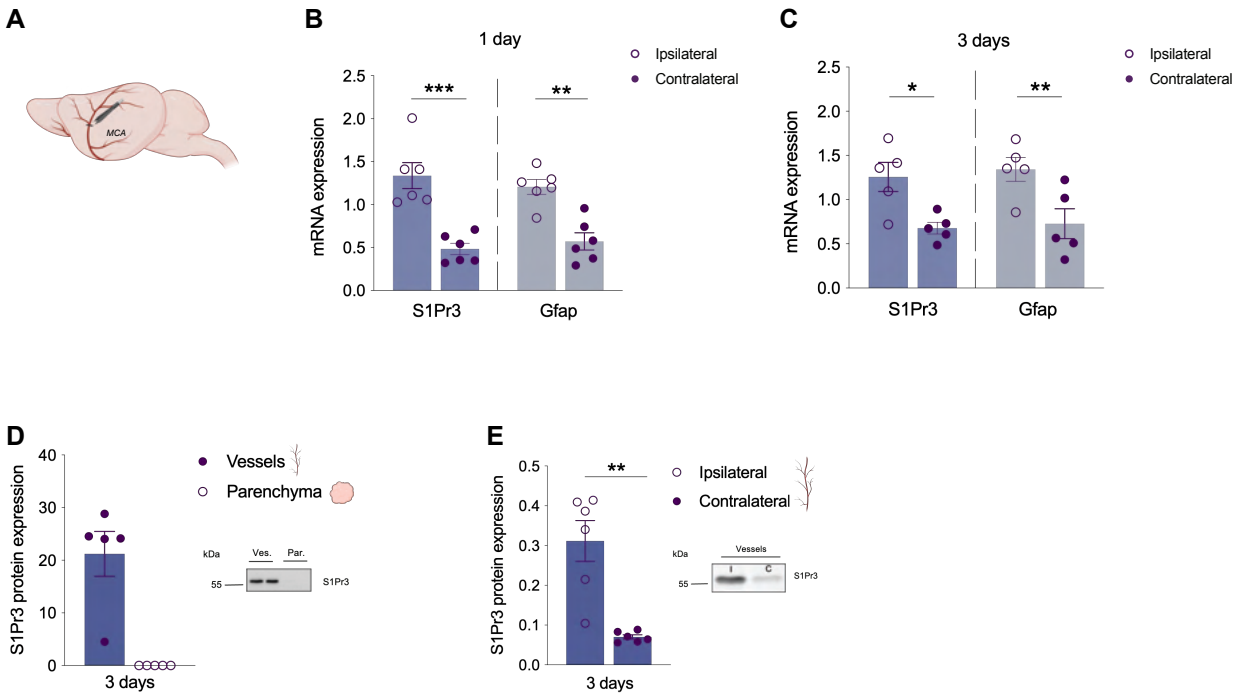

Fig. 8: S1Pr3 is up-regulated in a mouse model of stroke with permanent occlusion of the MCA. **A)** Schematic illustration of pMCAo procedure. **B)** S1Pr3 and Gfap gene expression (normalized to L14) in the ipsilateral and contralateral hemisphere (n = 6) 1 day after pMCAo. **C)** S1Pr3 and Gfap gene expression (normalized to L14) in the ipsilateral and contralateral hemisphere (n = 5) 3 days after pMCAo. **D)** S1Pr3 protein expression in the vessel and parenchyma fraction (normalized to β-actin) 3 days after pMCAo (n = 5). **E)** S1Pr3 protein expression of the vessel fractions in the ipsilateral and contralateral hemisphere (normalized to β-actin) 3 days after pMCAo (n = 6). Data expressed as mean ± SEM.

* denotes $P \leq 0.05$, ** denotes $P \leq 0.01$, *** denotes $P \leq 0.001$ for paired t-test when comparing the ipsilateral and contralateral hemisphere. Dotted line represents two independent statistical tests.

Gfap – glial fibrillary acidic protein; MCA – middle cerebral artery; pMCAo – permanent middle cerebral artery occlusion; S1Pr3 – sphingosine-1-phosphate receptor 3; SEM – standard error of the mean.

3.4. Pharmacological antagonism of S1Pr3 mitigates consequences of ischemic stroke

As previous results pointed towards deleterious effects of augmented S1Pr3 signaling on stroke outcome, we pharmacologically modulated S1Pr3 via systemic intraperitoneal injections of the S1Pr3 antagonist CAY10444. Because a previous study has reported S1Pr3 increase as early as 3–6 hours after tMCAo (Salas-Perdomo et al., 2019), we injected the S1Pr3 antagonist 4 hours after pMCAo. Following CAY10444 injection, mice underwent longitudinal T2-weighted MRI to assess infarct lesion and ASL imaging to investigate CBF 1 day and 3 days after stroke induction (**Fig. 9A**). Quantification of ASL imaging revealed significantly improved overall perfusion of mice treated with the S1Pr3 antagonist compared to the vehicle-treated mice 1 day post-tMCAo ($p = 0.0065$); (**Fig. 9B**). This improvement persisted also for 3 days after stroke ($p = 0.0033$); (**Fig. 9B**). Improved cerebral perfusion was further associated with significantly reduced infarct lesion 1 day ($p = 0.0491$) that did not reach significance at the 3 days timepoint ($p = 0.1313$); (**Fig. 9C**).

Currently, the only approved pharmaceutical reperfusion treatment is tPA, which has a limited administration time window (i.e., up to 4.5 hours) after stroke onset. Later administration of tPA is associated with an increased risk of secondary injury (Peña et al., 2017) therefore, the development of novel therapeutics is urgently needed. In order to investigate if the same CBF improvement and infarct volume reduction can be achieved when extending the therapeutic window of the S1Pr3 antagonist, a separate cohort of mice was subjected to CAY10444 injections 8 hours after the stroke surgery (**Fig. 9D**). As illustrated in Figure 9E and F, later treatment did not improve CBF (1 day – $p = 0.2271$; 3 days – $p = 0.3951$); (**Fig. 9E**) or reduce infarct volume (1 day – $p = 0.3248$; 3 days – $p = 0.1692$); (**Fig. 9F**). Unlike tPA, however, no side effects where observed when administering CAY104444 beyond 4 hours where it showed therapeutic effects .

Taken together, administration of the S1Pr3 antagonist as early as 4 hours after pMCAo improves CBF and reduces the infarct lesion, however, this beneficial effect is absent at later administration timepoints (i.e., 8 hours post-pMCAo).

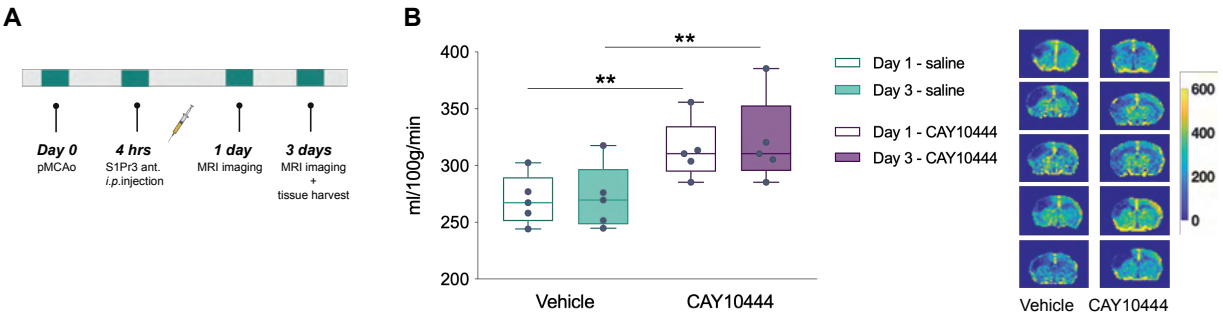
A
Day 0
pMCAo
4 hrs
S1Pr3 ant.
i.p.injection
1 day
MRI imaging
3 days
MRI imaging
+
tissue harvest
B
ml/100g/min
400
350
300
250
200
**
**
Vehicle
CAY10444
Day 1 - saline
Day 3 - saline
Day 1 - CAY10444
Day 3 - CAY10444
600
400
200
0
Vehicle
CAY10444

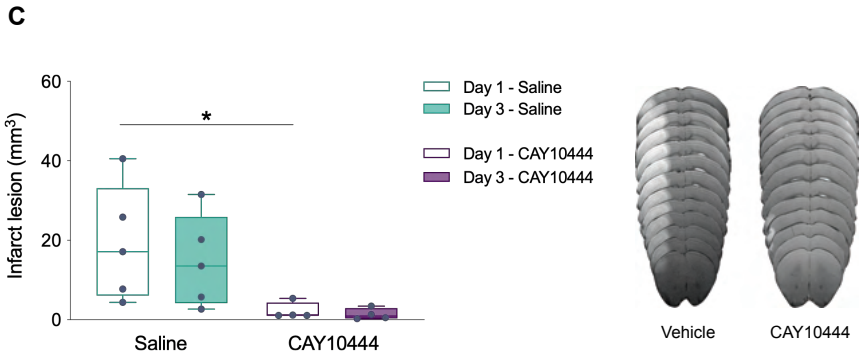
C
Infarct lesion (mm3)
60
40
20
0
*
Saline
CAY10444
Day 1 - Saline
Day 3 - Saline
Day 1 - CAY10444
Day 3 - CAY10444
Vehicle
CAY10444

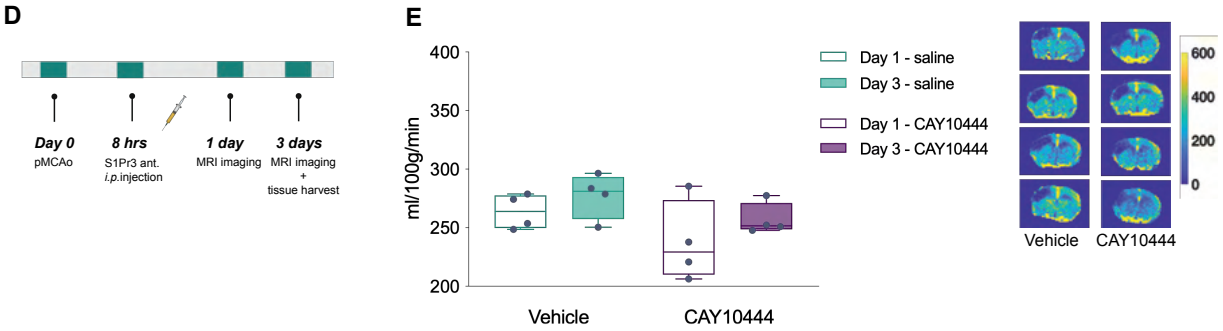
D
Day 0
pMCAo
8 hrs
S1Pr3 ant.
i.p.injection
1 day
MRI imaging
3 days
MRI imaging
+
tissue harvest
E
ml/100g/min
400
350
300
250
200
Vehicle
CAY10444
Day 1 - saline
Day 3 - saline
Day 1 - CAY10444
Day 3 - CAY10444
600
400
200
0
Vehicle
CAY10444

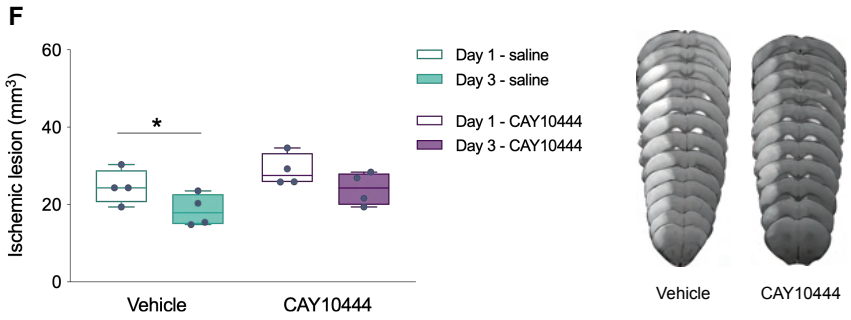
F
Ischemic lesion (mm3)
60
40
20
0
*
Vehicle
CAY10444
Day 1 - saline
Day 3 - saline
Day 1 - CAY10444
Day 3 - CAY10444
Vehicle
CAY10444

Fig. 9: S1Pr3 antagonist treatment early after stroke onset improves functional outcome. **A)** Overview of the experimental timeline. **B)** Analysis of longitudinally assessed CBF in WT mice after pMCAo treated with the S1Pr3 antagonist CAY10444 or vehicle (n = 5 per group). **C)** Quantification of longitudinally assessed ischemic lesion in WT mice after pMCAo treated with the S1Pr3 antagonist CAY10444 (n = 4) or vehicle (n = 5). Lesion size is presented as volume (mm^3). Analysis of the infarct lesion of CAY10444-treated group was performed only with four mice per group as the value from one mouse was excluded based on the Dixon's test for a single outlier. **D)** Overview of the experimental timeline. **E)** Analysis of longitudinally assessed CBF in WT mice after pMCAo treated with the S1Pr3 antagonist CAY10444 or vehicle (n = 4 per group). **F)** Quantification of longitudinally assessed ischemic lesion in WT mice after pMCAo treated with the S1Pr3 antagonist CAY10444 or vehicle (n = 4 per group). Lesion size is presented as volume (mm^3). Data expressed as mean ± SEM.

* denotes $P \leq 0.05$, ** denotes $P \leq 0.01$ after RM two-way ANOVA with Šidák post-hoc testing.

CBF – cerebral blood flow; MRI – magnetic resonance imaging; pMCAo – permanent middle cerebral artery occlusion; S1Pr3 – sphingosine-1-phosphate receptor 3; SEM – standard error of the mean; WT – wild type.

3.5. Stroke-induced alterations of S1Pr3 are detectable in plasma

Our results show an elevation of S1Pr3 in the brain after stroke, which associates with worse stroke outcome. To investigate S1Pr3's biomarker potential, we tested whether S1Pr3 levels are also altered in plasma after stroke using ELISA. Compared to sham-operated controls, S1Pr3 was significantly up-regulated 1 day after tMCAo ($p = 0.0321$); (**Fig. 10A**). We will next test circulating S1Pr3 plasma levels in stroke patients and age-matched controls to validate the suitability of S1Pr3 as a biomarker for stroke severity.

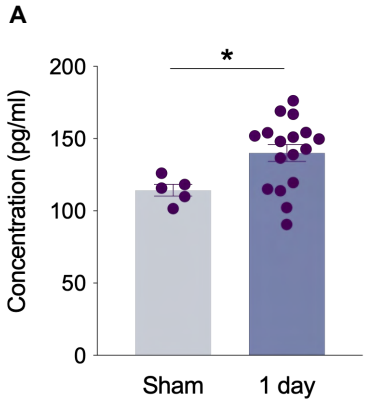

Fig. 10: S1Pr3 alterations post-stroke are detectable in plasma. **A)** S1Pr3 concentration in plasma 1 day after sham (n = 5) compared to tMCAo (n = 17) surgery. Data expressed as mean ± SEM.

* denotes P ≤ 0.05 for unpaired t-test.

S1Pr3 – sphingosine-1-phosphate receptor 3; SEM – standard error of the mean; tMCAo – transient middle cerebral artery occlusion.

3.6. Supplementary results

3.6.1. Ischemic stroke induces increase of S1Pr3 expression

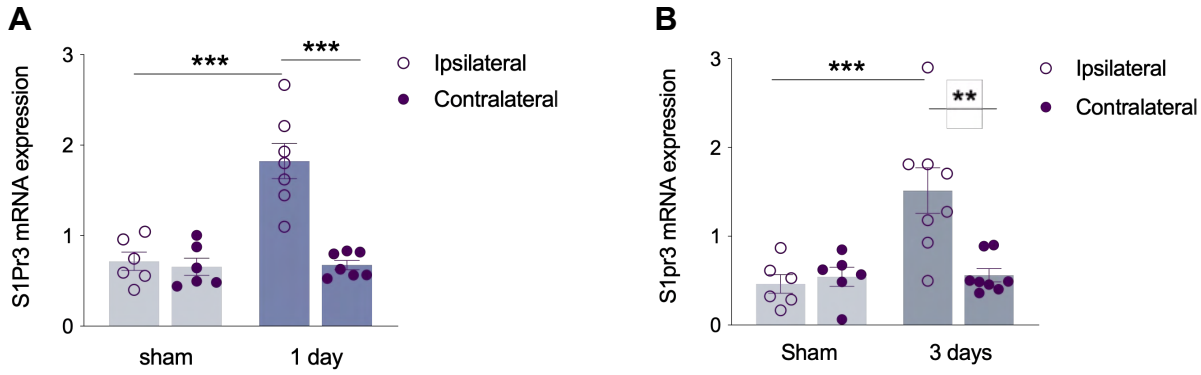

Supplementary Fig. 1: S1Pr3 is up-regulated in a mouse model of stroke following tMCAo. **A)** S1Pr3 gene expression (normalized to L14) 1 day after sham (n = 6) compared to tMCAo (n = 7) surgery in the ipsilateral and contralateral hemisphere. Ipsilateral: sham vs 1 day – p < 0.0001; contralateral: sham vs 1 day – p = 0.9934. **B)** S1Pr3 gene expression (normalized to L14) 3 days after sham (n = 6) compared to tMCAo surgery (n = 8) in the ipsilateral and contralateral hemisphere. Ipsilateral: sham vs 3 days – p = 0.0004; contralateral: sham vs 3 days – p = 0.9967. ** denotes P ≤ 0.01, *** denotes P ≤ 0.001 for RM two-way ANOVA with Šidák post-hoc testing when comparing multiple groups.

S1Pr3 – sphingosine-1-phosphate receptor 3; SEM – standard error of the mean; tMCAo – transient middle cerebral artery occlusion.

3.6.2. S1Pr3 is expressed by endothelial cells and astrocytes after stroke

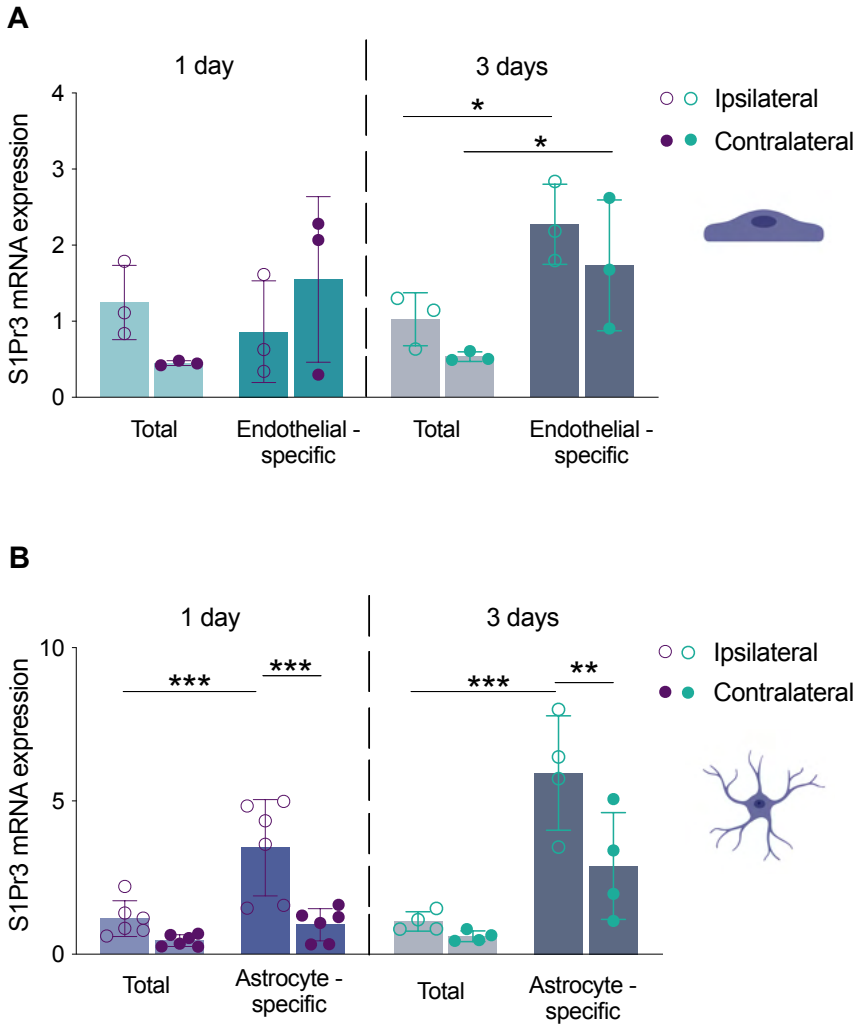

Supplementary Fig. 2: Establishment of techniques for astrocyte- and endothelial-specific S1Pr3 signaling alterations following tMCAo. **A)** Enrichment of S1Pr3 gene expression (normalized to L14) in the sample containing total RNA compared to the immunoprecipitated mRNA from endothelial cells in the ipsilateral and contralateral hemisphere 1 day (n = 3; ipsilateral: total vs endothelial-specific – p = 0.5824; contralateral: total vs endothelial-specific – p = 0.2149) and 3 days (n = 3; ipsilateral: total vs endothelial-specific – p = 0.0417; contralateral: total vs endothelial-specific – p = 0.0491) after tMCAo. **B)** Enrichment of S1Pr3 gene expression (normalized to L14) in the sample containing total RNA compared to the immunoprecipitated mRNA from astrocytes in the ipsilateral and contralateral hemisphere 1 day (n = 6; ipsilateral: total vs astrocyte-specific – p = 0.0004; contralateral: total vs astrocyte-specific – p = 0.5441) and 3 days (n = 4; ipsilateral: total vs astrocyte-specific – p = 0.0004; contralateral: total vs astrocyte-specific – p = 0.0536) after tMCAo. Data expressed as mean ± SEM.

* denotes P ≤ 0.05, ** denotes P ≤ 0.01, *** denotes P ≤ 0.001 for two-way ANOVA with Šidák post-hoc testing when comparing multiple groups. Dotted line represents two independent statistical tests. Dotted line represents two independent statistical tests.

S1Pr3 – sphingosine-1-phosphate receptor 3; SEM – standard error of the mean; tMCAo – transient middle cerebral artery occlusion.

3.6.3. VEGF expression is attenuated in S1Pr3$^{-/-}$ mice early after stroke onset

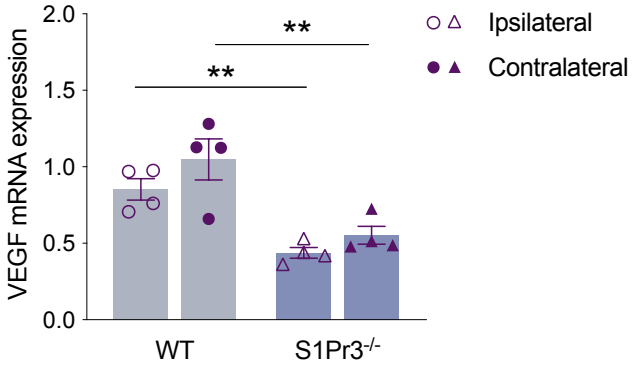

Supplementary Fig. 3: VEGF alterations in WT vs S1Pr3$^{-/-}$ mice 1 day post-tMCAo. VEGF relative gene expression (normalized to L14) 1 day after tMCAo in the ipsilateral and contralateral hemisphere of WT compared to S1Pr3$^{-/-}$ mice (n = 4; ipsilateral: WT vs S1Pr3$^{-/-}$ – p = 0.0084; contralateral: WT vs S1Pr3$^{-/-}$ – p = 0.0024). Data expressed as mean ± SEM.

** denotes P ≤ 0.01 for two-way ANOVA with Šidák post-hoc testing when comparing multiple groups.

S1Pr3$^{-/-}$ – sphingosine-1-phosphate receptor 3 knockout; SEM – standard error of the mean; tMCAo – transient middle cerebral artery occlusion; VEGF – vascular endothelial growth factor; WT – wild type.

3.6.4. Mean values ± SEM of presented data

Tab. 12: Mean values ± SEM

Fig. 6		1 day	3 days
6B	Ipsilateral	1.825 ± 0.1939	1.514 ± 0.2563
	Contralateral	0.6757 ± 0.05096	0.5613 ± 0.07483
6C	Ipsilateral	0.2587 ± 0.04322	0.5902 ± 0.1124
	Contralateral	0.1654 ± 0.02540	0.3261 ± 0.07896
6D	WT	13.30 ± 1.052	---
	$S1Pr3^{-/-}$	7.875 ± 1.835	---
6E	WT	22.22 ± 4.938	---
	$S1Pr3^{-/-}$	10.34 ± 1.866	---

Fig. 7		1 day	3 days
7E	Ipsilateral	0.8625 ± 0.3858	2.215 ± 0.3523
	Contralateral	1.549 ± 0.6279	2.252 ± 0.5953
7F	Ipsilateral	3.477 ± 0.6411	5.911 ± 1.867
	Contralateral	0.9600 ± 0.2149	2.878 ± 1.739
7G	Sox+/S1Pr3+_ipsilateral	61.87 ± 6.266	41.10 ± 7.367
	Sox+/S1Pr3+_contralateral	6.800 ± 2.479	3.800 ± 2.862
	Sox9-/S1Pr3+_ipsilateral	19.53 ± 9.453	4.747 ± 3.548

Fig. 8		1 day	3 days
8B, C	S1Pr3_ipsilateral	1.337 ± 0.1512	1.257 ± 0.1647
	S1Pr3_contralateral	0.4845 ± 0.06728	0.6780 ± 0.06745
	Gfap_ipsilateral	1.206 ± 0.08575	1.343 ± 0.1360
	Gfap_contralateral	0.5724 ± 0.1005	0.7276 ± 0.1688
8E	Ipsilateral	---	0.3116 ± 0.05121
	Contralateral	---	0.07022 ± 0.005431

Fig. 9		1 day	3 days
9B	Vehicle	269.7 ± 9.806	271.9 ± 12.77
	CAY10444	313.7 ± 11.60	321.3 ± 17.01
9C	Vehicle	19.11 ± 6.528	14.72 ± 5.194
	CAY10444	2.183 ± 1.064	1.393 ± 0.7184
9E	Vehicle	263.8 ± 7.479	277.3 ± 9.699
	CAY10444	237.6 ± 17.19	257.1 ± 6.849
9F	Vehicle	24.58 ± 2.231	18.50 ± 2.072
	CAY10444	28.88 ± 2.065	24.08 ± 2.134

Fig. 10		1 day	3 days
10A	Sham	114.3 ± 4.099	---
	1 day	140 ± 5.850	---

Suppl. Fig. 1		1 day	3 days
1A	Sham_ipsilateral	0.7165 ± 0.1012	0.4646 ± 0.1050
	Sham_contralateral	0.6573 ± 0.09484	0.5440 ± 0.1084
	tMCAo_ipsilateral	1.825 ± 0.1939	1.514 ± 0.2563
	tMCAo_contralateral	0.6757 ± 0.05096	0.5613 ± 0.07483

Suppl. Fig. 2		1 day	3 days
2A	Total_ipsilateral	1.247 ± 0.2823	1.027 ± 0.2008
	Total_contralateral	0.4504 ± 0.01766	0.5350 ± 0.03684
	Endothelial spec._ipsilateral	0.8625 ± 0.3858	2.275 ± 0.3035
	Endothelial spec._contralateral	1.549 ± 0.6279	1.735 ± 0.4958
2B	Total_ipsilateral	1.160 ± 0.2379	1.067 ± 0.1585
	Total_contralateral	0.4454 ± 0.07785	0.5866 ± 0.08826
	Astrocyte spec._ipsilateral	3.477 ± 0.6411	5.911 ± 0.9334
	Astrocyte spec._contralateral	0.9600 ± 0.2149	2.878 ± 0.8697

Suppl. Fig. 3		1 day	3 days
3	WT_ipsilateral	0.8526 ± 0.06999	---
	WT_contralateral	1.048 ± 0.1346	---
	$S1Pr3^{-/-}$_ipsilateral	0.4382 ± 0.03503	---
	$S1Pr3^{-/-}$_contralateral	0.5518 ± 0.05842	---

4. Discussion

Modulation of S1Prs has shown to be a promising target in various diseases including stroke. However, the current knowledge still lacks a cell-specific mechanisms of action for most of these receptors, which is crucial for development of optimal targeting and efficient therapeutic strategies. Here, we investigated how S1Pr3 expression is altered in stroke and how a general lack of S1Pr3 expression affects stroke outcome. Our experiments revealed a central role for S1Pr3 signaling during the acute phase after stroke that was verified by apparent functional improvement in the absence of S1Pr3. More specifically, we provide compelling evidence that astrocyte- but not endothelial-specific S1Pr3 signaling is a critical contributor to ischemic brain damage. Lastly, we determined the therapeutic window for systemic targeting of S1Pr3 after stroke. Together, our results suggest an apparent time-dependent augmentation of S1Pr3 signaling post-stroke that emerges as a potential target for the development of novel stroke therapies.

Our study reported an elevation of S1Pr3 during acute stages after stroke onset, which is in agreement with previously published analyses of S1Pr1-5 expression profiles at different timepoints after tMCAo. While all receptors presented with gradual increases towards their peak at day 4 post-stroke, S1Pr3 was the only S1Pr that rapidly increased at 1 day after reperfusion (Salas-Perdomo et al., 2019). Our results were further supported by another study investigating acute expression patterns of S1Prs 1 day post-tMCAo showing significant S1Pr3 up-regulation in the ischemic hemisphere (Lucaciu et al., 2020). These results provided initial evidence of S1Pr3 alterations after stroke, which required further investigation. In a context of ischemia/reperfusion (I/R)-related injuries of different organs other than the brain, S1Pr3 has been reported to have both beneficial and detrimental effects. During renal and hepatic I/R injury, S1Pr3 was linked to worse outcomes and its genetic or pharmacological inhibition provided protection (Jo et al., 2009; Park et al., 2010). Specifically, Jo et al. (2008) observed attenuated vascular permeability in $S1Pr3^{-/-}$ mice after renal I/R injury (Jo et al., 2009). In contrast to this, it has been reported that S1Pr3, either alone (Theilmeier et al., 2006; Yung et al., 2017) or together with S1Pr2 (Means et al., 2007), had a cardioprotective role in myocardial I/R injury.

Interestingly, each of these studies found different mechanisms for S1Pr3-associated protection in the heart (i.e., Akt-mediated pro-survival pathway, RhoA-induced protection against oxidative stress and NO-dependent protection). In a model of permanent hindlimb ischemia, S1Pr3 was necessary for blood flow recovery through activation of pro-angiogenesis receptors (e.g., vascular endothelial growth factor 2 or epidermal growth factor); (Walter et al., 2007). S1Pr3 activation has clearly diverse effects depending on the organ and pathology of interest. To identify the role of increased S1Pr3 in the brain during ischemia, we used $S1Pr3^{-/-}$ mouse. Our results revealed functional improvement presented as a reduced infarct lesion and improved neurological function in response to tMCAo compared to WT controls. These observations suggested S1Pr3-related damaging effects in acute stages after stroke. There is only one study using the $S1Pr3^{-/-}$ mouse line in the context of ischemic stroke (Nitzsche et al., 2021). However, they did not observe any differences in infarct size between $S1Pr3^{-/-}$ and littermate controls after pMCAo. Although, using littermate controls is a standard, without an additional WT control group it is uncertain if the littermate mice still carry S1Pr3 knockout in some cells, which could be responsible for some improvements that suppress the difference. While our results were obtained from tMCAo, Nitzsche et al. (2021) used a model of pMCAo. It has been reported that stroke-induced immune responses as well as effects of therapeutics might vary between different experimental models of stroke (Chu et al., 2014; Poittevin et al., 2013; Shimazu et al., 2005) suggesting another explanation of these contradictory results. The mechanism behind improvement associated with the lack of S1Pr3 is necessary to elucidate, as it could shed light on the opposite results, we and Nitzsche, et al. (2020) observed. Nevertheless, given the differences between experimental stroke models, we additionally verified our initial observations of S1Pr3 elevation post-tMCAo with a model of pMCAo. For the first time, we confirmed that S1Pr3 up-regulates independently of reperfusion. Together with previously published studies, our results confirmed S1Pr3 as a promising target under ischemic conditions. However, its multifaceted roles require identification of cell-specific functions in order to target S1Pr3 in a more specific manner and circumvent the potentially high risk of side effects.

Dusaban et al. (2017) investigated how astrocytes isolated from $S1Pr3^{-/-}$ mice compared to WT controls differ in response to an *in vitro* scratch injury (Dusaban et al., 2017).

Astrocytes lacking S1Pr3 presented with a reduced production of several pro-inflammatory cytokines, such as IL-6 and cyclooxygenase-2 (COX-2), and VEGF (Dusaban et al., 2017). IL-6 and COX-2 have been repeatedly reported to contribute to the aggravation of infarct size (Ahmad et al., 2009; Basic Kes et al., 2008; Hotter et al., 2019; Iadecola et al., 2001). Thus, the functional improvement we observed could be linked to an attenuated S1Pr3-driven pro-inflammatory response, which is blocked in mice lacking S1Pr3. Testing this hypothesis, we assessed the gene expression of IL-6 and COX-2 in S1Pr3$^{-/-}$ and WT mice 1 day post-tMCAo but failed to observe any differences (data not shown). Next, we tested the expression of VEGF. Stroke-related functions of VEGF strongly depend on time. While VEGF has an important function promoting angiogenesis at later post-stroke timepoints, during the acute stages post-stroke, it has been identified as a vascular permeabilization factor that contributes to BBB disruption (Chi et al., 2007; Fagan et al., 2004; H. T. Zhang et al., 2017). Supporting astrocyte-specific *in vitro* results reported by Dusaban et al. (2017), our data revealed a significant reduction of VEGF gene expression in the ipsilateral hemisphere of S1Pr3$^{-/-}$ mice compared to WT controls (**Supplementary Fig. 3**). These data are suggestive of an S1Pr3 contribution to BBB disruption in acute stages after stroke and hence, a potential mechanism of functional improvement after stroke in S1Pr3$^{-/-}$ mice.

Stroke-induced BBB disruption contributes to injury progression and neuronal dysfunction (Shi et al., 2016). BBB dysfunction was found to be a biomarker of poor functional outcome after stroke (Latour et al., 2004; Nadareishvili et al., 2019) and yet, techniques which enable to separate cerebral vessels including cell components of BBB (mural cells, endothelial cells and astrocytes) from brain parenchyma are limited. Available protocols use either enzymatic digestion (Yousif et al., 2007), which introduces alterations of expression profile or mechanical digestion, which overcomes this issue but the protocol design is suitable only for large amounts of tissue (i.e., whole brain); (Boulay et al., 2015; Y. K. Lee et al., 2019; Munikoti et al., 2012). Since we were interested in changes in the ischemic vs contralateral hemisphere post-stroke, we optimized a protocol previously published by Boulay et al. (2015) which allowed us to process brain hemispheres separately and also compare isolated vessel fractions that include astrocyte end-feet, ECs and pericytes to the parenchyma fraction (Matthes et al., 2021).

Using this method, we provide compelling evidence that S1Pr3 is exclusively associated with brain vessels in both experimental stroke models used in our study. Additionally, when looking at the vessels fraction, we detected significant increases of vessel-associated S1Pr3 in the ipsilateral hemisphere. RNA seq results from dissected MCA from male and female rats, which underwent 2 hours tMCAo, revealed an acute elevation of S1Pr3 in the occluded MCA compared to controls independently of sex, which further supported our observation of vessel-associated S1Pr3 expression (Rehnström et al., 2020). Another study using model of tMCAo that performed RNA seq analyses on isolated vessels (Callegari et al., 2019*, *preprint*) corroborated our results as they detected S1Pr3 mRNA in murine vessels. However, when comparing S1Pr3 expression between ischemic vs sham vessels, they did not find any difference. In their experimental design, the vessels were isolated only from the cortical part of the ischemic/control hemisphere, while the infarcted area after 60 min of MCA occlusion covers also subcortical areas. Thus, information about the expression in the rest of the hemisphere is missing, which could change the results substantially. Moreover, the parenchyma fraction was not used for internal comparison with vessels.

S1Prs are widely expressed in different cell types where they mediate a variety of different cell type-specific responses. S1Pr3 activation in VSMCs for instance, induces vasoconstriction (Murakami et al., 2010), while its activation in ECs results in vasodilation (Nofer et al., 2004) and angiogenesis (Yasuda et al., 2021). Depending on the cell type that is affected by certain insults, disease phenotypes may also differ. For instance, S1Pr3 in cardiomyocytes provides cardioprotection during myocardial I/R injury (Yung et al., 2017), while S1Pr3 expressed on dendritic cells contributes to inflammation of renal I/R injury (Bajwa et al., 2012). It is therefore of utmost importance to define cell-specific S1Prs mechanisms during disease. However, the number of studies investigating cell-specific S1P signaling alterations during disease is extremely low.

We opted for the RiboTag approach which has several advantages compared to the alternatives such as magnetic-activated cell sorting (MACS) or fluorescence-activated cell sorting (FACS). The main drawbacks of FACS are the length of the procedure and mechanical disruption during sorting, which affects RNA integrity (Sutermaster & Darling, 2019). Additionally, the yield is often very low, which requires pooling samples from

several animals. Both techniques commonly use enzymatic digestion, which introduces alterations in gene and protein expression (Mattei et al., 2020). Although MACS is generally superior to FACS, there is a lack of cell-specific surface markers, which results in contamination and ultimately to data misinterpretation (Pan & Wan, 2020). The isolation of astrocytes represents a particular challenge due to their highly complex morphology and absence of the reliable surface marker. There are numerous well-established protocols for astrocytes isolation from postnatal mouse brain for *in vitro* cell culture (Schildge et al., 2013; Taylor et al., 2007; Weinstein, 1997). However, expression profile and characteristics of the immature astrocytes greatly differ from the mature ones in the adult mouse brain (Batiuk et al., 2017; Cahoy et al., 2008). Additionally, in the controlled *in vitro* environment it is impossible to simulate the complexity of the healthy and diseased brain. Lastly, since we are interested in stroke-induced S1Pr3 alterations in young adult mice, an *in vitro* culture of isolated immature astrocytes was not suitable for our experimental design. Therefore, we initially tried to use MACS and the astrocyte cell surface antigen 2 (ACSA2) antibody for isolation of murine astrocytes from adult mouse brains, which was published as a novel astrocyte-specific surface marker (Batiuk et al., 2017; G. Kantzer et al., 2017). In contrast to these findings, however, we encountered contamination with oligodendrocytes, which was also observed by other studies (Pan & Wan, 2020; Schroeter et al., 2021). Additionally, we detected a distinct ACSA2 positive population of pericytes (data not shown). Considering the fact that S1Pr3 is highly expressed in mural cells (He et al., 2016), we decided to perform a RiboTag approach. In RiboTag, cell types are genetically identified, and hemagglutinin-tagged ribosomes enable immunoprecipitation of translating mRNAs. Furthermore, the tissue is dissociated mechanically and the whole protocol is performed on ice (Sanz et al., 2009), which reduces the risk of expression alterations.

Using Cnx43, a gap junction protein highly expressed in astrocytes (Y. Zhang et al., 2014), as a promoter, we observed a significant S1Pr3 up-regulation in the ischemic hemisphere after stroke. This finding supports several previous studies, which found *in vitro* inflammation-induced increase of S1Pr3 in astrocytes isolated from mice (Dusaban et al., 2017; Fischer et al., 2011; Hamby et al., 2012; Liddelow et al., 2017) and humans (Van Doorn et al., 2010). It also confirms an *in vivo* study showing 46-fold increase of S1Pr3 in

astrocytes after tMCAo (Zamanian et al., 2012). In the same study, they identified S1Pr3 as a marker of reactive astrocytes, which confirms our data obtained from multiplexed RNAscope localizing S1Pr3 expression along the ischemic lesion and strongly colocalizing with reactive astrocytes detected based on Gfap.

The same RiboTag approach was performed with an endothelial-specific Cdh5 promotor, which revealed no changes in endothelial S1Pr3 expression after stroke. The presence of ECs is gradually increased especially in the damaged area towards day 7 after stroke (Buscemi et al., 2019). While we did not detect any changes at day 1 and 3 post-stroke, endothelial-specific S1Pr3 signaling might be increased at later stages post-stroke at the time when angiogenesis occurs (S. Moon et al., 2021), which could be associated with regenerative effects. Thus, changes of S1Pr3 in ECs during chronic stages post-stroke remain to be elucidated. Regarding the potential involvement of other S1Prs, several studies have been published. Yanagida et al. (2017) showed endothelial S1Pr1 knockout-induced size selective opening of the BBB in the healthy brain (Yanagida et al., 2017). It was later corroborated *in vivo,* showing a crucial role of S1Pr1 in ECs in maintaining BBB integrity and promoting blood flow in hypoperfused areas during ischemic brain damage (Nitzsche et al., 2021). Contrary to that, S1Pr2 in ECs was reported to be up-regulated under inflammatory conditions *in vitro*, which was further associated with increased endothelial MMP9 activity, a known contributor to the BBB disruption (G. S. Kim et al., 2015). Our data regarding stroke-induced alterations of S1Pr1 expression in ECs and astrocytes revealed downregulation of S1Pr1 in the ipsilateral hemisphere 1 day and 3 days post-tMCAo. Since S1Pr1 has a crucial role in maintaining BBB integrity, its decreased expression in the ipsilateral hemisphere, which has a severely disrupted BBB, is in agreement with previously published data. Similar to S1Pr1, our data revealed a decrease of endothelial S1Pr4 expression in the ipsilateral hemisphere 1 day after tMCAo, which corroborates recently published data following stroke. These data imply S1Pr4 is another S1Pr involved in maintaining BBB integrity (Hansen et al., 2021). Taken together, our data provide evidence of an astrocyte-specific source of S1Pr3 up-regulation after stroke without contribution of ECs at early stages after stroke. However, cell-specific contribution of S1Pr3 beyond 3 days after ischemic brain damage remains to be investigated in order to develop most effective therapeutic strategies.

S1Pr3 has been shown to be a regulator of blood flow by several studies (Cantalupo et al., 2017; Levkau et al., 2004; Murakami et al., 2010). Based on that and our own observations that showed post-stroke improvement in S1Pr3$^{-/-}$ mice, we hypothesized that systemic blocking of S1Pr3 might be beneficial for stroke outcome. Indeed, injection of the S1Pr3 specific antagonist CAY10444 4 hours after pMCAo reduced infarct lesion and for the first time, we also provided evidence of improvement of CBF. Gaire et al. (2018) achieved the same reduction of infarct volume in a model of tMCAo by injecting CAY10444 immediately after reperfusion (Gaire et al., 2018). In this study, the beneficial effect of S1Pr3 antagonism was attributed to attenuation of microglial activation together with reduction of neuronal damage (Gaire et al., 2018). Our observation of CAY10444-induced improvement of perfusion is in line with Murakami et al. (2010) who showed a restoration of S1P-induced reduction of blood flow after administration of TY52156, an S1Pr3 selective antagonist, *ex vivo* and *in vivo* (Murakami et al., 2010). Further extending the therapeutic time window to 8 hours post-pMCAo, however, revealed no functional improvement. While the S1Pr3 increase is gradual between 3–6 hours post-tMCAo, above 6 hours the gene expression rises rapidly (Salas-Perdomo et al., 2019). When S1Pr3 expression is close to the basal levels, 4 hours post-occlusion antagonist injection is beneficial, while after 4 additional hours, S1Pr3 may reach levels where the single administration could not effectively antagonize all S1Pr3. Thus, more experiments of single S1Pr3 antagonist injection between 4–8 hours or alternatively, several injections after stroke onset are necessary to investigate how far the time window can be extended.

When targeting S1P signaling systemically, several factors should be taken into consideration. Among them are specificity, plasma half-life or undesirable effects on other organs. The ubiquitous S1Prs expression makes systemic S1Prs modulation particularly complicated. Such an example is S1Pr3 whose activation in cardiomyocytes had a protective effect during myocardial ischemia (Means et al., 2007; Theilmeier et al., 2006), while our data using S1Pr3$^{-/-}$ and pharmacological inhibition points towards its detrimental role in experimental stroke. In our study, we have not observed any side effects associated with S1Pr3 pharmacological inhibition, however, here we investigated only the acute effects of CAY10444, thus the long-term impact of S1Pr3 antagonism needs to be still addressed.

This is especially important to mention considering the immunomodulatory drug Fingolimod, which has gained increased attention in the stroke field. It is currently undergoing several clinical trials although, studies investigating the effect of Fingolimod in experimental stroke have reported inconsistent results (Czech et al., 2009; Salas-Perdomo et al., 2019; Wei et al., 2011). On the one hand, the action of Fingolimod has been associated with attenuated influx of lymphocytes into the brain (Liesz et al., 2011; Salas-Perdomo et al., 2019), reduced infarct lesions, improved neurological outcome or BBB protection (Czech et al., 2009; Wei et al., 2011). While the majority of these studies used tMCAo, Liesz et al. (2011) observed no Fingolimod-associated effect on reduction of infarct lesion or improvement of neurological function in a model of pMCAo (Liesz et al., 2011). Some studies additionally revealed no improvement of BBB integrity or attenuation of neuroinflammation (Kraft et al., 2013; Salas-Perdomo et al., 2019). The mechanism of Fingolimod action was mainly attributed to internalization of S1Pr1 followed by inhibition of lymphocyte egress from lymphoid organs (Matloubian et al., 2004). S1Pr1 is crucial for maintaining vascular integrity (Fischl et al., 2019) and our results (data not shown) together with others showed that S1Pr1 is decreased (Lucaciu et al., 2020; E. Moon et al., 2015) early after stroke onset. That might be the reason why systemic modulation with Fingolimod, which induces further S1Pr1 downregulation, could not improve BBB integrity. Fingolimod is a nonspecific agent and even though it is clear that it acts as a functional S1Pr1 antagonist, its activation of other S1Prs, particularly S1Pr3, remains to be fully elucidated in conditions like stroke. Some studies showed evidence of Fingolimod's action as an S1Pr3 agonist (Dusaban et al., 2017; Sensken et al., 2008), which could potentially be a reason for one of its side effects such as bradycardia, which has been reported in association with S1Pr3 signaling (Camm et al., 2014; Dusaban et al., 2017; Murakami et al., 2010; Sanna et al., 2004). Furthermore, Fingolimod does not target S1Pr2, which is also elevated after tMCAo (Y. K. Lee et al., 2019; Lucaciu et al., 2020). S1Pr2 up-regulation post-stroke has been linked to disruption of vascular integrity and increased BBB permeability induced by MMP9 activity (G. S. Kim et al., 2015) and pharmacological inhibition of S1Pr2 showed promising results in improving stroke outcome (G. S. Kim et al., 2015; Y. K. Lee et al., 2019; Sapkota et al., 2019). These findings undermine the suitability of Fingolimod in stroke therapy and imply more specific S1Prs modulators to be preferable.

Current knowledge about the role of S1P signaling during ischemia supports the importance of organ- and cell-specific investigations, which can be later harnessed for the development of effective therapeutic strategies. In this respect, the route of administration should be also reconsidered. The commonly used intraperitoneal and oral administrations act systemically and might have adverse effects like, for instance, in case of Fingolimod and additionally, might fail to effectively reach the CNS. Thus, intranasal administration could be an alternative for more brain-targeted delivery of S1Prs modulators (Lochhead & Thorne, 2012).

Finally, with the aim to confirm and translate our results into clinic, we started with the evaluation of S1Pr3 alterations in murine plasma. As we hypothesized, S1Pr3 was significantly up-regulated in murine plasma samples 1 day post-tMCAo compared to the control group. In line with our observation, Sun et al. (2012) reported elevated S1Pr3 plasma concentration associated with inflammation and additionally, they identified S1Pr3 as a biomarker of acute lung injury severity (X. Sun et al., 2012). While they revealed ECs as a source of shed S1Pr3 in plasma during lung injury, it remains to be elucidated for stroke in the future as well as the confirmation of our observations in plasma samples obtained from stroke patients.

5. Abstract

Stroke is a leading cause of long-term disability worldwide. Its highly complex pathogenesis is characterized by a deleterious cycle of vascular dysfunction and inflammation. Recently, the bioactive phospholipid sphingosine-1-phosphate (S1P), has gained increasing attention in cardiovascular diseases due to its involvement in both vascular function and immune cell responses. Altered S1P levels have been reported in several cardiovascular and inflammation-associated diseases, including stroke. S1P signals via five ubiquitously expressed S1P receptors, S1Pr1-5. Previous *in vitro* studies revealed alterations of S1Pr3 signaling under inflammatory conditions. During vascular adaptation to disease models of middle cerebral artery occlusion (MCAo), we determined the expression pattern of S1Pr3 in brain tissue with qPCR and western blot. Transient MCAo in endothelial- and astrocyte-specific RiboTag transgenic mice allowed us to determine changes in S1P signaling through immunoprecipitation of translating mRNAs from both cell types. For modulation of S1Pr3 signaling, we used $S1Pr3^{-/-}$ mice or pharmacological S1Pr3 inhibition administered 4 and 8 hours after permanent MCAo. Stroke outcome was determined by infarct size evaluation, neuroscore, and assessment of cerebral blood flow (CBF) using magnetic resonance imaging.

S1Pr3 expression was significantly increased 1 day and 3 days post-ischemia in the ipsilateral hemisphere of WT mice on the gene and protein level. Mice lacking S1Pr3 revealed improved neurological function and reduced ischemic lesion during the acute phase after experimental stroke. Using vessel-parenchyma fractionation of brain tissue, we detected the majority of S1Pr3 associated with cerebral vessels. RiboTag analysis unveiled an augmentation of astrocyte- but not endothelial-specific S1Pr3 expression 1 day and 3 days post-stroke. RiboTag results were further confirmed using *in situ* hybridization colocalization of Gfap and Sox9, astrocytic markers and S1Pr3 in the ischemic hemisphere. Single administration of an S1Pr3 antagonist 4 hours after permanent MCAo led to significant CBF improvements in the ipsilateral hemisphere 1 day post-stroke that persisted up to 3 days. Consequently, infarct size was significantly reduced in mice treated with S1Pr3 antagonist. However, later administration at 8 hours post-stroke did not improve CBF or reduced infarct size.

In conclusion, our findings point to an important involvement of the S1P/S1Pr3 signaling axis during stroke, and a potential contribution of astrocytes-specific S1Pr3 signaling during the acute phase post-stroke. Modulating S1Pr3-mediated vascular responses may emerge as a viable target to improving stroke outcome.

6. List of Figures

7. List of Tables

8. References

Ahmad, M., Zhang, Y., Liu, H., Rose, M. E., & Graham, S. H. (2009). Prolonged opportunity for neuroprotection in experimental stroke with selective blockade of cyclooxygenase-2 activity. *Brain Research*, *1279*, 168–173. https://doi.org/10.1016/j.brainres.2009.05.020

Allen, N. J., & Eroglu, C. (2017). Cell Biology of Astrocyte-Synapse Interactions. *Neuron*, *96*(3), 697–708. https://doi.org/10.1016/j.neuron.2017.09.056

Allende, M. L., Dreier, J. L., Mandala, S., & Proia, R. L. (2004). Expression of the Sphingosine 1-Phosphate Receptor, S1P1, on T-cells Controls Thymic Emigration. *Journal of Biological Chemistry*, *279*(15), 15396–15401. https://doi.org/10.1074/jbc.M314291200

Allende, M. L., Tuymetova, G., Lee, B. G., Bonifacino, E., Wu, Y. P., & Proia, R. L. (2010). S1P1 receptor directs the release of immature B cells from bone marrow into blood. *Journal of Experimental Medicine*, *207*(5), 1113–1124. https://doi.org/10.1084/jem.20092210

Andriezen, W. L. (1893). The neuroglia elements in the human brain. *The British Medical Journal.* 2, 227–230. doi: 10.1136/bmj.2.1700.227

Araque, A., Parpura, V., Sanzgiri, R. P., & Haydon, P. G. (1999). Tripartite synapses: Glia, the unacknowledged partner. *Trends in Neurosciences*, *22*(5), 208–215. https://doi.org/10.1016/S0166-2236(98)01349-6

Armulik, A., Genové, G., Mäe, M., Nisancioglu, M. H., Wallgard, E., Niaudet, C., He, L., Norlin, J., Lindblom, P., Strittmatter, K., Johansson, B. R., & Betsholtz, C. (2010). Pericytes regulate the blood-brain barrier. *Nature*, *468*(7323), 557–561. https://doi.org/10.1038/nature09522

Bajwa, A., Huang, L., Ye, H., Dondeti, K., Song, S., Rosin, D. L., Lynch, K. R., Lobo, P. I., Li, L., & Okusa, M. D. (2012). Dendritic Cell Sphingosine 1-Phosphate Receptor-3 Regulates Th1–Th2 Polarity in Kidney Ischemia–Reperfusion Injury. *The Journal of Immunology*, *189*(5), 2584–2596. https://doi.org/10.4049/jimmunol.1200999

Bak, L. K., Schousboe, A., & Waagepetersen, H. S. (2006). The glutamate/GABA-glutamine cycle: Aspects of transport, neurotransmitter homeostasis and ammonia transfer. *Journal of Neurochemistry*, *98*(3), 641–653. https://doi.org/10.1111/j.1471-4159.2006.03913.x

Basic Kes, V., Simundic, A. M., Nikolac, N., Topic, E., & Demarin, V. (2008). Pro-inflammatory and anti-inflammatory cytokines in acute ischemic stroke and their relation to early neurological deficit and stroke outcome. *Clinical Biochemistry*, *41*(16–17), 1330–1334. https://doi.org/10.1016/j.clinbiochem.2008.08.080

Batiuk, M. Y., De Vin, F., Duqué, S. I., Li, C., Saito, T., Saido, T., Fiers, M., Belgard, T. G., & Holt, M. G. (2017). An immunoaffinity-based method for isolating ultrapure adult

astrocytes based on ATP1B2 targeting by the ACSA-2 antibody. *Journal of Biological Chemistry*, *292*(21), 8874–8891. https://doi.org/10.1074/jbc.M116.765313

Batiuk, M. Y., Martirosyan, A., Wahis, J., de Vin, F., Marneffe, C., Kusserow, C., Koeppen, J., Viana, J. F., Oliveira, J. F., Voet, T., Ponting, C. P., Belgard, T. G., & Holt, M. G. (2020). Identification of region-specific astrocyte subtypes at single cell resolution. *Nature Communications*, *11*(1), 1–15. https://doi.org/10.1038/s41467-019-14198-8

Becerra-Calixto, A., & Cardona-Gómez, G. P. (2017). The role of astrocytes in neuroprotection after brain stroke: Potential in cell therapy. *Frontiers in Molecular Neuroscience*, *10*(April), 1–12. https://doi.org/10.3389/FNMOL.2017.00088

Bell, A. H., Miller, S. L., Castillo-Melendez, M., & Malhotra, A. (2020). The Neurovascular Unit: Effects of Brain Insults During the Perinatal Period. *Frontiers in Neuroscience*, *13*(January), 1–19. https://doi.org/10.3389/fnins.2019.01452

Ben Haim, L., & Rowitch, D. H. (2016). Functional diversity of astrocytes in neural circuit regulation. *Nature Reviews Neuroscience*, *18*(1), 31–41. https://doi.org/10.1038/nrn.2016.159

Benarroch, E. E. (2016). Astrocyte signaling and synaptic homeostasis. *Neurology*, *87*(7), 726–735. https://doi.org/10.1212/WNL.0000000000003019

Bernardo-Castro, S., Sousa, J. A., Brás, A., Cecília, C., Rodrigues, B., Almendra, L., Machado, C., Santo, G., Silva, F., Ferreira, L., Santana, I., & Sargento-Freitas, J. (2020). Pathophysiology of Blood–Brain Barrier Permeability Throughout the Different Stages of Ischemic Stroke and Its Implication on Hemorrhagic Transformation and Recovery. *Frontiers in Neurology*, *11*(December), 1–24. https://doi.org/10.3389/fneur.2020.594672

Betz, A. L., Firth, J. A., & Goldstein, G. W. (1980). Polarity of the blood-brain barrier: Distribution of enzymes between the luminal and antiluminal membranes of brain capillary endothelial cells. *Brain Research*, *192*(1), 17–28. https://doi.org/10.1016/0006-8993(80)91004-5

Beuker, C., Strecker, J. K., Rawal, R., Schmidt-Pogoda, A., Ruck, T., Wiendl, H., Klotz, L., Schäbitz, W. R., Sommer, C. J., Minnerup, H., Meuth, S. G., & Minnerup, J. (2021). Immune Cell Infiltration into the Brain After Ischemic Stroke in Humans Compared to Mice and Rats: a Systematic Review and Meta-Analysis. *Translational Stroke Research*, *12*(6), 976–990. https://doi.org/10.1007/s12975-021-00887-4

Blutstein, T., & Haydon, P. G. (2013). The Tripartite Synapse. A Role for Glial Cells in Modulating Synaptic Transmission. In *The Synapse: Structure and Function*. Elsevier. https://doi.org/10.1016/B978-0-12-418675-0.00005-5

Boehme, A. K., Esenwa, C., & Elkind, M. S. V. (2017). Stroke Risk Factors, Genetics, and Prevention. *Circulation Research*, *120*(3), 472–495. https://doi.org/10.1161/CIRCRESAHA.116.308398

Boulay, A. C., Saubaméa, B., Declèves, X., & Cohen-Salmon, M. (2015). Purification of

mouse brain vessels. *Journal of Visualized Experiments*, *2015*(105), 1–8. https://doi.org/10.3791/53208

Brait, V. H., Arumugam, T. V., Drummond, G. R., & Sobey, C. G. (2012). Importance of T lymphocytes in brain injury, immunodeficiency, and recovery after cerebral ischemia. *Journal of Cerebral Blood Flow and Metabolism*, *32*(4), 598–611. https://doi.org/10.1038/jcbfm.2012.6

Brunkhorst, R., Vutukuri, R., & Pfeilschifter, W. (2014). Fingolimod for the treatment of neurological diseases—state of play and future perspectives3. *Frontiers in Cellular Neuroscience*, *8*(September). https://doi.org/10.3389/fncel.2014.00283

Bryan, A. M., & Del Poeta, M. (2018). Sphingosine-1-phosphate receptors and innate immunity. *Cellular Microbiology*, *20*(5), 1–18. https://doi.org/10.1111/cmi.12836

Buscemi, L., Price, M., Bezzi, P., & Hirt, L. (2019). Spatio-temporal overview of neuroinflammation in an experimental mouse stroke model. *Scientific Reports*, *9*(1), 1–13. https://doi.org/10.1038/s41598-018-36598-4

Busch, S. A., & Silver, J. (2007). The role of extracellular matrix in CNS regeneration. *Current Opinion in Neurobiology*, *17*(1), 120–127. https://doi.org/10.1016/j.conb.2006.09.004

Bush, T. G., Puvanachandra, N., Horner, C. H., Polito, A., Ostenfeld, T., Svendsen, C. N., Mucke, L., Johnson, M. H., & Sofroniew, M. V. (1999). Leukocyte infiltration, neuronal degeneration, and neurite outgrowth after ablation of scar-forming, reactive astrocytes in adult transgenic mice. *Neuron*, *23*(2), 297–308. https://doi.org/10.1016/S0896-6273(00)80781-3

Cabezas, R., Ávila, M., Gonzalez, J., El-Bachá, R. S., Báez, E., García-Segura, L. M., Coronel, J. C. J., Capani, F., Cardona-Gomez, G. P., & Barreto, G. E. (2014). Astrocytic modulation of blood brain barrier: Perspectives on Parkinson's disease. *Frontiers in Cellular Neuroscience*, *8*(AUG), 1–11. https://doi.org/10.3389/fncel.2014.00211

Cahoy, J. D., Emery, B., Kaushal, A., Foo, L. C., Zamanian, J. L., Christopherson, K. S., Xing, Y., Lubischer, J. L., Krieg, P. A., Krupenko, S. A., Thompson, W. J., & Barres, B. A. (2008). A transcriptome database for astrocytes, neurons, and oligodendrocytes: A new resource for understanding brain development and function. *Journal of Neuroscience*, *28*(1), 264–278. https://doi.org/10.1523/JNEUROSCI.4178-07.2008

Callegari, K., Dash, S., Uchida, H., Lee, Y., Ito, A., Zhang, T., Xiang, J., & Sanchez, T. (2019). Translationally relevant transcriptomic alterations in mouse ischemic cerebral microvessels. *BioRxiv*. https://doi.org/10.1101/829820

Camerer, E., Regard, J. B., Cornelissen, I., Srinivasan, Y., Duong, D. N., Palmer, D., Pham, T. H., Wong, J. S., Pappu, R., & Coughlin, S. R. (2009). Sphingosine-1-phosphate in the plasma compartment regulates basal and inflammation-induced vascular leak in mice. *Journal of Clinical Investigation*, *119*(7), 1871–1879. https://doi.org/10.1172/jci38575

Camm, J., Hla, T., Bakshi, R., & Brinkmann, V. (2014). Cardiac and vascular effects of fingolimod: Mechanistic basis and clinical implications. *American Heart Journal*, *168*(5), 632–644. https://doi.org/10.1016/j.ahj.2014.06.028

Cantalupo, A., & Di Lorenzo, A. (2016). S1P signaling and de novo biosynthesis in blood pressure homeostasis. *Journal of Pharmacology and Experimental Therapeutics*, *358*(2), 359–370. https://doi.org/10.1124/jpet.116.233205

Cantalupo, A., Gargiulo, A., Dautaj, E., Liu, C., Zhang, Y., Hla, T., & Di Lorenzo, A. (2017). S1PR1 (Sphingosine-1-Phosphate Receptor 1) Signaling Regulates Blood Flow and Pressure. *Hypertension*, *70*(2), 426–434. https://doi.org/10.1161/HYPERTENSIONAHA.117.09088

Chauhan, G., & Debette, S. (2016). Genetic Risk Factors for Ischemic and Hemorrhagic Stroke. *Current Cardiology Reports*, *18*(12). https://doi.org/10.1007/s11886-016-0804-z

Chen, Y., Bodhankar, S., Murphy, S. J., Vandenbark, A. A., Alkayed, N. J., & Offner, H. (2012). Intrastriatal B-cell administration limits infarct size after stroke in B-cell deficient mice. *Metabolic Brain Disease*, *27*(4), 487–493. https://doi.org/10.1007/s11011-012-9317-7

Chi, O. Z., Hunter, C., Liu, X., & Weiss, H. R. (2007). Effects of anti-VEGF antibody on blood-brain barrier disruption in focal cerebral ischemia. *Experimental Neurology*, *204*(1), 283–287. https://doi.org/10.1016/j.expneurol.2006.11.001

Chu, H. X., Broughton, B. R. S., Ah Kim, H., Lee, S., Drummond, G. R., & Sobey, C. G. (2015). Evidence That Ly6Chi Monocytes Are Protective in Acute Ischemic Stroke by Promoting M2 Macrophage Polarization. *Stroke*, *46*(7), 1929–1937. https://doi.org/10.1161/STROKEAHA.115.009426

Chu, H. X., Kim, H. A., Lee, S., Moore, J. P., Chan, C. T., Vinh, A., Gelderblom, M., Arumugam, T. V., Broughton, B. R., Drummond, G. R., & Sobey, C. G. (2014). Immune cell infiltration in malignant middle cerebral artery infarction: Comparison with transient cerebral ischemia. *Journal of Cerebral Blood Flow and Metabolism*, *34*(3), 450–459. https://doi.org/10.1038/jcbfm.2013.217

Czech, B., Pfeilschifter, W., Mazaheri-Omrani, N., Strobel, M. A., Kahles, T., Neumann-Haefelin, T., Rami, A., Huwiler, A., & Pfeilschifter, J. (2009). The immunomodulatory sphingosine 1-phosphate analog FTY720 reduces lesion size and improves neurological outcome in a mouse model of cerebral ischemia. *Biochemical and Biophysical Research Communications*, *389*(2), 251–256. https://doi.org/10.1016/j.bbrc.2009.08.142

Daneman, R., Prat, A. (2008). The blood brain barrier. *Neuroimmune Pharmacology*, 21–38. https://doi.org/10.1007/978-0-387-72573-4_4

Deitmer, J. W., Theparambil, S. M., Ruminot, I., Noor, S. I., & Becker, H. M. (2019). Energy Dynamics in the Brain: Contributions of Astrocytes to Metabolism and pH Homeostasis. *Frontiers in Neuroscience*, *13*(December), 1–7. https://doi.org/10.3389/fnins.2019.01301

Dirnagl, U., Iadecola, C., & Moskowitz, M. A. (1999). Pathobiology of ischaemic stroke: an integrated view. *Trends in Neurosciences*, *22*(9), 391–397. https://doi.org/10.1016/S0166-2236(99)01401-0

Dong, Y. F., Guo, R. B., Ji, J., Cao, L. L., Zhang, L., Chen, Z. Z., Huang, J. Y., Wu, J., Lu, J., & Sun, X. L. (2018). S1PR3 is essential for phosphorylated fingolimod to protect astrocytes against oxygen-glucose deprivation-induced neuroinflammation via inhibiting TLR2/4-NFκB signalling. *Journal of Cellular and Molecular Medicine*, *22*(6), 3159–3166. https://doi.org/10.1111/jcmm.13596

Doyle, K. P., Quach, L. N., Solé, M., Axtell, R. C., Nguyen, T. V. V., Soler-Llavina, G. J., Jurado, S., Han, J., Steinman, L., Longo, F. M., Schneider, J. A., Malenka, R. C., & Buckwalter, M. S. (2015). B-lymphocyte-mediated delayed cognitive impairment following stroke. *Journal of Neuroscience*, *35*(5), 2133–2145. https://doi.org/10.1523/JNEUROSCI.4098-14.2015

Doyle, K. P., Simon, R. P., & Stenzel-Poore, M. P. (2008). Mechanisms of ischemic brain damage. *Neuropharmacology*, *55*(3), 310–318. https://doi.org/10.1016/j.neuropharm.2008.01.005

Dusaban, S. S., Chun, J., Rosen, H., Purcell, N. H., & Brown, J. H. (2017). Sphingosine 1-phosphate receptor 3 and RhoA signaling mediate inflammatory gene expression in astrocytes. *Journal of Neuroinflammation*. https://doi.org/10.1186/s12974-017-0882-x

Fagan, S. C., Hess, D. C., Hohnadel, E. J., Pollock, D. M., & Ergul, A. (2004). Targets for vascular protection after acute ischemic stroke. *Stroke*, *35*(9), 2220–2225. https://doi.org/10.1161/01.STR.0000138023.60272.9e

Fan, X., Liu, L., Shi, Y., Guo, F., He, X., Zhao, X., Zhong, D., & Li, G. (2021). Recent advances of the function of sphingosine 1-phosphate (S1P) receptor S1P3. *Journal of Cellular Physiology*, *236*(3), 1564–1578. https://doi.org/10.1002/jcp.29958

Faura, J., Bustamante, A., Miró-Mur, F., & Montaner, J. (2021). Stroke-induced immunosuppression: implications for the prevention and prediction of post-stroke infections. *Journal of Neuroinflammation*, *18*(1), 1–14. https://doi.org/10.1186/s12974-021-02177-0

Finley, A., Chen, Z., Esposito, E., Cuzzocrea, S., Sabbadini, R., & Salvemini, D. (2013). Sphingosine 1-Phosphate Mediates Hyperalgesia via a Neutrophil-Dependent Mechanism. *PLoS ONE*, *8*(1), 1–9. https://doi.org/10.1371/journal.pone.0055255

Fischer, I., Alliod, C., Martinier, N., Newcombe, J., Brana, C., & Pouly, S. (2011). Sphingosine kinase 1 and sphingosine 1-phosphate receptor 3 are functionally upregulated on astrocytes under pro-inflammatory conditions. *PLoS ONE*, *6*(8). https://doi.org/10.1371/journal.pone.0023905

Fischl, A. S., Wang, X., Falcon, B. L., Almonte-Baldonado, R., Bodenmiller, D., Evans, G., Stewart, J., Wilson, T., Hipskind, P., Manro, J., Uhlik, M. T., Chintharlapalli, S., Gerald, D., Alsop, D. C., Benjamin, L. E., & Bhatt, R. S. (2019). Inhibition of sphingosine phosphate

receptor 1 signaling enhances the efficacy of VEGF receptor inhibition. *Molecular Cancer Therapeutics*, *18*(4), 856–867. https://doi.org/10.1158/1535-7163.MCT-18-0548

G. Kantzer, C., Boutin, C., Herzig, I. D., Wittwer, C., Reiß, S., Tiveron, M. C., Drewes, J., Rockel, T. D., Ohlig, S., Ninkovic, J., Cremer, H., Pennartz, S., Jungblut, M., & Bosio, A. (2017). Anti-ACSA-2 defines a novel monoclonal antibody for prospective isolation of living neonatal and adult astrocytes. *Glia*, *65*(6), 990–1004. https://doi.org/10.1002/glia.23140

Gaire, B. P., Song, M. R., & Choi, J. W. (2018). Sphingosine 1-phosphate receptor subtype 3 (S1P3) contributes to brain injury after transient focal cerebral ischemia via modulating microglial activation and their M1 polarization. *Journal of Neuroinflammation*, *15*(1), 1–14. https://doi.org/10.1186/s12974-018-1323-1

Golfier, S., Kondo, S., Schulze, T., Takeuchi, T., Vassileva, G., Achtman, A. H., Gräler, M. H., Abbondanzo, S. J., Wiekowski, M., Kremmer, E., Endo, Y., Lira, S. A., Bacon, K. B., & Lipp, M. (2010). Shaping of terminal megakaryocyte differentiation and proplatelet development by sphingosine-1-phosphate receptor S1P 4 . *The FASEB Journal*, *24*(12), 4701–4710. https://doi.org/10.1096/fj.09-141473

Gottschalk, M. (2020). Look-Locker FAIR TrueFISP for arterial spin labelling on mouse at 9.4 T. *NMR in Biomedicine*, *33*(3), 1–11. https://doi.org/10.1002/nbm.4191

Grassi, S., Mauri, L., Prioni, S., Cabitta, L., Sonnino, S., Prinetti, A., & Giussani, P. (2019). Sphingosine 1-phosphate receptors and metabolic enzymes as druggable targets for brain diseases. *Frontiers in Pharmacology*, *10*(July), 1–20. https://doi.org/10.3389/fphar.2019.00807

Guérit, S., Fidan, E., Macas, J., Czupalla, C. J., Figueiredo, R., Vijikumar, A., Yalcin, B. H., Thom, S., Winter, P., Gerhardt, H., Devraj, K., & Liebner, S. (2021). Astrocyte-derived Wnt growth factors are required for endothelial blood-brain barrier maintenance. *Progress in Neurobiology*, *199*. https://doi.org/10.1016/j.pneurobio.2020.101937

Hamby, M. E., Coppola, G., Ao, Y., Geschwind, D. H., Khakh, B. S., & Sofroniew, M. V. (2012). Inflammatory mediators alter the astrocyte transcriptome and calcium signaling elicited by multiple G-protein-coupled receptors. *Journal of Neuroscience*, *32*(42), 14489–14510. https://doi.org/10.1523/JNEUROSCI.1256-12.2012

Hansen, L., Lohfink, N., Vutukuri, R., Kestner, R. I., Trautmann, S., Hecht, M., Wagner, P. V., Spitzer, D., Khel, M. I., Macas, J., Ferreirós, N., Gurke, R., Günther, S., Pfeilschifter, W., & Devraj, K. (2021). Endothelial sphingosine-1-phosphate receptor 4 regulates blood-brain barrier permeability and promotes a homeostatic endothelial phenotype. *Journal of Neuroscience, September*, JN-RM-0188-21. https://doi.org/10.1523/JNEUROSCI.0188-21.2021.

Hartings, J. A., Rolli, M. L., Lu, X. C. M., & Tortella, F. C. (2003). Delayed Secondary Phase of Peri-Infarct Depolarizations after Focal Cerebral Ischemia: Relation to Infarct Growth and Neuroprotection. *Journal of Neuroscience*, *23*(37), 11602–11610. https://doi.org/10.1523/jneurosci.23-37-11602.2003

Hasegawa, Y., Suzuki, H., Sozen, T., Rolland, W., & Zhang, J. H. (2010). Activation of sphingosine 1-phosphate receptor-1 by FTY720 is neuroprotective after ischemic stroke in rats. *Stroke*, *41*(2), 368–374. https://doi.org/10.1161/STROKEAHA.109.568899

He, L., Vanlandewijck, M., Raschperger, E., Andaloussi Maë, M., Jung, B., Lebouvier, T., Ando, K., Hofmann, J., Keller, A., & Betsholtz, C. (2016). Analysis of the brain mural cell transcriptome. *Scientific Reports*, *6*(Icmc), 1–13. https://doi.org/10.1038/srep35108

Hla, T., & Maciag, T. (1990). An abundant transcript induced in differentiating human endothelial cells encodes a polypeptide with structural similarities to G-protein-coupled receptors. *Journal of Biological Chemistry*, *265*(16), 9308–9313. https://doi.org/10.1016/s0021-9258(19)38849-0

Hotter, B., Hoffmann, S., Ulm, L., Meisel, C., Fiebach, J. B., & Meisel, A. (2019). IL-6 Plasma levels correlate with cerebral perfusion deficits and infarct sizes in stroke patients without associated infections. *Frontiers in Neurology*, *10*(FEB), 1–8. https://doi.org/10.3389/fneur.2019.00083

Hu, X., Li, P., Guo, Y., Wang, H., Leak, R. K., Chen, S., Gao, Y., & Chen, J. (2012). Microglia/macrophage polarization dynamics reveal novel mechanism of injury expansion after focal cerebral ischemia. *Stroke*, *43*(11), 3063–3070. https://doi.org/10.1161/STROKEAHA.112.659656

Huwiler, A., & Zangemeister-Wittke, U. (2018). The sphingosine 1-phosphate receptor modulator fingolimod as a therapeutic agent: Recent findings and new perspectives. *Pharmacology and Therapeutics*, *185*, 34–49. https://doi.org/10.1016/j.pharmthera.2017.11.001

Iadecola, C., & Anrather, J. (2011). The immunology of stroke: From mechanisms to translation. *Nature Medicine*, *17*(7), 796–808. https://doi.org/10.1038/nm.2399

Iadecola, C., Niwa, K., Nogawa, S., Zhao, X., Nagayama, M., Araki, E., Morham, S., & Ross, M. E. (2001). Reduced susceptibility to ischemic brain injury and N-methyl-D-aspartate-mediated neurotoxicity in cyclooxygenase-2-deficient mice. *Proceedings of the National Academy of Sciences of the United States of America*, *98*(3), 1294–1299. https://doi.org/10.1073/pnas.98.3.1294

Ishii, I., Friedman, B., Ye, X., Kawamura, S., McGiffert, C., Contos, J. J. A., Kingsbury, M. A., Zhang, G., Brown, J. H., & Chun, J. (2001). Selective Loss of Sphingosine 1-Phosphate Signaling with No Obvious Phenotypic Abnormality in Mice Lacking Its G Protein-coupled Receptor, LP B3/EDG-3. *Journal of Biological Chemistry*, *276*(36), 33697–33704. https://doi.org/10.1074/jbc.M104441200

Jaillard, C., Harrison, S., Stankoff, B., Aigrot, M. S., Calver, A. R., Duddy, G., Walsh, F. S., Pangalos, M. N., Arimura, N., Kaibuchi, K., Zalc, B., & Lubetzki, C. (2005). Edg8/S1P5: An oligodendroglial receptor with dual function on process retraction and cell survival. *Journal of Neuroscience*, *25*(6), 1459–1469. https://doi.org/10.1523/JNEUROSCI.4645-04.2005

Jäkel, S., & Dimou, L. (2017). Glial cells and their function in the adult brain: A journey through the history of their ablation. *Frontiers in Cellular Neuroscience*, *11*(February), 1–17. https://doi.org/10.3389/fncel.2017.00024

Jayaraj, R. L., Azimullah, S., Beiram, R., Jalal, F. Y., & Rosenberg, G. A. (2019). Neuroinflammation: Friend and foe for ischemic stroke. *Journal of Neuroinflammation*, *16*(1), 1–24. https://doi.org/10.1186/s12974-019-1516-2

Jickling, G. C., Liu, D., Stamova, B., Ander, B. P., Zhan, X., Lu, A., & Sharp, F. R. (2014). Hemorrhagic transformation after ischemic stroke in animals and humans. *Journal of Cerebral Blood Flow and Metabolism*, *34*(2), 185–199. https://doi.org/10.1038/jcbfm.2013.203

Jo, S. K., Bajwa, A., Ye, H., Vergis, A. L., Awad, A. S., Kharel, Y., Lynch, K. R., & Okusa, M. D. (2009). Divergent roles of sphingosine kinases in kidney ischemia-reperfusion injury. *Kidney International*, *75*(2), 167–175. https://doi.org/10.1038/ki.2008.400

John Lin, C. C., Yu, K., Hatcher, A., Huang, T. W., Lee, H. K., Carlson, J., Weston, M. C., Chen, F., Zhang, Y., Zhu, W., Mohila, C. A., Ahmed, N., Patel, A. J., Arenkiel, B. R., Noebels, J. L., Creighton, C. J., & Deneen, B. (2017). Identification of diverse astrocyte populations and their malignant analogs. *Nature Neuroscience*, *20*(3), 396–405. https://doi.org/10.1038/nn.4493

Jozefczuk, E., Guzik, T. J., & Siedlinski, M. (2020). Significance of sphingosine-1-phosphate in cardiovascular physiology and pathology. *Pharmacological Research*, *156*(March), 104793. https://doi.org/10.1016/j.phrs.2020.104793

Kim, G. S., Yang, L., Zhang, G., Zhao, H., Selim, M., McCullough, L. D., Kluk, M. J., & Sanchez, T. (2015). Critical role of sphingosine-1-phosphate receptor-2 in the disruption of cerebrovascular integrity in experimental stroke. *Nature Communications*, *6*. https://doi.org/10.1038/ncomms8893

Kim, J. S. (2019). tPA helpers in the treatment of acute ischemic stroke: Are they ready for clinical use? *Journal of Stroke*, *21*(2), 160–174. https://doi.org/10.5853/jos.2019.00584

Kimura, A., Ohmori, T., Kashiwakura, Y., Ohkawa, R., Madoiwa, S., Mimuro, J., Shimazaki, K., Hoshino, Y., Yatomi, Y., & Sakata, Y. (2008). Antagonism of sphingosine 1-phosphate receptor-2 enhances migration of neural progenitor cells toward an area of brain infarction. *Stroke*, *39*(12), 3411–3417. https://doi.org/10.1161/STROKEAHA.108.514612

Kleinschnitz, C., Kraft, P., Dreykluft, A., Hagedorn, I., Göbel, K., Schuhmann, M. K., Langhauser, F., Helluy, X., Schwarz, T., Bittner, S., Mayer, C. T., Brede, M., Varallyay, C., Pham, M., Bendszus, M., Jakob, P., Magnus, T., Meuth, S. G., Iwakura, Y., … Wiendl, H. (2013). Regulatory T cells are strong promoters of acute ischemic stroke in mice by inducing dysfunction of the cerebral microvasculature. *Blood*, *121*(4), 679–691. https://doi.org/10.1182/blood-2012-04-426734

Kleinwort, A., Lührs, F., Heidecke, C. D., Lipp, M., & Schulze, T. (2018). S1P signalling

differentially affects migration of peritoneal B cell populations in vitro and influences the production of intestinal IgA in vivo. *International Journal of Molecular Sciences*, *19*(2), 1–13. https://doi.org/10.3390/ijms19020391

Koh, S. H., & Park, H. H. (2017). Neurogenesis in Stroke Recovery. *Translational Stroke Research*, *8*(1), 3–13. https://doi.org/10.1007/s12975-016-0460-z

Kono, M., Belyantseva, I. A., Skoura, A., Frolenkov, G. I., Starost, M. F., Dreier, J. L., Lidington, D., Bolz, S. S., Friedman, T. B., Hla, T., & Proia, R. L. (2007). Deafness and stria vascularis defects in S1P2 receptor-null mice. *Journal of Biological Chemistry*, *282*(14), 10690–10696. https://doi.org/10.1074/jbc.M700370200

Kono, M., Mi, Y., Liu, Y., Sasaki, T., Allende, M. L., Wu, Y. P., Yamashita, T., & Proia, R. L. (2004). The sphingosine-1-phosphate receptors S1P1, S1P2, and S1P3 function coordinately during embryonic angiogenesis. *Journal of Biological Chemistry*, *279*(28), 29367–29373. https://doi.org/10.1074/jbc.M403937200

Kraft, P., Göb, E., Schuhmann, M. K., Göbel, K., Deppermann, C., Thielmann, I., Herrmann, A. M., Lorenz, K., Brede, M., Stoll, G., Meuth, S. G., Nieswandt, B., Pfeilschifter, W., & Kleinschnitz, C. (2013). FTY720 ameliorates acute ischemic stroke in mice by reducing thrombo-infammation but not by direct neuroprotection. *Stroke*, *44*(11), 3202–3210. https://doi.org/10.1161/STROKEAHA.113.002880

Kretz, M., Euwens, C., Hombach, S., Eckardt, D., Teubner, B., Traub, O., Willecke, K., & Ott, T. (2003). Altered connexin expression and wound healing in the epidermis of connexin-deficient mice. *Journal of Cell Science*, *116*(16), 3443–3452. https://doi.org/10.1242/jcs.00638

Kroll, A., Cho, H. E., & Kang, M. H. (2020). Antineoplastic Agents Targeting Sphingolipid Pathways. *Frontiers in Oncology*, *10*(May), 1–12. https://doi.org/10.3389/fonc.2020.00833

Lambertsen, K. L., Finsen, B., & Clausen, B. H. (2019). Post-stroke inflammation—target or tool for therapy? *Acta Neuropathologica*, *137*(5), 693–714. https://doi.org/10.1007/s00401-018-1930-z

Latour, L. L., Kang, D. W., Ezzeddine, M. A., Chalela, J. A., & Warach, S. (2004). Early blood-brain barrier disruption in human focal brain ischemia. *Annals of Neurology*, *56*(4), 468–477. https://doi.org/10.1002/ana.20199

Lee, M. J., Thangada, S., Claffey, K. P., Ancellin, N., Liu, C. H., Kluk, M., Volpi, M., Sha'afi, R. I., & Hla, T. (1999). Vascular endothelial cell adherens junction assembly and morphogenesis induced by sphingosine-1-phosphate. *Cell*, *99*(3), 301–312. https://doi.org/10.1016/S0092-8674(00)81661-X

Lee, Y. K., Uchida, H., Smith, H., Ito, A., & Sanchez, T. (2019). The isolation and molecular characterization of cerebral microvessels. *Nature Protocols*, *14*(11), 3059–3081. https://doi.org/10.1038/s41596-019-0212-0

Levkau, B., Hermann, S., Theilmeier, G., Van Der Giet, M., Chun, J., Schober, O., & Schäfers, M. (2004). High-density lipoprotein stimulates myocardial perfusion in vivo. *Circulation*, *110*(21), 3355–3359. https://doi.org/10.1161/01.CIR.0000147827.43912.AE

Liddelow, S. A., Guttenplan, K. A., Clarke, L. E., Bennett, F. C., Bohlen, C. J., Schirmer, L., Bennett, M. L., Münch, A. E., Chung, W. S., Peterson, T. C., Wilton, D. K., Frouin, A., Napier, B. A., Panicker, N., Kumar, M., Buckwalter, M. S., Rowitch, D. H., Dawson, V. L., Dawson, T. M., … Barres, B. A. (2017). Neurotoxic reactive astrocytes are induced by activated microglia. *Nature*, *541*(7638), 481–487. https://doi.org/10.1038/nature21029

Liesz, A., Sun, L., Zhou, W., Schwarting, S., Mracsko, E., Zorn, M., Bauer, H., Sommer, C., & Veltkamp, R. (2011). FTY720 reduces post-ischemic brain lymphocyte influx but does not improve outcome in permanent murine cerebral ischemia. *PLoS ONE*, *6*(6). https://doi.org/10.1371/journal.pone.0021312

Liesz, A., Suri-Payer, E., Veltkamp, C., Doerr, H., Sommer, C., Rivest, S., Giese, T., & Veltkamp, R. (2009). Regulatory T cells are key cerebroprotective immunomodulators in acute experimental stroke. *Nature Medicine*, *15*(2), 192–199. https://doi.org/10.1038/nm.1927

Liu, C. Y., Yang, Y., Ju, W. N., Wang, X., & Zhang, H. L. (2018). Emerging roles of astrocytes in neuro-vascular unit and the tripartite synapse with emphasis on reactive gliosis in the context of alzheimer's disease. *Frontiers in Cellular Neuroscience*, *12*(July), 1–12. https://doi.org/10.3389/fncel.2018.00193

Liu, Y., Wada, R., Yamashita, T., Mi, Y., Deng, C. X., Hobson, J. P., Rosenfeldt, H. M., Nava, V. E., Chae, S. S., Lee, M. J., Liu, C. H., Hla, T., Spiegel, S., & Proia, R. L. (2000). Edg-1, the G protein-coupled receptor for sphingosine-1-phosphate, is essential for vascular maturation. *Journal of Clinical Investigation*, *106*(8), 951–961. https://doi.org/10.1172/JCI10905

Llovera, G., Simats, A., & Liesz, A. (2021). Modeling stroke in mice: transient middle cerebral artery occlusion via the external carotid artery. *Journal of Visualized Experiments*, *2021*(171), 1–19. https://doi.org/10.3791/62573

Lo, E. H. (2008). A new penumbra: Transitioning from injury into repair after stroke. In *Nature Medicine* (Vol. 14, Issue 5, pp. 497–500). https://doi.org/10.1038/nm1735

Lochhead, J. J., & Thorne, R. G. (2012). Intranasal delivery of biologics to the central nervous system. *Advanced Drug Delivery Reviews*, *64*(7), 614–628. https://doi.org/10.1016/j.addr.2011.11.002

Lucaciu, A., Kuhn, H., Trautmann, S., Ferreirós, N., Steinmetz, H., Pfeilschifter, J., Brunkhorst, R., Pfeilschifter, W., Subburayalu, J., & Vutukuri, R. (2020). A sphingosine 1-phosphate gradient is linked to the cerebral recruitment of t helper and regulatory t helper cells during acute ischemic stroke. *International Journal of Molecular Sciences*, *21*(17), 1–20. https://doi.org/10.3390/ijms21176242

Magistretti, P., Pellerin, L., Rothman, D. (1999). *Energy on Demand*. Science, *283*(January), 496-497. https://doi.org/10.1126/science.283.5401.496

Malone, K., Diaz Diaz, A. C., Shearer, J. A., Moore, A. C., & Waeber, C. (2021). The effect of fingolimod on regulatory T cells in a mouse model of brain ischaemia. *Journal of Neuroinflammation*, *18*(1), 1–15. https://doi.org/10.1186/s12974-021-02083-5

Matloubian, M., Lo, C. G., Cinamon, G., Lesneski, M. J., Xu, Y., Brinkmann, V., Allende, M. L., Proia, R. L., & Cyster, J. G. (2004). Lymphocyte egress from thymus and peripheral lymphoid organs is dependent on S1P receptor 1. *Nature*, *427*(6972), 355–360. https://doi.org/10.1038/nature02284

Mattei, D., Ivanov, A., van Oostrum, M., Pantelyushin, S., Richetto, J., Mueller, F., Beffinger, M., Schellhammer, L., Berg, J. Vom, Wollscheid, B., Beule, D., Paolicelli, R. C., & Meyer, U. (2020). Enzymatic dissociation induces transcriptional and proteotype bias in brain cell populations. *International Journal of Molecular Sciences*, *21*(21), 1–20. https://doi.org/10.3390/ijms21217944

Matthes, F., Matuskova, H., Arkelius, K., Ansar, S., Lundgaard, I., & Meissner, A. (2021). An Improved Method for Physical Separation of Cerebral Vasculature and Parenchyma Enables Detection of Blood-Brain-Barrier Dysfunction. *NeuroSci*, *2*(1), 59–74. https://doi.org/10.3390/neurosci2010004

Matthias, K., Kirchhoff, F., Seifert, G., Hüttmann, K., Matyash, M., Kettenmann, H., & Steinhäuser, C. (2003). Segregated expression of AMPA-type glutamate receptors and glutamate transporters defines distinct astrocyte populations in the mouse hippocampus. *Journal of Neuroscience*, *23*(5), 1750–1758. https://doi.org/10.1523/jneurosci.23-05-01750.2003

McBride, D. W., & Zhang, J. H. (2017). Precision Stroke Animal Models: the Permanent MCAO Model Should Be the Primary Model, Not Transient MCAO. *Translational Stroke Research*, *8*(5), 397–404. https://doi.org/10.1007/s12975-017-0554-2

McConnell, H. L., Kersch, C. N., Woltjer, R. L., & Neuwelt, E. A. (2017). The translational significance of the neurovascular unit. *Journal of Biological Chemistry*, *292*(3), 762–770. https://doi.org/10.1074/jbc.R116.760215

Means, C. K., Xiao, C. Y., Li, Z., Zhang, T., Omens, J. H., Ishii, I., Chun, J., & Brown, J. H. (2007). Sphingosine 1-phosphate S1P2 and S1P3 receptor-mediated Akt activation protects against in vivo myocardial ischemia-reperfusion injury. *American Journal of Physiology - Heart and Circulatory Physiology*, *292*(6), 2944–2951. https://doi.org/10.1152/ajpheart.01331.2006

Meisel, C., Schwab, J. M., Prass, K., Meisel, A., & Dirnagl, U. (2005). Central nervous system injury-induced immune deficiency syndrome. *Nature Reviews Neuroscience*, *6*(10), 775–786. https://doi.org/10.1038/nrn1765

Moon, E., Han, J. E., Jeon, S., Ryu, J. H., Choi, J. W., & Chun, J. (2015). Exogenous S1P Exposure Potentiates Ischemic Stroke Damage That Is Reduced Possibly by Inhibiting

S1P Receptor Signaling. *Mediators of Inflammation*, *2015*, 11–14. https://doi.org/10.1155/2015/492659

Moon, S., Chang, M. S., Koh, S. H., & Choi, Y. K. (2021). Repair mechanisms of the neurovascular unit after ischemic stroke with a focus on vegf. *International Journal of Molecular Sciences*, *22*(16). https://doi.org/10.3390/ijms22168543

Munikoti, V. V., Hoang-Minh, L. B., & Ormerod, B. K. (2012). Enzymatic digestion improves the purity of harvested cerebral microvessels. *Journal of Neuroscience Methods*, *207*(1), 80–85. https://doi.org/10.1016/j.jneumeth.2012.03.011

Muoio, V., Persson, P. B., & Sendeski, M. M. (2014). The neurovascular unit - concept review. *Acta Physiologica*, *210*(4), 790–798. https://doi.org/10.1111/apha.12250

Murakami, A., Takasugi, H., Ohnuma, S., Koide, Y., Sakurai, A., Takeda, S., Hasegawa, T., Sasamori, J., Konno, T., Hayashi, K., Watanabe, Y., Mori, K., Sato, Y., Takahashi, A., Mochizuki, N., & Takakura, N. (2010). Sphingosine 1-phosphate (S1P) regulates vascular contraction via S1P 3 receptor: Investigation based on a new S1P3 receptor antagonist. *Molecular Pharmacology*, *77*(4), 704–713. https://doi.org/10.1124/mol.109.061481

Nadareishvili, Z., Simpkins, A. N., Hitomi, E., Reyes, D., & Leigh, R. (2019). Post-stroke blood-brain barrier disruption and poor functional outcome in patients receiving thrombolytic therapy. *Cerebrovascular Diseases*, *47*(3–4), 135–142. https://doi.org/10.1159/000499666

Nawashiro, H., Brenner, M., Fukui, S., Shima, K., & Hallenbeck, J. M. (2000). High susceptibility to cerebral ischemia in GFAP-null mice. *Journal of Cerebral Blood Flow and Metabolism*, *20*(7), 1040–1044. https://doi.org/10.1097/00004647-200007000-00003

Nian, K., Harding, I. C., Herman, I. M., & Ebong, E. E. (2020). Blood-Brain Barrier Damage in Ischemic Stroke and Its Regulation by Endothelial Mechanotransduction. *Frontiers in Physiology*, *11*(December). https://doi.org/10.3389/fphys.2020.605398

Nitzsche, A., Poittevin, M., Benarab, A., Bonnin, P., Faraco, G., Uchida, H., Favre, J., Garcia-Bonilla, L., Garcia, M. C. L., Léger, P. L., Thérond, P., Mathivet, T., Autret, G., Baudrie, V., Couty, L., Kono, M., Chevallier, A., Niazi, H., Tharaux, P. L., … Camerer, E. (2021). Endothelial S1P1 signaling counteracts infarct expansion in ischemic stroke. *Circulation Research*, 363–382. https://doi.org/10.1161/CIRCRESAHA.120.316711

Nofer, J. R., Van Der Giet, M., Tölle, M., Wolinska, I., Von Wnuck Lipinski, K., Baba, H. A., Tietge, U. J., Gödecke, A., Ishii, I., Kleuser, B., Schäfers, M., Fobker, M., Zidek, W., Assmann, G., Chun, J., & Levkau, B. (2004). HDL induces NO-dependent vasorelaxation via the lysophospholipid receptor S1P3. *Journal of Clinical Investigation*, *113*(4), 569–581. https://doi.org/10.1172/JCI200418004

Obermeier, B., Daneman, R., & Ransohoff, R. M. (2013). Development, maintenance and disruption of the blood-brain barrier. *Nature Medicine*, *19*(12), 1584–1596. https://doi.org/10.1038/nm.3407

Okamoto, Y., Wang, F., Yoshioka, K., Takuwa, N., & Takuwa, Y. (2011). Sphingosine-1-phosphate-specific G protein-coupled receptors as novel therapeutic targets for atherosclerosis. *Pharmaceuticals*, *4*(1), 117–137. https://doi.org/10.3390/ph4010117

Olesch, C., Ringel, C., Brüne, B., & Weigert, A. (2017). Beyond Immune Cell Migration: The Emerging Role of the Sphingosine-1-phosphate Receptor S1PR4 as a Modulator of Innate Immune Cell Activation. *Mediators of Inflammation*, *2017*. https://doi.org/10.1155/2017/6059203

Pan, J., & Wan, J. (2020). Methodological comparison of FACS and MACS isolation of enriched microglia and astrocytes from mouse brain. *Journal of Immunological Methods*, *486*(August), 112834. https://doi.org/10.1016/j.jim.2020.112834

Pankratz, N., Schick, U. M., Zhou, Y., Zhou, W., Ahluwalia, T. S., Allende, M. L., Auer, P. L., Bork-Jensen, J., Brody, J. A., Chen, M. H., Clavo, V., Eicher, J. D., Grarup, N., Hagedorn, E. J., Hu, B., Hunker, K., Johnson, A. D., Leusink, M., Lu, Y., … Ganesh, S. K. (2016). Meta-analysis of rare and common exome chip variants identifies S1PR4 and other loci influencing blood cell traits. *Nature Genetics*, *48*(8), 867–876. https://doi.org/10.1038/ng.3607

Papadopoulos, M. C., Manley, G. T., Krishna, S., & Verkman, A. S. (2004). Aquaporin-4 facilitates reabsorption of excess fluid in vasogenic brain edema. *The FASEB Journal*, *18*(11), 1291–1293. https://doi.org/10.1096/fj.04-1723fje

Park, S. W., Kim, M., Chen, S. W. C., Brown, K. M., D'Agati, V. D., & Lee, H. T. (2010). Sphinganine-1-phosphate protects kidney and liver after hepatic ischemia and reperfusion in mice through S1P 1 receptor activation. *Laboratory Investigation*, *90*(8), 1209–1224. https://doi.org/10.1038/labinvest.2010.102

Peña, I. Dela, Borlongan, C., Shen, G., & Davis, W. (2017). Strategies to extend thrombolytic time window for ischemic stroke treatment: An unmet clinical need. In *Journal of Stroke* (Vol. 19, Issue 1, pp. 50–60). Korean Stroke Society. https://doi.org/10.5853/jos.2016.01515

Perea, G., Navarrete, M., & Araque, A. (2009). Tripartite synapses: astrocytes process and control synaptic information. *Trends in Neurosciences*, *32*(8), 421–431. https://doi.org/10.1016/j.tins.2009.05.001

Perego, C., Fumagalli, S., Zanier, E. R., Carlino, E., Panini, N., Erba, E., & De Simoni, M. G. (2016). Macrophages are essential for maintaining a M2 protective response early after ischemic brain injury. *Neurobiology of Disease*, *96*, 284–293. https://doi.org/10.1016/j.nbd.2016.09.017

Poittevin, M., Deroide, N., Azibani, F., Delcayre, C., Giannesini, C., Levy, B. I., Pocard, M., & Kubis, N. (2013). Glatiramer Acetate administration does not reduce damage after cerebral ischemia in mice. *Journal of Neuroimmunology*, *254*(1–2), 55–62. https://doi.org/10.1016/j.jneuroim.2012.09.009

Prager, B., Spampinato, S. F., & Ransohoff, R. M. (2015). Sphingosine 1-phosphate

signaling at the blood-brain barrier. *Trends in Molecular Medicine*, *21*(6), 354–363. https://doi.org/10.1016/j.molmed.2015.03.006

Proia, R. L., & Hla, T. (2015). Emerging biology of sphingosine-1-phosphate: Its role in pathogenesis and therapy. *Journal of Clinical Investigation*, *125*(4), 1379–1387. https://doi.org/10.1172/JCI76369

Pyne, N. J., & Pyne, S. (2017). Sphingosine 1-phosphate receptor 1 signaling in mammalian cells. *Molecules*, *22*(3). https://doi.org/10.3390/molecules22030344

Pyne, S., Adams, D. R., & Pyne, N. J. (2016). Sphingosine 1-phosphate and sphingosine kinases in health and disease: Recent advances. *Progress in Lipid Research*, *62*, 93–106. https://doi.org/10.1016/j.plipres.2016.03.001

Qiu, Y. M., Zhang, C. L., Chen, A. Q., Wang, H. L., Zhou, Y. F., Li, Y. N., & Hu, B. (2021). Immune Cells in the BBB Disruption After Acute Ischemic Stroke: Targets for Immune Therapy? *Frontiers in Immunology*, *12*(June). https://doi.org/10.3389/fimmu.2021.678744

Rehnström, M., Frederiksen, S. D., Ansar, S., & Edvinsson, L. (2020). Transcriptome profiling revealed early vascular smooth muscle cell gene activation following focal ischemic stroke in female rats – comparisons with males. *BMC Genomics*, *21*(1), 1–19. https://doi.org/10.1186/s12864-020-07295-2

Rodrigo, R., Fernández-Gajardo, R., Gutiérrez, R., Matamala, J. M., Carrasco, R., Miranda-Merchak, A., & Feuerhake, W. (2013). Oxidative Stress and Pathophysiology of Ischemic Stroke: Novel Therapeutic Opportunities. *CNS & Neurological Disorders -Drug Targets*, *12*, 0–0.

Salas-Perdomo, A., Miró-Mur, F., Gallizioli, M., Brait, V. H., Justicia, C., Meissner, A., Urra, X., Chamorro, A., & Planas, A. M. (2019). Role of the S1P pathway and inhibition by fingolimod in preventing hemorrhagic transformation after stroke. *Scientific Reports*, *9*(1), 1–13. https://doi.org/10.1038/s41598-019-44845-5

Sanchez, T., Skoura, A., Wu, M. T., Casserly, B., Harrington, E. O., & Hla, T. (2007). Induction of vascular permeability by the sphingosine-1-phosphate receptor-2 (S1P2R) and its downstream effectors ROCK and PTEN. *Arteriosclerosis, Thrombosis, and Vascular Biology*, *27*(6), 1312–1318. https://doi.org/10.1161/ATVBAHA.107.143735

Sanna, M. G., Liao, J., Jo, E., Alfonso, C., Ahn, M. Y., Peterson, M. S., Webb, B., Lefebvre, S., Chun, J., Gray, N., & Rosen, H. (2004). Sphingosine 1-Phosphate (S1P) Receptor Subtypes S1P1 and S1P3, Respectively, Regulate Lymphocyte Recirculation and Heart Rate. *Journal of Biological Chemistry*, *279*(14), 13839–13848. https://doi.org/10.1074/jbc.M311743200

Sanz, E., Yang, L., Su, T., Morris, D. R., McKnight, G. S., & Amieux, P. S. (2009). Cell-type-specific isolation of ribosome-associated mRNA from complex tissues. *Proceedings of the National Academy of Sciences of the United States of America*, *106*(33), 13939–13944. https://doi.org/10.1073/pnas.0907143106

Sapkota, A., Gaire, B. P., Kang, M. G., & Choi, J. W. (2019). S1P2 contributes to microglial activation and M1 polarization following cerebral ischemia through ERK1/2 and JNK. *Scientific Reports*, *9*(1), 1–13. https://doi.org/10.1038/s41598-019-48609-z

Schildge, S., Bohrer, C., Beck, K., & Schachtrup, C. (2013). Isolation and culture of mouse cortical astrocytes. *Journal of Visualized Experiments : JoVE*, *71*, 1–7. https://doi.org/10.3791/50079

Schroeter, C. B., Herrmann, A. M., Bock, S., Vogelsang, A., Eichler, S., Albrecht, P., Meuth, S. G., & Ruck, T. (2021). Article one brain—all cells: A comprehensive protocol to isolate all principal cns-resident cell types from brain and spinal cord of adult healthy and eae mice. *Cells*, *10*(3), 1–25. https://doi.org/10.3390/cells10030651

Schwab, S. R., Pereira, J. P., Matloubian, M., Xu, Y., Huang, Y., & Cyster, J. G. (2005). Immunology: Lymphocyte sequestration through S1P lyase inhibition and disruption of S1P gradients. *Science*, *309*(5741), 1735–1739. https://doi.org/10.1126/science.1113640

Selvaraj, U. M., & Stowe, A. M. (2017). Long-term T cell responses in the brain after an ischemic stroke. *Discovery Medicine*, *24*(134), 323–333.

Sensken, S. C., Stäubert, C., Keul, P., Levkau, B., Schöneberg, T., & Gräler, M. H. (2008). Selective activation of G alpha i mediated signalling of S1P3 by FTY720-phosphate. *Cellular Signalling*, *20*(6), 1125–1133. https://doi.org/10.1016/j.cellsig.2008.01.019

Shao, Z., Tu, S., & Shao, A. (2019). Pathophysiological mechanisms and potential therapeutic targets in intracerebral hemorrhage. *Frontiers in Pharmacology*, *10*(September), 1–8. https://doi.org/10.3389/fphar.2019.01079

Shi, Y., Zhang, L., Pu, H., Mao, L., Hu, X., Jiang, X., Xu, N., Stetler, R. A., Zhang, F., Liu, X., Leak, R. K., Keep, R. F., Ji, X., & Chen, J. (2016). Rapid endothelial cytoskeletal reorganization enables early blood-brain barrier disruption and long-term ischaemic reperfusion brain injury. *Nature Communications*, *7*. https://doi.org/10.1038/ncomms10523

Shimazu, T., Inoue, I., Araki, N., Asano, Y., Sawada, M., Furuya, D., Nagoya, H., & Greenberg, J. H. (2005). A peroxisome proliferator-activated receptor-γ agonist reduces infarct size in transient but not in permanent ischemia. *Stroke*, *36*(2), 353–359. https://doi.org/10.1161/01.STR.0000152271.21943.a2

Sofroniew, M. V. (2015). Astrocyte barriers to neurotoxic inflammation. *Nature Reviews Neuroscience*, *16*(5), 249–263. https://doi.org/10.1038/nrn3898

Sofroniew, M. V. (2020). Astrocyte Reactivity: Subtypes, States, and Functions in CNS Innate Immunity. *Trends in Immunology*, *41*(9), 758–770. https://doi.org/10.1016/j.it.2020.07.004

Sofroniew, M. V, & Vinters, H. V. (2009). *Astrocytes: biology and pathology*. https://doi.org/10.1007/s00401-009-0619-8

Sun, W., Cornwell, A., Li, J., Peng, S., Joana Osorio, M., Aalling, N., Wang, S., Benraiss, A., Lou, N., Goldman, S. A., & Nedergaard, M. (2017). SOX9 is an astrocyte-specific nuclear marker in the adult brain outside the neurogenic regions. *Journal of Neuroscience*, *37*(17), 4493–4507. https://doi.org/10.1523/JNEUROSCI.3199-16.2017

Sun, X., Singleton, P. A., Letsiou, E., Zhao, J., Belvitch, P., Sammani, S., Chiang, E. T., Moreno-Vinasco, L., Wade, M. S., Zhou, T., Liu, B., Parastatidis, I., Thomson, L., Ischiropoulos, H., Natarajan, V., Jacobson, J. R., MacHado, R. F., Dudek, S. M., & Garcia, J. G. N. (2012). Sphingosine-1-phosphate receptor-3 is a novel biomarker in acute lung injury. *American Journal of Respiratory Cell and Molecular Biology*, *47*(5), 628–636. https://doi.org/10.1165/rcmb.2012-0048OC

Sutermaster, B. A., & Darling, E. M. (2019). Considerations for high-yield, high-throughput cell enrichment: fluorescence versus magnetic sorting. *Scientific Reports*, *9*(1), 1–9. https://doi.org/10.1038/s41598-018-36698-1

Sweeney, M. D., Ayyadurai, S., & Zlokovic, B. V. (2016). Pericytes of the neurovascular unit: Key functions and signaling pathways. *Nature Neuroscience*, *19*(6), 771–783. https://doi.org/10.1038/nn.4288

Takata, N., & Hirase, H. (2008). Cortical layer 1 and layer 2/3 astrocytes exhibit distinct calcium dynamics in vivo. *PLoS ONE*, *3*(6). https://doi.org/10.1371/journal.pone.0002525

Taylor, A. R., Robinson, M. B., & Milligan, C. E. (2007). In vitro methods to prepare astrocyte and motoneuron cultures for the investigation of potential in vivo interactions. *Nature Protocols*, *2*(6), 1499–1507. https://doi.org/10.1038/nprot.2007.208

Temburni, M. K., & Jacob, M. H. (2001). New functions for glia in the brain. *Proceedings of the National Academy of Sciences of the United States of America*, *98*(7), 3631–3632. https://doi.org/10.1073/pnas.081073198

Theilmeier, G., Schmidt, C., Herrmann, J., Keul, P., Schäfers, M., Herrgott, I., Mersmann, J., Larmann, J., Hermann, S., Stypmann, J., Schober, O., Hildebrand, R., Schulz, R., Heusch, G., Haude, M., Lipinski, K. V. W., Herzog, C., Schmitz, M., Erbel, R., … Levkau, B. (2006). High-density lipoproteins and their constituent, sphingosine-1-phosphate, directly protect the heart against ischemia/reperfusion injury in vivo via the S1P3 lysophospholipid receptor. *Circulation*, *114*(13), 1403–1409. https://doi.org/10.1161/CIRCULATIONAHA.105.607135

Theparambil, S. M., Hosford, P. S., Ruminot, I., Kopach, O., Reynolds, J. R., Sandoval, P. Y., Rusakov, D. A., Barros, L. F., & Gourine, A. V. (2020). Astrocytes regulate brain extracellular pH via a neuronal activity-dependent bicarbonate shuttle. *Nature Communications*, *11*(1), 1–15. https://doi.org/10.1038/s41467-020-18756-3

Thomsen, M. S., Routhe, L. J., & Moos, T. (2017). The vascular basement membrane in the healthy and pathological brain. *Journal of Cerebral Blood Flow and Metabolism*, *37*(10), 3300–3317. https://doi.org/10.1177/0271678X17722436

Van Doorn, R., Van Horssen, J., Verzijl, D., Witte, M., Ronken, E., Van Het Hof, B.,

Lakeman, K., Dijkstra, C. D., Van Der Valk, P., Reijerkerk, A., Alewijnse, A. E., Peters, S. L. M., & De Vries, H. E. (2010). Sphingosine 1-phosphate receptor 1 and 3 are upregulated in multiple sclerosis lesions. *Glia*, *58*(12), 1465–1476. https://doi.org/10.1002/glia.21021

Van Echten-Deckert, G., & Alam, S. (2018). Sphingolipid metabolism - An ambiguous regulator of autophagy in the brain. *Biological Chemistry*, *399*(8), 837–850. https://doi.org/10.1515/hsz-2018-0237

Venkataraman, K., Lee, Y. M., Michaud, J., Thangada, S., Ai, Y., Bonkovsky, H. L., Parikh, N. S., Habrukowich, C., & Hla, T. (2008). Vascular endothelium as a contributor of plasma sphingosine 1-phosphate. *Circulation Research*, *102*(6), 669–676. https://doi.org/10.1161/CIRCRESAHA.107.165845

Walter, D. H., Rochwalsky, U., Reinhold, J., Seeger, F., Aicher, A., Urbich, C., Spyridopoulos, I., Chun, J., Brinkmann, V., Keul, P., Levkau, B., Zeiher, A. M., Dimmeler, S., & Haendeler, J. (2007). Sphingosine-1-phosphate stimulates the functional capacity of progenitor cells by activation of the CXCR4-dependent signaling pathway via the S1P3 receptor. *Arteriosclerosis, Thrombosis, and Vascular Biology*, *27*(2), 275–282. https://doi.org/10.1161/01.ATV.0000254669.12675.70

Walzer, T., Chiossone, L., Chaix, J., Calver, A., Carozzo, C., Garrigue-Antar, L., Jacques, Y., Baratin, M., Tomasello, E., & Vivier, E. (2007). Natural killer cell trafficking in vivo requires a dedicated sphingosine 1-phosphate receptor. *Nature Immunology*, *8*(12), 1337–1344. https://doi.org/10.1038/ni1523

Wang, L., Xiong, X., Zhang, L., & Shen, J. (2021). Neurovascular Unit: A critical role in ischemic stroke. *CNS Neuroscience and Therapeutics*, *27*(1), 7–16. https://doi.org/10.1111/cns.13561

Wang, Z., Higashikawa, K., Yasui, H., Kuge, Y., Ohno, Y., Kihara, A., Midori, Y. A., Houkin, K., & Kawabori, M. (2020). FTY720 Protects Against Ischemia–Reperfusion Injury by Preventing the Redistribution of Tight Junction Proteins and Decreases Inflammation in the Subacute Phase in an Experimental Stroke Model. *Translational Stroke Research*, *11*(5), 1103–1116. https://doi.org/10.1007/s12975-020-00789-x

Watts, M. E., Pocock, R., & Claudianos, C. (2018). Brain energy and oxygen metabolism: Emerging role in normal function and disease. *Frontiers in Molecular Neuroscience*, *11*(June), 1–13. https://doi.org/10.3389/fnmol.2018.00216

Wei, Y., Yemisci, M., Kim, H. H., Yung, L. M., Shin, H. K., Hwang, S. K., Guo, S., Qin, T., Alsharif, N., Brinkmann, V., Liao, J. K., Lo, E. H., & Waeber, C. (2011). Fingolimod provides long-term protection in rodent models of cerebral ischemia. *Annals of Neurology*, *69*(1), 119–129. https://doi.org/10.1002/ana.22186

Weichand, B., Weis, N., Weigert, A., Grossmann, N., Levkau, B., & Brüne, B. (2013). Apoptotic cells enhance sphingosine-1-phosphate receptor 1 dependent macrophage migration. *European Journal of Immunology*, *43*(12), 3306–3313. https://doi.org/10.1002/eji.201343441

Weinstein, D. E. (1997). Isolation and Purification of Primary Rodent Astrocytes. *Current Protocols in Neuroscience*, *00*(1), 1–9. https://doi.org/10.1002/0471142301.ns0305s00

Williamson, M. R., Fuertes, C. J. A., Dunn, A. K., Drew, M. R., & Jones, T. A. (2021). Reactive astrocytes facilitate vascular repair and remodeling after stroke. *Cell Reports*, *35*(4), 109048. https://doi.org/10.1016/j.celrep.2021.109048

World Health Organization, 2020: The top 10 causes of death. https://www.who.int/news-room/fact-sheets/detail/the-top-10-causes-of-death (29.01.2022)

Xing, C., Arai, K., Lo, E. H., & Hommel, M. (2012). Pathophysiologic cascades in ischemic stroke. *International Journal of Stroke : Official Journal of the International Stroke Society*, *7*(5), 378–385. https://doi.org/10.1111/j.1747-4949.2012.00839.x

Xu, D., Gao, Q., Wang, F., Peng, Q., Wang, G., Wei, Q., Lei, S., Zhao, S., Zhang, L., & Guo, F. (2021). Sphingosine-1-phosphate receptor 3 is implicated in BBB injury via the CCL2-CCR2 axis following acute intracerebral hemorrhage. *CNS Neuroscience and Therapeutics*, *27*(6), 674–686. https://doi.org/10.1111/cns.13626

Xu, S., Lu, J., Shao, A., Zhang, J. H., & Zhang, J. (2020). Glial Cells: Role of the Immune Response in Ischemic Stroke. *Frontiers in Immunology*, *11*(February), 294. https://doi.org/10.3389/fimmu.2020.00294

Yanagida, K., & Hla, T. (2017). Vascular and Immunobiology of the Circulatory Sphingosine 1-Phosphate Gradient. *Annual Review of Physiology*, *79*(October 2016), 67–91. https://doi.org/10.1146/annurev-physiol-021014-071635

Yanagida, K., Liu, C. H., Faraco, G., Galvani, S., Smith, H. K., Burg, N., Anrather, J., Sanchez, T., Iadecola, C., & Hla, T. (2017). Size-selective opening of the blood-brain barrier by targeting endothelial sphingosine 1-phosphate receptor 1. *Proceedings of the National Academy of Sciences of the United States of America*, *114*(17), 4531–4536. https://doi.org/10.1073/pnas.1618659114

Yao, X., Derugin, N., Manley, G. T., & Verkman, A. S. (2015). Reduced brain edema and infarct volume in aquaporin-4 deficient mice after transient focal cerebral ischemia. *Neuroscience Letters*, *584*, 368–372. https://doi.org/10.1016/j.neulet.2014.10.040

Yasuda, S., Sumioka, T., Iwanishi, H., Okada, Y., Miyajima, M., Ichikawa, K., Reinach, P. S., & Saika, S. (2021). Loss of sphingosine 1-phosphate receptor 3 gene function impairs injury-induced stromal angiogenesis in mouse cornea. *Laboratory Investigation*, *101*(2), 245–257. https://doi.org/10.1038/s41374-020-00505-1

Yin, K., & Yang, X. (2016). *Non-Neuronal Mechanisms of Brain Damage and Repair After Stroke*. 93–108. https://doi.org/10.1007/978-3-319-32337-4

Yousif, S., Marie-Claire, C., Roux, F., Scherrmann, J. M., & Declèves, X. (2007). Expression of drug transporters at the blood-brain barrier using an optimized isolated rat brain microvessel strategy. *Brain Research*, *1134*(1), 1–11. https://doi.org/10.1016/j.brainres.2006.11.089

Yung, B. S., Brand, C. S., Xiang, S. Y., Gray, C. B. B., Means, C. K., Rosen, H., Chun, J., Purcell, N. H., Brown, J. H., & Miyamoto, S. (2017). Selective coupling of the S1P3 receptor subtype to S1P-mediated RhoA activation and cardioprotection. *Journal of Molecular and Cellular Cardiology*, *103*, 1–10. https://doi.org/10.1016/j.yjmcc.2016.12.008

Zaheer, Z., Robinson, T., & Mistri, A. K. (2011). Thrombolysis in acute ischaemic stroke: An update. In *Therapeutic Advances in Chronic Disease* (Vol. 2, Issue 2, pp. 119–131). https://doi.org/10.1177/2040622310394032

Zamanian, J. L., Xu, L., Foo, L. C., Nouri, N., Zhou, L., Giffard, R. G., & Barres, B. A. (2012). Genomic analysis of reactive astrogliosis. *Journal of Neuroscience*, *32*(18), 6391–6410. https://doi.org/10.1523/JNEUROSCI.6221-11.2012

Zhang, H. T., Zhang, P., Gao, Y., Li, C. L., Wang, H. J., Chen, L. C., Feng, Y., Li, R. Y., Li, Y. L., & Jiang, C. L. (2017). Early VEGF inhibition attenuates blood-brain barrier disruption in ischemic rat brains by regulating the expression of MMPs. *Molecular Medicine Reports*, *15*(1), 57–64. https://doi.org/10.3892/mmr.2016.5974

Zhang, S., Shang, D., Shi, H., Teng, W., & Tian, L. (2021). Function of Astrocytes in Neuroprotection and Repair after Ischemic Stroke. *European Neurology*, *84*(6), 426–434. https://doi.org/10.1159/000517378

Zhang, Y., Chen, K., Sloan, S. A., Bennett, M. L., Scholze, A. R., O'Keeffe, S., Phatnani, H. P., Guarnieri, P., Caneda, C., Ruderisch, N., Deng, S., Liddelow, S. A., Zhang, C., Daneman, R., Maniatis, T., Barres, B. A., & Wu, J. Q. (2014). An RNA-sequencing transcriptome and splicing database of glia, neurons, and vascular cells of the cerebral cortex. *Journal of Neuroscience*, *34*(36), 11929–11947. https://doi.org/10.1523/JNEUROSCI.1860-14.2014

Zhao, S. C., Ma, L. S., Chu, Z. H., Xu, H., Wu, W. Q., & Liu, F. (2017). Regulation of microglial activation in stroke. *Acta Pharmacologica Sinica*, *38*(4), 445–458. https://doi.org/10.1038/aps.2016.162

Zhou, J., & van Zijl, P. C. M. (2012). Defining an Acidosis-Based Ischemic Penumbra from pH-Weighted MRI. *Translational Stroke Research*, *3*(1), 76–83. https://doi.org/10.1007/s12975-011-0110-4

9. Acknowledgements

First of all, I want to thank my supervisor Prof. Dr. Anja Meissner for giving me the opportunity to work on this and also on many other projects throughout the past four years. I feel very grateful for having such an amazing supervisor, who I connected with on a professional and most importantly, on a personal level. Thank you for your endless support on this journey, for being always open for discussion (anytime during the day and week), exposing me to challenges which helped me to grow in the best way possible and helping me accomplish great things.

Next, I would like to thank my co-supervisor Prof. Dr. Gabor Petzold for his support and valuable input throughout my PhD journey. Thank you for helping me drive this project forward and involving me in different collaborations, which I truly enjoyed.

I would like to thank Prof. Dr. Sebastian Zimmer and Prof. Dr. Susanne Schoch for their willingness to be part of my committee and taking time to consider my work.

I am grateful for the opportunity to work in such a friendly environment in both labs in Bonn and Lund. Theresa, I would like to thank you (and *Ficus benjamina*) for your emotional and professional support throughout my PhD. I would like to thank Nancy for having her doors always open and being there for us. Nelli for giving me proper training in the lab, all the fun we had together and being a friend, I can always rely on. A big thank goes to former (Andrea and Christof) and current members (Stephanie and her legendary gatherings, Gulia, Christian, Somayyeh, Nicole and Jan) of the AG Petzold group. Next, I would like to thank Stefano. You helped me to go through difficult times and you were always open for any discussion, celebrating my achievements and most importantly, joining me on the journey towards the victory over the cryostat (-16/-30 forever). Moni and Steffi, thank you for always having a glass of white wine and delicious food for me and all the great laughs we had on our hikes and during exit games. Many thanks go also to Nora and Pietro and our Inline skater group, which brought us back to life after lockdown. Thank both of you for making me laugh so much and giving me support and creating a safe space in Campus. My sincere acknowledgement also goes to Lund. Lotte, thank you for all your help during the time I was in Sweden and for your willingness to take your time to correct my thesis, I am very grateful for that!

Next, a huge thank you goes to the Czech Republic. I would like to thank Ráďa for contributing to our regular podcast and being such an incredibly supportive friend, Štěpánka for making me laugh also at times when I did not feel like laughing and always helping me to look at things from above and showing me that not everything is always as dramatic as I see it. Big thank you goes also to Markét for being my big motivation and Sarah for being my true fan and staying with me during my ups and downs. Thank you all for always being there for me!

Finally, any of this would be possible without my mum and sister. Ze srdce vám děkuji za vaši láskyplnou podporu a důvěru. Děkuji, že tu pro mě vždy jste, podporujete mě ve všech mých rozhodnutích a motivujete mě v dobách, kdy žádnou motivaci nemám!